CU-167
AT 30-1-GEN-72

PUPIN CYCLOTRON LABORATORY
AND PEGRAM LABORATORY

THE BETA SPECTRUM OF He^6: LIMITS ON THE AXIAL VECTOR AND PSEUDOSCALAR COUPLING CONSTANTS OF BETA DECAY

BY

ARTHUR Z. SCHWARZSCHILD

MAY 1, 1957

COLUMBIA UNIVERSITY
DEPT. OF PHYSICS
NEW YORK 27, N.Y.

The Beta Spectrum of He^6 : Limits on the Axial Vector and Pseudoscalar Coupling Constants of Beta Decay

Arthur Z. Schwarzschild

A Dissertation

Submitted in partial fulfillment of the requirements for the degree of Doctor of Philosophy in the Faculty of Pure Science, of Columbia University.

ABSTRACT

We have performed a careful measurement of the shape of the beta spectrum of He^6. A detailed study of the phenomenon of electron scattering in our thin lens magnetic spectrometer enabled us to interpret the spectrum shape from the end point at $W_0 = 3.50 \pm .02$ Mev. down to $1/14\ W_0 = 0.250$ Mev. The experimental shape has been compared with the theoretically predicted shape for allowed spectra. The influence of the pseudoscalar interaction on the shape of the He^6 spectrum has also been considered. From these measurements we have been able to set limits on the Fierz interference in the Gamow-Teller interaction as well as on the magnitude of the pseudoscalar coupling constants. These limits have been interpreted in terms of the relative magnitudes of the axial vector, pseudoscalar, and tensor coupling constants using the two component theory of the neutrino and assuming that the complete beta decay Hamiltonian proposed by Lee and Yang is or is not invariant under time reversal. We have also calculated the effect on the spectrum shape of the production of inner Bremsstrahlung in beta decay and have shown this effect to be at the limit of experimental detectability.

ACKNOWLEDGEMENTS

The author wishes to express his sincere thanks to Prof. C. S. Wu. Prof. Wu suggested this problem and many of the procedures used to overcome the numerous experimental difficulties. Her constant guidance and encouragement were invaluable in the successful completion of this experiment.

The continued efforts of Mr. Brice Rustad and Mr. Ottmar Kistner in all the aspects of this project are gratefully acknowledged. Thanks go to Mr. R. Graeser and Mr. E. Caruso for their technical assistance.

To many members of the staff of Brookhaven National Laboratory the author expresses his appreciation. It is a pleasure to thank Dr. M. Fox and the Reactor Department for their hospitality, Dr. D. E. Alburger for kindly lending us his thin lens spectrometer, and Dr. Charles Baker and the members of the cyclotron crew for their generous assistance.

The author thanks Dr. Paul Martin for his suggestions regarding the calculation of the effect of Inner Bremsstrahlung on the shape of the beta spectrum. The help of Dr. E. Melkonian in the computer calculations of the numerous least square analyses is gratefully acknowledged.

The many discussions with Mrs. N. Benczer-Koller and Mr. J. Sucher were most helpful in the completion of this work and the writing of the dissertation.

Thanks are due to Prof. W. W. Havens for his continued interest in this project.

The work described in this paper was partially supported by the United States Atomic Energy Commission.

TABLE OF CONTENTS

INTRODUCTION

Experimental investigations of the shapes of the continuous β-spectra of both allowed and forbidden β-decay provide pertinent information necessary to specify the form of the β-decay Hamiltonian. In particular, the Fierz interference terms between Scalar and Vector interactions and between Tensor and Axial vector interaction have been found to be very small. Together with the results of the β-ν angular correlation experiments, this information has led us to believe that the Scalar and Tensor interactions are the predominant ones in β-decay. The recent evidence indicating that the β-decay Hamiltonian is not invariant under parity transformation and charge conjugation, as well as the present speculation that the Hamiltonian may not be invariant under time reversal, has cast some doubts on the old interpretation of the experimental results.

We have attempted a precise measurement of the allowed β-spectrum of He^6 in order to obtain a lower limit on the Fierz interference. We have interpreted these measurements in terms of the various combinations of possible invariance properties of the β-decay Hamiltonian and the properties of the neutrino field.

It has also been indicated by several authors that the shape of the β-spectrum of He^6 may afford information regarding the magnitude of the pseudoscalar coupling constant in β-decay. There is at present little indication that the pseudoscalar interaction plays any role in the β-decay. From a precise measurement of the He^6 spectral shape we have been able to set limits on the magnitude of the pseudoscalar coup-

ling constant.

Historically, the measurements of the shapes of β-spectra have been beset with instrumental difficulties of various types. The most significant experimental distortion of the spectral shapes was due to the scattering of electrons in the spectrometer source and detector. Rather complete studies of these phenomena have been reported in the literature, and many of these studies were performed in this laboratory. Since the maximum energy of the He^6 spectrum is large, distortion of spectral shape due to electron scattering in the spectrometer baffle system has been found to be more serious than scattering in the source and detector.

In order to obtain a precise measurement of the He^6 spectrum, we have studied the phenomenon of baffle scattering extensively. By measuring the spectrum of electrons transmitted by our magnetic spectrometer with the use of a scintillation spectrometer, we have been able to obtain a quantitative measure of the baffle scattering effect.

We have also considered the possibility of small deviations of the theoretically predicted spectrum shape due to the emission of inner bremsstrahlung in the β-decay as well as the very small effect of the finite nuclear recoil energy.

The precise measurements, together with extensive investigation of the scattering effects and other small corrections, have enabled us to make a significant comparison of the He^6 spectrum shape with that predicted by the theory over the range of energies from 1/14 of maximum energy to the end point of the spectrum.

I. THE THEORY OF ALLOWED β-DECAY

The Shape of the Allowed Spectrum

The β decay reaction can be represented by the following equation:

$$n \longrightarrow \bar{\nu} + p + e^- \tag{1-1}$$

The rate of decay from a complex nucleus is given by the usual first order perturbation formula for transitions from a discrete quantum state to a continuum of final states:

$$P(\epsilon) = \frac{\hbar}{2\pi} |H|^2 \rho(\epsilon) \tag{1-2}$$

$P(\epsilon)$ is the probability of emission of an electron into a unit energy interval, $\rho(\epsilon)$ is the density of final states available to the system of electron and neutrino, and recoil, and H is the matrix element of the interaction Hamiltonian.

Since the specific nature of the forces involved in the decay are not known, one can only appeal to general invariance principles of physics, and to the desire for simplicity, to limit the choice of the form of the Hamiltonian.

Fermi's original theory[1] proposed that the Hamiltonian was a function only of the field operators of the four particles involved in the decay, and that no derivative operators were to be included. Except for the attempts of Konipinski and Uhlenbeck to explain some unfortunately incorrectly measured β-spectra by introducing derivative operators, almost all the theoretical work to date has considered only

the "simplest" case of interactions not involving such operators. Experiment indicates that most β-decay phenomena can be explained within the framework of this simplifying assumption.

The invariance requirements on the Lagrangian and also on the β-decay Hamiltonian which had been assumed until recently were invariance under:

a. Proper Lorentz transformations

b. Space inversion (or parity transformation) (P)

c. Charge Conjugation (C)

d. Time reversal (T)

The Hamiltonian density which conforms to both the above mentioned simplicity requirement (ie. no derivative operators) and to the invariance requirement (a) above is:

$$\begin{aligned}\mathcal{H} = {} & (\psi_p^+ \gamma_4 \psi_n)(C_S \psi_e^+ \gamma_4 \psi_\nu + C_S' \psi_e^+ \gamma_4 \gamma_5 \psi_\nu) \\ & + (\psi_p^+ \gamma_4 \gamma_\mu \psi_n)(C_V \psi_e^+ \gamma_4 \gamma_\mu \psi_\nu + C_V' \psi_e^+ \gamma_4 \gamma_\mu \gamma_5 \psi_\nu) \\ & + \tfrac{1}{2}(\psi_p^+ \gamma_4 \sigma_{\lambda\mu} \psi_n)(C_T \psi_e^+ \gamma_4 \sigma_{\lambda\mu} \psi_\nu + C_T' \psi_e^+ \gamma_4 \sigma_{\lambda\mu} \gamma_5 \psi_\nu) \\ & + (\psi_p^+ \gamma_4 \gamma_\mu \gamma_5 \psi_n)(-C_A \psi_e^+ \gamma_4 \gamma_\mu \gamma_5 \psi_\nu - C_A' \psi_e^+ \gamma_4 \gamma_\mu \psi_\nu) \qquad (1\text{-}3) \\ & + (\psi_p^+ \gamma_4 \gamma_5 \psi_n)(C_P \psi_e^+ \gamma_4 \gamma_5 \psi_\nu + C_P' \psi_e^+ \gamma_4 \psi_\nu) \\ & + \text{Hermitian conjugate}.\end{aligned}$$

The terms involved in (1-3) are as follows: $\psi_p, \psi_n, \psi_e + \psi_\nu$ are the field operators of the proton, neutron, electron and neutrino, respectively; the matrices γ_μ are $\gamma_i \equiv -i\beta\alpha_i$; $\gamma_4 = \beta$; $\sigma_{\lambda\mu} \equiv -\frac{1}{2} i (\gamma_\lambda\gamma_\mu - \gamma_\mu\gamma_\lambda)$; $\gamma_5 \equiv \gamma_1\gamma_2\gamma_3\gamma_4$ where β and $\vec{\alpha}$ are the usual 4 X 4 Dirac matrices.(2) The C_i , C_i' are the coupling constants, named according to the transformation properties of the heavy particle part of the Hamiltonian.

Until recently it was believed that the Hamiltonian must be invariant also under transformations (P), (C), and (T) mentioned above. In this case either all the values C_i' must be zero (or all C_i must be zero depending upon the transformation properties of the neutrino field.(3)) In this case the Hamilton (1-3) reduces to the usual Hamiltonian discussed in the previous β-decay literature.

The recent experiment of Wu etal(4) has shown that the β-decay Hamiltonian is <u>not</u> invariant under p and c transformations. We therefore include all ten coupling constants of Eq. (1-3) according to the proposals of Lee and Yang.(5)

For the present discussion we shall also <u>not</u> assume that $\mathcal{H}$ is invariant under charge conjugation or time reversal.

The Hamiltonian of Eq. (1-3) may be rewritten in terms of the 4 X 4 matrices $\beta, \vec{\alpha}, \vec{\nabla} + \gamma_5$ in the following manner:

<u>Non-Relativistic</u> <u>Relativistic</u>

$$\mathcal{H} = (\psi_p^+ \beta \psi_N)\left[C_S \psi_e^+ \beta \psi_\nu + C_S' \psi_e^+ \beta\gamma_5 \psi_\nu\right]$$

$$+ (\psi_p^+ \psi_N)\left[C_V \psi_e^+ \psi_\nu + C_V' \psi_e^+ \gamma_5 \psi_\nu\right] \qquad -\left[\psi_p^+ \vec{\alpha} \psi_N\right]\cdot\left[C_V \psi_e^+ \vec{\alpha} \psi_\nu + C_V' \psi_e^+ \vec{\alpha}\gamma_5 \psi_\nu\right]$$

(cont'd)

$$+\left(\psi_p^{+}\beta\vec{\sigma}\,\psi_n\right)\cdot\left[C_T\,\psi_e^{+}\beta\vec{\sigma}\,\psi_\nu + C_T'\,\psi_e^{+}\beta\vec{\sigma}\gamma_5\psi_\nu\right] \quad + \left[\psi_p^{+}\beta\vec{\alpha}\psi_N\right]\cdot\left[C_T\psi_e^{+}\beta\vec{\alpha}\,\psi_\nu + C_T'\,\psi_e^{+}\beta\vec{\alpha}\gamma_5\psi_\nu\right]$$

$$+\left(\psi_p^{+}\vec{\sigma}\,\psi_n\right)\cdot\left[C_A\,\psi_e\vec{\sigma}\,\psi_\nu + C_A'\,\psi_e^{+}\vec{\sigma}\,\psi_\nu\right] \quad - \left[\psi_p^{+}\gamma_5\psi_N\right]\left[C_A\psi_e^{+}\gamma_5\psi_\nu + C_A'\,\psi_e^{+}\psi_\nu\right]$$

$$+ \quad \left[\psi_f^{+}\beta\gamma_5\psi_N\right]\left[C_P\psi_e^{+}\beta\gamma_5\psi_\nu + C_P'\,\psi_e\beta\psi_\nu\right]$$

$$+ \text{ Hermitian Conjugate.}$$

Although this form does not evidence the elegant symmetry of Eq.(1-3), it is more useful for the present discussion. The valuation of $|H|^2$ in Eq. (1-2) involves the calculation of the matrix element $H = \sum_k \int \mathcal{H}\, d\tau_k$; where $\mathcal{H}$ is integrated over the nuclear volume, the 4 field operators being replaced by the wave functions of the 4 particles, all taken at the same point and summed over all nucleons.

If the nucleus is sufficiently heavy, the nuclear recoil momentum is small compared to the momenta of neutrino and electron. If the rest mass of the neutrino is assumed to be zero then we have the following relation:

$$\epsilon_0 = \epsilon_\nu + \epsilon_e \qquad (1\text{-}4)$$

where ϵ_0 is the available total decay energy and $\epsilon_\nu + \epsilon_e$ are neutrino and electron energies.

The term $\rho(\epsilon)$ in Eq. (1-2) then becomes the density of states available to an electron and neutrino where $\epsilon \equiv \epsilon_e$. According to the usual calculation of phase space available to the two particles, electron and neutrino,

$$\rho(\epsilon) \approx \int d\omega_e d\eta\, \delta(\epsilon_0 - q - \epsilon)\, q^2 \eta^2 dq \int d\omega_\nu\, \Omega^2 \tag{1-5}$$

$\eta + q$ are the momenta of the electron and neutrino respectively (all units are: for energy: m_0c^2 and for momentum: m_0c where m_0 is one electron rest mass and c is the velocity of light; (m_0c^2 = 511 kev)) Ω is the volume over which the electron and neutrino wave functions are to be normalized and we have written

$$d\vec{\eta} = \eta^2 d\omega_e d\eta \quad + \quad d\vec{q} = q^2 d\omega_\nu dq \tag{1-6}$$

(The integrals over dw_e and dw_ν are to be performed if the angular correlation between $\vec{\eta}$ and $\vec{q}$ is not measured.)

After integrating over angles, and over the neutrino momentum, and retaining only those terms which are dependent upon the electron energy in the β-spectrum, we have:

$$\rho(\epsilon) = k\eta\, \epsilon(\epsilon_0 - \epsilon)^2 d\epsilon\, \Omega^2 \tag{1-7}$$

and

$$P(\epsilon)\, d\epsilon = k\eta\, \epsilon\, (\epsilon_0 - \epsilon)^2 |H|^2 d\epsilon\, \Omega^2 \tag{1-8}$$

For the discussion of the evaluation of $|\mathcal{H}|^2$ we shall assume that the coulomb field of the nucleus, into which the electron is emitted, is turned off. The effects of the coulomb field will be discussed below. We desire to find the dependence of

$|H|^2$ upon the electron energy in order to obtain the spectrum shape.

In the Eq. (1-3a) some of the terms are titled "non-relativistic" and some, "relativistic." This nomenclature refers to the nucleon velocities in the nucleus. The operators appearing in the terms labled "relativistic" connect the large compcnents with the small components of the spinors describing the nucleons. The operators appearing in the terms labled "non relativistic" do not mix the large and small parts of the nucleon spinors. Since v/c for the nucleons is ~ 1/10 the relativistic terms are small. The selection rules for nuclear spin change in the decay for the relativistic terms are different from those for the non-relativistic terms, which further reduces their value for allowed decay. We shall therefore consider these terms to be negligible, except for the Pseudoscaler coupling.

In evaluating the matrix element $|H|$ we shall now take the spatial dependence of the spinor wave functions of the electron and neutrino to be plane waves of the form $e^{i\vec{k}\cdot\vec{r}}$. The possibility of using spherical waves will be discussed below. Since the wave length of the electron emitted in the decay is generally large compared to the nuclear radius, a series expansion of the spatial part of the lepton wave functions

$$\left[\psi_\nu \psi_e\right]_{\text{spatial}} = e^{i(\vec{\eta}+\vec{q})\cdot\vec{r}} = \sum_{n=0}^{\infty}\left[-\frac{i(\vec{\eta}+\vec{q})\cdot\vec{r}}{n!}\right]^n$$

is useful.

It can be shown that the terms of the summation (1-9)decrease by two to three orders of magnitude for each successive term (r < Radius of Nucleus). It can also be shown that the n^{th} term in the summation corresponds to decay in which n units of orbital angular momentum are carried off by the neutrino-electron system. If we consider only those terms which arise in $|H|^2$ from the first term of Eq. 9,we perform the "allowed" approximation and will obtain the so called allowed spectrum shape. We shall now consider only the allowed decay. In this case, as can be seen from (1-9), the spatial parts of the electron and neutrino wave functions are constant over the nuclear volume and may be removed from the integral over the nuclear volume.

The Matrix element can now be re-written:

$$|H|^2 = \sum_{m_f} \sum_{ev} \left| S_j \sum_k (\psi_e^+ O_j [C_j + C_j' \gamma_5] \psi_\nu)(\int \psi_p^+ O_j \psi_N \, d\tau_k) \right|^2 \qquad (1\text{-}10)$$

where Σ_{mf} is the sum over the different orientations of the final nucleus. Averaging over the initial spin states is implied in Eq. 10) S_j indicates the sum of terms arising from the five interactions indicated in 3a,where the respective operators are symbolized by O_j ,and $\sum_k$ indicates summation over the k nucleons of the nucleus. $\sum_{ev}$ indicates summation over the possible spin states of electron and neutrino.

We wish to study the term $\int \psi_p^+ O_j \psi_N \, d\tau$ which appears in (1-10). In the non-relativistic approximation for the nuclear wave functions, those operators which differ only by a factor β are simply related. (The β-matrix does not mix terms of different spin). The following relations exist between the matrix elements:

$$M_F' \equiv \int \psi_p^* \beta \psi_N \, d\tau = -\int \psi_p^* \psi_N \, d\tau \qquad \Delta J = 0 \quad \text{no parity change} \qquad (1\text{-}11)$$

$$\vec{M}_{GT} \equiv \int \psi_p \beta \vec{\sigma} \psi_N \, d\tau = -\int \psi_p \vec{\sigma} \psi_N \, d\tau \qquad \Delta J = 0,1 \text{ (no } 0 \to 0\text{)} \quad \text{no parity change} \qquad (1\text{-}12)$$

$$\int \psi_p \beta \gamma_5 \psi_N \, d\tau = 0 \qquad (1\text{-}13)$$

It is the equality of the scalar and vector nuclear matrix elements and of the tensor and axial vector matrix elements which gives rise to the terms M_F and M_{GT} corresponding to the Fermi and the Gamow-Teller selection rules of allowed β-decay. The selection rules indicated at the right of Eqs. (1-11) and (1-12) refer to the nuclear spin change in the β-decay. Unless these selection rules hold, the indicated nuclear matrix element is zero, and the decay cannot proceed via this type of interaction in the allowed approximation.

After performing the indicated sums of equation (1-10)

and substituting the notation of (1-11) (1-12) for the nuclear matrix elements one obtains:

$$P(\epsilon) = k\eta(\epsilon_0-\epsilon)^2\int d\omega_e\, d\omega_\nu \left[\sum_F'\left(1+a_F\frac{\vec{\eta}\cdot\vec{q}}{q\epsilon}+\frac{b_F}{\epsilon}\right)|M_F|^2+\sum_{GT}\left(1+\frac{a_{GT}}{3}\frac{\vec{\eta}\cdot\vec{q}}{q\epsilon}+\frac{b_{GT}}{\epsilon}\right)|M_{GT}|^2\right] \quad (1\text{-}14)$$

where

$$\sum_F = |C_S|^2+|C_V|^2+|C_S'|^2+|C_V'|^2 \qquad \sum_{GT} = |C_T|^2+|C_A|^2+|C_T'|^2+|C_A'|^2 \quad (1\text{-}14a)$$

$$a_F\sum_F = -|C_S|^2+|C_V|^2-|C_S'|^2+|C_V'|^2 \qquad a_{GT}\sum_{GT} = |C_T|^2-|C_A|^2+|C_T'|^2-|C_A'|^2 \quad (1\text{-}14b)$$

$$b_F\sum_F = C_S^*C_V+C_SC_V^*+C_S'^*C_V'+C_S'C_V'^* \qquad b_{GT}\sum_{GT} = C_T^*C_A+C_A^*C_T+C_T'^*C_A'+C_A'^*C_T' \quad (1\text{-}14c)$$

$$M_F = \sum_{m_f} M_F' \qquad \vec{M}_{GT} = \sum_{m_f}\vec{M}_{GT}' \quad (1\text{-}15)$$

We wish now to identify the terms of Eq. (1-14).

Terms of the form $a_i\frac{\vec{\eta}\cdot\vec{q}}{q\epsilon}$ are a result of the decay due to any of the four individual interactions, the constant a being the electron-neutrino angular correlation coefficient for different interactions. When integration is performed over the angles between electron and neutrino, the terms with co-efficients a will contribute nothing to the electron spectrum.

Terms of the form $\frac{b}{\epsilon}$ are the Fierz interference terms. It is most important to note that interference occurs only between S and V and between Tand A interactions, but not between S and A, or S and T, or V and A, or V and T. There is no interference

between the Fermi and Gamow-Teller components of the interaction.

Upon integration over $dw_e dw_z$ Eq. (1-14) reduces to

$$P(\epsilon) = k'\eta\epsilon(\epsilon_o-\epsilon)^2\left[\sum_F |M_F|^2 + \sum_{GT} |M_{GT}|^2 + \frac{1}{\epsilon}\left(\sum_F b_F |M_F|^2 + \sum_{GT} b_{GT} |M_{GT}|^2\right)\right] \quad (1\text{-}16)$$

For the decay of He^6 where $\Delta J = 1$ in the allowed approximation we have

$$P(\epsilon) = k'\eta\epsilon(\epsilon_o-\epsilon)^2 |M_{GT}|^2 \sum_{GT}\left[1 + \frac{b_{GT}}{\epsilon}\right] \quad (1\text{-}17)$$

Coulomb Effects

In the previous section we have considered that the electron emitted in beta-decay may be described by a plane wave. This approximation neglects the effect of the Coulomb field of the nucleus.

The shape factors presented in the previous section have been calculated by Tholhoek and De Groot[6] using spherical waves for the neutrino and coulomb wave functions for the electrons. They used the old Hamiltonian in which all $C_i' = 0$. The method of calculation and the "allowed approximation" are similar to those used in the absence of Coulomb effects. The shape factors for the resulting spectrum are quite similar.

Including the Coulomb effect, the energy distribution for allowed spectra is given by [5]

$$P(\epsilon) = k' \eta \epsilon (\epsilon_0 - \epsilon)^2 F(Z,\epsilon) \left[\Sigma_F |M_F|^2 + \Sigma_{GT} |M_{GT}|^2 + \frac{\gamma}{\epsilon} \left(\Sigma_F b_F |M_F|^2 + \Sigma_{GT} b_{GT} |M_{GT}|^2 \right) \right] \quad (1\text{-}18)$$

This equation differs from the Eq. (1-21) by the factor $F(Z,\epsilon)$ multiplying the total distribution, and the factor of

$\gamma = \sqrt{1 - \alpha^2 Z^2}$ in the interference term.

$\alpha = \frac{e^2}{\hbar c} = \frac{1}{137}$ Z = charge of daughter nucleus

$F(Z, \epsilon)$ is called the Fermi function and is essentially equal to the ratio of the square of the electron wave function calculated in a coulomb field and evaluated at the nuclear radius to the square of the free electron wave function evaluated at the same point. The function $F(Z, \epsilon)$ has been calculated for all Z and in convenient intervals of energy by Feister[7] and by Rose.[8]

Both Rose[9] and Reitz[10] have calculated the effect of atomic screening of the Coulomb potential of the nucleus on the function $F(Z, \epsilon)$. For the case of $\epsilon_\beta > 0.200$ MEV and Z small, as in the region of analysis of the He^6 spectrum, the screening correction is extremely small compared to the experimental accuracy.

The Coupling Constants

Previous experiments and analyses to determine the relative magnitude of the coupling constants of β-decay can be grouped in five classes.

a) study of spectral shapes of allowed and forbidden spectra

b) study of β-ν angular correlation experiments

c) study of f-τ values and decay rates

d) study of K capture to positron branching ratios

e) β-decay from oriented nuclei

A discussion of the first three methods, and the results of experiments have been presented by C. S. Wu.[11] For a discussion of the fourth method the reader is referred to the experimental paper of Sherr and Miller.[12] The fifth method is discussed extensively in the recent papers of Lee and Yang[5], as well as in the paper of C. S. Wu etal.[4]

The interpretations of the experimental evidence depends intimately upon the form chosen for the β-decay Hamiltonian which, in turn, depends upon the invariance requirements set. Until the recent theoretical speculations of Lee and Yang and the experimental verification of the lack of conservation of parity by Wu etal[4] and by Lederman etal,[13] the Hamiltonian was assumed to be invariant under Parity Transformation, charge conjugation, and time reversal, aside from the assumed strict invariance under proper Lorentz transformations.

Experiments mentioned above have shown that the Hamiltonian is not invariant under parity transformation or charge conjugation. No evidence regarding invariance under time reversal is yet known--although several experiments have been proposed to test for its validity.

Lee and Yang have recently proposed a "two component theory" for the neutrino. According to this theory, the neutrino field takes the form of a two component spinor satisfying the equation:

$$\vec{\sigma} \cdot \vec{\nabla} \psi_\nu = i \frac{\partial \psi_\nu}{\partial t} \tag{1-19}$$

The theory presumes a zero mass for the neutrino. The neutrino Hamiltonian is not invariant under space inversion (parity) or charge conjugation. The authors have shown that "all calculations using conventional theory of the neutrino with the Hamiltonian of Eq.(1-3) (or 1-3a) concerning β-decay give the same results as the two component theory" if the choice of coupling constants is:

$$C_i = \pm C_i' \tag{1-20}$$

The sign chosen in equation (1-20) is to be the same for all five sets of interactions, and the choice depends upon whether a neutrino (right handed screw) or an anti-neutrino is emitted in the β-decay of the neutron.

Table I gives the conditions imposed upon the coupling constants of the Hamiltonian of Eq. 3 (and 3a) according to the invariance assumptions and the neutrino picture assumed.

TABLE I

	Invariance assumed and specific description of the neutrino if any. (all include proper Lorentz invariance)	Requirements upon the coupling constants of Hamiltonian of Eq.3 and (3a)
1	Invariance under T, C, P (the "old" assumption now known to be incorrect.)	All C_i real All $C_i' = 0$ (or all $C_i = 0$ For purposes of discussion we shall assume all $C_i' = 0$
2	Invariance not required for P, C, or T.	No requirements on any C_i or C_i'
3	Invariance under T (and CP)	All C_i and C_i' are real
4	Two component neutrino picture invariance not required on T	All $C_i = \pm C_i'$
5	Two component neutrino picture. Invariance required under T (and CP)	All $C_i = \pm C_i'$ All C_i real

II. SMALL CORRECTIONS TO THE ALLOWED β-SPECTRUM SHAPE

Equation (1-18) of Chapter I has presented the theoretical energy distribution for an "allowed" spectrum. Experimental investigations of shapes of allowed spectra have shown that within the limits of experimental accuracy, the predictions of Eq. (1-18) are correct. They have further shown that the interference terms b_F and b_{GT} are smaller than ~15 per cent.[11] This evidence provides certain relations between the coupling constants C_i and C_i' of Eq. (1-3).

We shall attempt to set a lower limit on the magnitude of the interference terms b_{GT} from an investigation of the β-spectrum of He^6. Since the theory of Chapter I leading to equation (1-18) is only an approximate one, we must consider possible theoretically predictable deviations of the β-spectrum of He^6 from the form of Eq. (1-18). Such considerations will be the subject of this chapter.

In particular the three phenomena: (1) Pseudoscalar interaction (2) Inner Bremsstrahlung correction and (3) Recoil correction will be discussed below.

The first is the possible contribution of pseudoscalar coupling to the allowed β-decay. It will be shown that consideration of this interaction, and comparison with experimental results, will enable us to set experimental limits on the relative magnitude of the pseudoscalar coupling constants in β-decay.

The second phenomenon is the effect upon the β-spectrum

shape of the emission of real electromagnetic radiation during the β-decay process. The existence of "inner Bremsstrahlung" emission from a β-active nucleus is well known. However, no quantitative evaluation of the influence of this process upon the β-spectrum shape has appeared in the literature. It will be shown in this chapter and in the final discussion of the analysis of the β-spectrum of He^6 that this effect is not detectable with present techniques except as a possible shift in the maximum energy of allowed β-decays.

The theory of Chapter I considers essentially the β-decay from an infinitely heavy nucleus. Because of the low atomic weight of He^6 and the rather large energy available for β-decay, this decay is one of the most likely to show deviations due to the finite recoil energy of the nucleus. This effect is the third phenomenon discussed below. It is shown that corrections to the spectrum shape due to recoil energy are extremely small compared to the presently obtainable experimental accuracy.

Within the currently accepted framework of the theory of β-decay, no other corrections to the usual allowed spectrum shape which might be greater than several tenths percent (over the energy range which we shall consider) are known.

The Pseudoscalar Interaction in the β-decay of low Z Nuclei (for $\Delta J = 1$ no)

In the discussion of Chapter I, the possible influence of the pseudoscalar coupling has not been considered for allowed β-decay. The pseudoscalar matrix element $\left|\int \beta \gamma_5\right|^2$ is necessarily small because γ_5 connects only large and small components of the nuclear spinor wave functions. However, since little is known of the magnitudes of the pseudoscalar coupling constants, the possibility of very large C_p and C_p' must be considered.

In 1953 both Fujita and Yamada[14] and Alaga, Kofoed-Hansen, and Winther[15] calculated, independently, an estimate for the effect of pseudoscalar coupling on the shape of the allowed β-spectra of He^6 and B^{12}. From the data available to them at that time they were able to set rather large upper limits on C_p/C_T.

In order to obtain the shape of the spectrum including the pseudoscalar coupling, one must evaluate the nuclear matrix elements in terms of the electron energy and of the $\left|\int \vec{\sigma}\right|^2$ matrix element which appears in the Gamow-Teller interaction.

Upon examination of the pseudoscalar matrix elements the following properties become clear.

1. If the plane wave approximation for the lepton wave function is made, and only the term constant over the nuclear volume is retained, the pseudoscalar nuclear matrix element becomes zero for a transition in which the parity of the nuclear wave function is unchanged. Therefore higher order (forbidden) terms must be in-

cluded in order to obtain non-zero value for the pseudoscalar matrix element.

2. The operator γ_5 connects only the large and small components of the nuclear wave function, and therefore some model must be chosen to determine the "relativistic" components of the nucleon wave functions.

Alaga et al have assumed that the H_{int} between the nucleons can be described as a simple scalar central potential. By performing a Foldy-Wouthhuysen transformation to find the "relativistic components" of the spinor wave functions and carrying the approximation to order $\frac{1}{M^3}$ in the nuclear mass, they have found the correction factor for the β-spectrum.

The result for the electron distribution is:

$$P(\epsilon)d\epsilon = K(\epsilon_0-\epsilon)^2\eta\epsilon\, d\epsilon\, G_T^2 |\int \beta\vec{\sigma}|^2 \times$$

$$\left\{1+\left[\frac{\eta^2+(\epsilon_0-\epsilon)^2}{3}-\frac{2}{9}\frac{\eta^2(\epsilon_0-\epsilon)}{\epsilon}\right]\left(\frac{C_p}{C_T 2M}\right)^2-\frac{2}{3}\left(\frac{\eta^2}{\epsilon}-(\epsilon_0-\epsilon)\right)\frac{C_p}{C_T 2M}\right\}$$

(2-1)

This result is essentially the same as that of Fujita and Yamada, who use a similar approximation to show that

$$\int \beta\gamma_5 r = \frac{i}{2M}\int \vec{\sigma} \quad .$$

Since the Hamiltonian used by these authors conformed to all the invariance requirements of the old theory, they did not take account of the parity non-conserving terms of Eqs. 3a (They assumed all $C'=0$) They also assumed that the coupling constants were real and that in light of the experimental evidence available to them, $C_A \cong 0$. (Thus they have not calculated interference terms between Pseudoscalar and Axial Vector)

Recently, Morita (private communication) has recalculated the spectral distribution including the pseudoscalar coupling with the complete Hamiltonian of Eq. 3a. The approximation for the $\int \beta\gamma_5 r$ is the same as above. The spectral distribution is then

$$P(\epsilon)d\epsilon = K(\epsilon_0-\epsilon)^2 \eta\, \epsilon\, F(Z,\epsilon)\, d\epsilon \;\times$$

$$\left\{ \xi_{GT} + \left(\frac{\eta^2+q^2}{3} - \frac{2}{9}\frac{\eta^2 q^2}{\epsilon}\right)\frac{\xi_P}{(2M)^2} + \frac{\xi_{GT}\, b_{GT}}{\epsilon} \right. \qquad (2-2)$$

$$- \left(C_T^* C_P + C_T C_P^* + C_T' C_P'^* + C_T'^* C_P'\right)\frac{1}{2M}\frac{1}{3}\left(\frac{\eta^2}{\epsilon} - (\epsilon_0-\epsilon)\right)$$

$$\left. + \left(C_A^* C_P + C_P^* C_A + C_A'^* C_P' + C_P'^* C_A'\right)\frac{1}{2M}\frac{1}{3}\frac{\epsilon_0-\epsilon}{\epsilon} \right\} \left| \int \beta\vec{\sigma} \right|^2$$

where

$$\xi_P \equiv |C_P|^2 + |C_P'|^2$$

The terms of the bracket of [2-2] are identified as follows: The first and third are the usual terms of Gamow-Teller decay, the second is due to decay directly by the pseudoscalar interaction, and the fourth and fifth terms are the interference between pseudoscalar, and tensor and axial vector interaction respectively. We shall neglect the second term of (2-2) because of the very small co-efficient $(\frac{1}{2M})^2 \sim 10^{-7}$.

As mentioned in Alaga's paper, Ruderman[16] has shown that in the case of pseudoscaler meson theory with pseudoscalar coupling, the pseudoscalar nuclear matrix element of β-decay may be much larger than that obtained in the above approximation.

Since one of the purposes of this experiment will be to set an upper limit on the energy dependent co-efficients of Eg.(25a), the possibility of a larger pseudoscalar matrix element than calculated by A, K, and W, and by F and Y, and used in our correction factor will not invalidate our results.

Effect of Inner Bremsstrahlung on β-spectral shape

The effect of emission of inner Bremsstrahlung in the β-decay process has long been known. All of the experiments on inner Bremsstrahlung have been measurements of the intensity and spectral distribution of the Bremsstrahlung. However, the effect upon the shape of the β-spectrum due to the possibility of real radiation by the nucleus in the creation process of the β-particle has not been previously considered. The effect is quite small. However, it was felt that a quantitative estimate of the distortion of

the spectrum due to this effect should be calculated.

The inner Bremsstrahlung process has been considered by Knipp and Uhlenbeck as two step process:

$$\underset{(A)}{n} \longrightarrow \underset{(B)}{p + \tilde{\nu} + e} \longrightarrow \underset{(C)}{p + \tilde{\nu} + e + \gamma} \qquad (2\text{-}3)$$

The β-decay theory presented above considers only the intermediate state, and the spectrum there derived should be corrected for possible radiation. The gross effect is to depress the energy of the whole β-spectrum, the additional energy being carried off by the Bremsstrahlung.

Knipp and Uhlenbeck[17] calculated the probability

$$\Phi = \frac{\alpha \eta}{\pi \eta_0 k} \left\{ \frac{\epsilon_e^2 + \epsilon^2}{\epsilon_e \eta} \log(\epsilon + \eta) - 2 \right\} \qquad (2\text{-}4)$$

for emission of a γ-ray of energy k by an electron of energy ϵ_e and momentum η_e, which, after γ-emission, has energy ϵ and momentum η. (Note that this refers only to Inner Bremsstrahlung.)

In order to find the inner Bremsstrahlung spectrum one performs an integration over ϵ_e i.e.

$$S(k) = \int_{1+k}^{\epsilon_0} d\epsilon_e \, P(\epsilon_e) \Phi(\epsilon_e, k) \qquad (2\text{-}5)$$

where $S(k)$ is the γ spectrum, and $P(\epsilon_e)$ is the probability distribution of the β-spectrum.

It is found experimentally[18] that both as to shape and total magnitude $S(k)$ calculated from the above formula is in

reasonably good agreement with the measured Bremsstrahlung distribution, thus suggesting the validity of the approximations used by Knipp and Uhlenbeck to derive Φ .

We have calculated the effect of the β-spectrum, shape by using this same probability function Φ .

We note that $\epsilon_e - \epsilon = k$.

If we consider an interval $d\epsilon$ of the β-spectrum, then

$$P(\epsilon)d\epsilon = \left[P'(\epsilon) + \int_{\epsilon}^{\epsilon_o} \Phi(\epsilon_e, \eta_k) P'(\epsilon_e)\, d\epsilon_e - \int_{o}^{\epsilon-1} \Phi(\epsilon, \eta, k)\, P'(\epsilon_e)\, dk\right] d\epsilon \quad (2\text{-}6)$$

where $P'(\epsilon)$ is the probability distribution of electron energies at step (B) of Eq. (2-3), and $P(\epsilon)$ is the probability distribution of electrons at step (C). ϵ_o is the maximum energy available for decay.

The second and third terms of (2-6) are identified as follows: The first is the probability of an electron at step B of (2-3) of energy higher than ϵ losing sufficient energy by radiation to end up in step c at an energy between ϵ and $\epsilon + d\epsilon$. The second term is the probability of an electron initially in energy range $\epsilon \to \epsilon + d\epsilon$ losing energy by radiation to remove it from the range $\epsilon \to \epsilon + d\epsilon$.

Since we are interested only in the change of spectral shape due to this phenomenon, we have calculated:

$$I(\epsilon) \equiv \frac{P(\epsilon)\, d\epsilon}{P'(\epsilon) d\epsilon} = 1 + \frac{\int_{\epsilon}^{\epsilon_o} \Phi(\epsilon, \eta)\, P'(\epsilon_e)\, d\epsilon_e}{P'(\epsilon_e)} - \int_{o}^{\epsilon-1} \Phi(\epsilon, \eta, k)\, dk \quad . \quad (2\text{-}7)$$

which is the correction factor for the β-spectrum.

Since the order of the correction is very small, it was considered sufficiently accurate to neglect the Fermi function in $P'(\epsilon)d\epsilon$, so that

$$P'(\epsilon_e)d\epsilon_e = (\epsilon_0 - \epsilon_e)^2 \eta_e^2 \epsilon_e d\epsilon_e$$

was used in the second term of Eq. (2-7)

It should be noted that both of the integrals in (2-7) exhibit an infra-red divergence. However, if a cut-off is chosen for the integrals, then the difference between them is cut-off independent in the limit of small cut-off.

The result of this rather tedious integration is:

$$\begin{aligned} I(\epsilon) = 1 + \frac{5}{12}\frac{\alpha}{\pi}\Bigg(& \frac{\ln(\epsilon+\eta)}{12\eta}\left[\frac{\epsilon_0^2-3}{\epsilon} + 6\epsilon_0 + \epsilon(24\ln(\epsilon_0-\epsilon)-49)\right] \\ & - \frac{2}{3}\frac{\epsilon_0}{\epsilon} + 2\ln\frac{2\epsilon+1}{\epsilon_0-\epsilon} + 2\ln(\epsilon-1)\left[1 - \frac{\epsilon}{\eta}\ln(\epsilon+\eta)\right. \\ & \left. - \frac{\sqrt{2}\,\epsilon}{\sqrt{\epsilon+1}}\int_0^1 \frac{\ln(1-y)\,dy}{\sqrt{y}\sqrt{1+\frac{\epsilon-1}{2}y}}\right) \end{aligned} \qquad (2\text{-}8)$$

For the evaluation of $I(\epsilon)$, simplification of the above formula is not feasible because of the cancellation of large terms. For evaluation of the last integral we have made the following approximation:

$$\int_0^1 \frac{\ln(1-y)\,dy}{\sqrt{y}\sqrt{1+\frac{\epsilon-1}{2}y}} \approx \int_0^{\alpha} \frac{\ln(1-y)\,dy}{\sqrt{y}\sqrt{1+\frac{\epsilon-1}{2}y}} + \frac{1}{\sqrt{1+\frac{\alpha}{2}}\sqrt{1+\frac{\epsilon-1}{2}\left(\frac{1+\alpha}{2}\right)}} \int_{\alpha}^{1} \ln(1-y)\,dy \quad (2\text{-}9)$$

The first integral on the right side of (2-9) is evaluated numerically, and the second integral can be performed exactly. To within three significant figures, (2-9) is independent of α for the range $.8 < \alpha < .95$.

We have calculated $I(\epsilon)$ for several values of ϵ_0 over the spectrum range for each ϵ_0. The results are shown in Fig. 1.

The correction factor is constant to within the limits of accuracy of any of the β-spectra measurements which have been reported. If however, one considers the measurement of the β-decay energy by straight line extrapolation of the Kurie Plot of an allowed β- spectrum, then the inclusion of the correction factor $I(\epsilon)$ may displace the end point by ~0.1 percent. This is not far from the accuracy which has been quoted in some recent end-point measurements. If the techniques of end point measurements are improved, the correction will have to be included in order to obtain correct decay energies.

Effect of Nuclear Recoil on β-Spectrum Shape

In the evaluation of the phase space density available to the electron and neutrino and recoil in Chapter I, it has been assumed that the energy of the recoiling nuclues is zero. In the decay of He^6 this energy has a maximum value of ~ 4 K.E.V..

Kofoed-Hansen [19] has calculated the correction factor for the β-spectrum if the above assumption is relaxed. It is

$$R(\epsilon) = 1 + \frac{3\epsilon}{M} - \frac{\epsilon_0}{M} + a_i\left(\frac{m_\beta^2}{M\epsilon} - \frac{3\epsilon}{M}\right), \tag{2-10}$$

where a_i is the correlation coefficient of Eq. (1-14), and M is the nuclear mass. He has shown that $R(\epsilon)$ represents less than 0.2 per cent correction for the He^6 spectrum.

Expected Energy and Momentum Distribution for the β-Spectrum of He^6:

The theoretical distribution of electron energies for the He^6 β-Spectrum including all the effects discussed in this chapter, is given by

$$P(\epsilon)d\epsilon = [P'(\epsilon)d\epsilon]\, I(\epsilon)\, R(\epsilon), \tag{2-11}$$

where $P'(\epsilon)$ is the distribution of Eq. (2-2) including the effect of the pseudoscalar interaction, $I(\epsilon)$ is the inner Bremsstrahlung correction factor of Eq. (2-8) and $R(\epsilon)$ is the recoil correction factor of Eq. (2-10).

Rewriting Eq. (2-11) in complete form, we have:

$$P(\epsilon)d\epsilon = \left[K\left|\beta\vec{\nabla}\right|^2(\epsilon_0-\epsilon)^2\eta\epsilon\, F(z,\epsilon)\, I(\epsilon)\, R(\epsilon)\right] \times$$

$$\left[\Sigma_{GT} + \frac{\epsilon_0}{3M}\,\mathrm{Re}\left(C_A C_p^* + C_A' C_p'^*\right) + \frac{1}{\epsilon}\left(\Sigma_{GT}\, b_{GT} + \frac{\epsilon_0}{3M}\,\mathrm{Re}\left(C_A C_p^* + C_A' C_p'^*\right)\right)\right. \tag{2-12}$$

$$\left. -\left(2\epsilon-\epsilon_0-\frac{1}{\epsilon}\right)\frac{1}{3M}\,\mathrm{Re}\left(C_p C_T^* + C_p' C_T'^*\right) + \frac{\Sigma_p}{(2M)^2}\left(\frac{\eta^2-(\epsilon_0-\epsilon)^2}{3} - \frac{2}{9}\,\eta^2\,\frac{(\epsilon_0-\epsilon)}{\epsilon}\right)\right] d\epsilon .$$

If we now make the following approximations:

1. $\dfrac{\Sigma_p}{(2M)^2} \ll\ll \Sigma_{GT}$

2. $\dfrac{\epsilon_0}{3M}\,\mathrm{Re}\left(C_A C_p^* + C_A' C_p'^*\right) \ll \Sigma_{GT}$

$M = 1837$

$\epsilon_0 \sim 8$

$\eta = \sqrt{1-\alpha^2 z^2} \approx 1$

(2-13)

Eq. (2-12) can be reduced to:

$$P(\epsilon)d\epsilon = \left\{\left[K\left|\beta\vec{\nabla}\right|^2\Sigma_{GT}\right](\epsilon_0-\epsilon)^2\eta\epsilon\, F(z,\epsilon)\, I(\epsilon) R(\epsilon)\right\} d\epsilon \times$$

$$\left[1 + \frac{1}{\epsilon}\left\{b_{GT} + \frac{\epsilon_0}{3M}\,\frac{\mathrm{Re}\left(C_A C_p^* + C_A' C_p'^*\right)}{\Sigma_{GT}}\right\} - \left(2\epsilon-\epsilon_0-\frac{1}{\epsilon}\right)\left\{\frac{1}{3M}\,\frac{\mathrm{Re}\left(C_p C_T^* + C_T'^* C_p'\right)}{\Sigma_{GT}}\right\}\right] \tag{2-14}$$

The momentum distribution is given by:

$$P(\eta)d\eta = K(\epsilon_0-\epsilon)^2\eta^2 F(Z,\epsilon) I(\epsilon) R(\epsilon)\, d\eta \quad \times$$

$$\left[1 + \frac{1}{\epsilon}\left(b_{GT} + \frac{\epsilon_0}{3M}\frac{Re(C_A C_P^* + C_A' C_P'^*)}{\Sigma_{GT}} - \left(2\epsilon - \epsilon_0 - \frac{1}{\epsilon}\right)\left(\frac{1}{3M}\frac{Re(C_P C_T^* + C_P' C_T'^*)}{\Sigma_{GT}}\right)\right)\right] \quad (2\text{-}15)$$

We shall compare the experimental spectrum with the above equation in an attempt to set upper limits upon the two co-efficients

$$b_{GT} + \frac{\epsilon_0}{3M}\frac{Re(C_A C_P^* + C_A' C_P'^*)}{\Sigma_{GT}} \quad \text{and} \quad \frac{1}{3M}\frac{Re(C_P C_T^* + C_P' C_T'^*)}{\Sigma_{GT}}$$

For the sake of comparison of the above form with the older theory of β-decay we re-write the bracket of Eq. (2-15) on the assumption that all $C_i' = 0$, and all C_i are real:

$$[\;] = 1 + \frac{1}{\epsilon}\left\{\frac{2C_A C_T}{C_A^2 + C_T^2} + \frac{2\epsilon_0 C_A C_P}{C_A^2 + C_T^2}\right\} - \left(2\epsilon - \epsilon_0 - \frac{1}{\epsilon}\right)\left\{\frac{2}{3M}\frac{C_P C_T}{C_A^2 + C_T^2}\right\}$$

(2-16)

III. THE DECAY OF He^6: THE DECAY SCHEME, MAXIMUM ENERGY, MATRIX ELEMENTS AND SUITABILITY OF He^6 β-DECAY FOR DETECTION OF SMALL EFFECTS IN β-DECAY

Several authors have mentioned the advantages of a high energy β-spectrum for detection of the small effects of Fierz interference and other deviations from "allowed shape." Winther and Kofoed-Hanson[20] indicated the advantage of high energy spectra for detection of Fierz interference by the curves reproduced in Fig. 2. Fig. 2a shows a theoretical straight line "Kurie Plot" with end point ϵ_0, and a theoretical "Kurie Plot" with Fierz interference correction factor $1 + \frac{b}{\epsilon}$ normalized at the points $\epsilon_1 = \epsilon_0 - .2 \quad mc^2$ and $\epsilon_2 = .2 \quad mc^2$. Δm is the maximum deviation of the two curves. Fig. 2b shows a plot of $\frac{\Delta m}{K}$ for various values of b as a function of ϵ_0. It is clear that an end point of $\epsilon_0 > 10\ mc^2$ is most suitable for detection of this effect.

It is also necessary that the β-decay used for detection of small effects contain only one β-group of any significant intensity.

It is preferable to investigate a spectrum which proceeds by only one of either the Fermi or Gamow-Teller type transitions. Otherwise, the distortions in the spectrum produced by interference phenomena within the two types of interactions cannot, in general, be separated.

On the basis of the above mentioned criteria, the β-decay of He^6 is most suitable for the study of small deviations from allowed shape.

The decay scheme of He^6 is shown in figure 3. The β-decay of He^6 has the highest energy of any known β-decay in which interfering groups are not present. The decay scheme shows the two lowest excited states of Li^6. The 3.57 Mev analogue state of the He^6 ground state cannot be fed by β-decay from He^6, because of energy conservation. The 2.189 Mev state of Li^6 has spin and parity 3^+. Beta decay from He^6 to this level must be of the unique second forbidden type, and should have log $f\tau$ ~ 12. On this basis the β-decay branching ratio would be ~10^{-11} to this state. The extensive investigation of levels of Li^6 by heavy particle excitation[21] excludes the possibility of other excited states of Li^6 below 3.5 Mev. Also, several searches[22] for γ rays from the decay of He^6 have given negative results.

Several measurements[23] of the half-life of He^6 give an average value of $\tau_{1/2}$ = .82 sec.

The energy difference between the ground states of He^6 and Li^6 can be obtained by combining the following separate Q value measurements.

Reaction	Q (Mev)	Reference
$Li^7 + H^3 \longrightarrow He^6 + He^4$	9.79 ± .03	25
$H^3 \longrightarrow He^3 + \beta$	0.0186 ± .0002	26, 27
$Li^6 + H^1 \longrightarrow He^4 + He^3$	4.023 ± .002	28, 29
$H^1 + Li^7 \longrightarrow He^4 + He^4$	17.343 ± .007	28, 27

They yield an energy difference of 3.55 ± .03 Mev for Li^6 - He^6 mass difference--the error being almost completely due to the $Li^7(t,d)He^6$ Q value uncertainty.

Measurements of the He^6 β-decay end-point have been performed by Perez-Mendez and Brown[30], who obtained 3.215 Mev, and more recently by Wu, et al[31], who obtained 3.50 ± .05 Mev. It will be shown that the results of this experiment indicate that:

$$W_o = 3.50 \pm .03 \text{ Mev.}$$

The ft value for the He^6 decay is 808±32 sec. This is the lowest known ft for any β-decay. Recent estimates of the matrix element $\left|\int \beta \vec{\sigma}\right|^2$ --the only one involved significantly in the decay of He^6 -- have been made by A.I. Baz[32]

Baz presents estimates for $\left|\int \vec{\sigma}\right|^2$ on the basis of pure l-s and pure j-j coupling, as well as intermediate coupling models for the nucleus. The extent of intermediate coupling is determined by fitting the measured magnetic moment of Li^6 to that predicted by different mixture couplings.

The results are best summarized as follows:

Coupling	$\lvert\int\vec{\sigma}\rvert^2$
pure L-S	6
pure j-j	3.34
intermediate	5.25

The author points out that the intermediate coupling chosen also leads to calculation of the quadrupole moment of Li^6 which is in good agreement with experiment.

The value of $\lvert\int\vec{\sigma}\rvert^2$ can be calculated from the values of B and x discussed by Kofoed-Hansen and Winther.[33] Taking B=2787±70 and x=.560±.012, one obtains $\lvert\int\vec{\sigma}\rvert^2$ =6.17±.20. However, if only the recently determined ft values of H^3-He^3 (ft=1060 sec) and O^{14}-N^{14} (ft = 3090) beta decays are used, one obtains B = 2520 and x = .59, and therefrom, $\lvert\int\vec{\sigma}\rvert^2$ = 5.28 for He^6, in excellent agreement with the intermediate coupling estimate of Baz.

The relatively large matrix element of He^6 beta decay suggests again that this decay is suitable for detection of small effects in beta decay. Since the "allowed" matrix element is large, it is suggested that higher order effects upon the spectrum shape, which are neglected in the discussion of Chapter I, are likely to be smaller than usual.

The low Z of the product nucleus Li^6 also insures that errors in estimation of the effects of the coulomb field, and of the effect of finite nuclear size, will be less serious in their effect upon the spectral shape.

IV. PRODUCTION AND PURITY OF He^6

Production of He^6

He^6 was produced by the nuclear reaction $Be^9(n,\alpha)He^6$. The threshold neutron energy for this reaction is 0.64 Mev.

A very fine $Be(OH)_2$ powder[34] was placed loosely on six thin aluminum trays inside a 4" x 5" x 6" copper vacuum box. Immediately outside this box was a 1/4" x 1" x 5" water cooled Be block which, upon bombardment with 20 Mev. deuterons, formed the neutron source by the reaction $Be^9(d,n)Li^{10}$. The whole target assembly was placed directly in front of the Brookhaven 60" cyclotron window in the external beam of the cyclotron. The Be block target was electrically insulated from the ground so that the deuteron current could be measured.

A schematic diagram of the pumping and purifying system for the gaseous activity is shown in Fig. 4. A vacuum tank containing several liters of 200 proof ethyl alcohol was at one end of the pumping system. The tank was slightly warmed to maintain a vapor pressure of ~12 cm. Hg above the alcohol. Alcohol vapor diffused over the bombarded $Be(OH)_2$ powder and carried the activity with it through 40 ft. of 5/16" copper tubing into the experimental area. The alcohol was then liquefied in a dry ice trap. (Approximately three pints were condensed in 12 hours' running time.) Above this trap the vapor pressure was 5μ. A liquid nitrogen trap condensed the remaining alcohol and reduced the pressure to ~5×10^{-4} mm Hg.

After the activity was purified by passage through an activated charcoal trap, it was compressed by a small 7 liter/sec. oil diffusion pump. Pump vapors were trapped in another liquid nitrogen trap. The activity, now at fore-pump pressure of ~ 5μ, passed over red hot calcium (in a stainless steel tube) for further purification, and then diffused into the spectrometer source volume. Another liquid nitrogen trap in the pumping line between the mechanical fore-pump and the spectrometer source volume removed the fore-pump vapors. A throttling valve on the fore-pump side of the source volume could increase the activity in the spectrometer by a factor of three. However, a compromise had to be reached between the throttling and the pumping efficiency of the small diffusion pump. If the pressure in the source volume rose above ~15μ, the diffusion pump efficiency dropped quite rapidly. It is estimated that the total transit time of the activity from the target to the source volume was approximately 3 sec., or about 4 half lives of He^6. With a cyclotron beam of 60 microamperes deuterons on the target, about 10^6 atoms/sec. were delivered to the spectrometer source volume. However, this quantity was quite sensitive to the pressure conditions throughout the system.

Purity of He^6

The He^6 production and purifying system was patterned almost identically after the one used by Rustad and Ruby[34] for the neutrino angular correlation experiments on He^6. The essential difference is that in those experiments the Brookhaven reactor was used as the neutron source rather than the cyclotron. Since the old He^6

generator was still installed in the reactor, many of the purity tests on the gas were performed with that system. The $Be(OH)_2$ powder used for both He^6 generators came from the same batch produced by the Brush Beryllium Company.

The He^6 produced at the reactor was tested for purity by a careful study of the gross decay curve of the activity and by a study of the decay rate of radiations emitted in limited energy ranges. The activity was passed through a 5 cm^3 lucite volume which was fitted with a .001" aluminum window. The volume could be isolated from the pumping system by two electrically operated solenoid valves. The activity was detected with a 1" thick plastifluor scintillation spectrometer. The decay of the activity was recorded with the use of a moving tape pen recorder. The decay was followed, accepting both the whole spectrum, and also small portions of the β-spectra at different energies, by using an Atomic Single Channel Analyzer.

The results of these studies showed that a 2 per cent Ne^{23} activity was present, and was not reduced with the use of charcoal traps. N^{16} activity was effectively removed by the charcoal traps. No other activities were found greater than ~0.2 per cent.

Similar but less extensive tests were performed with the cyclotron He^6 generator. Half-life measurements indicated that the percentage of Ne^{23} had risen to about 55 per cent due to the higher energy of the neutrons at the cyclotron. The contaminant activity was definitely identified as Ne^{23} by four indications:

1. The contaminant ratio was not affected by the hot

calcium trap -- Ne does not react chemically with Ca.

2. The half-life of 37 sec. was in agreement with the published value for Ne^{23} (see Fig. 5)

3. γ rays of 1.6 Mev. and 0.44 Mev. were detected in the source, in agreement with the decay scheme of Schmidt et al for Ne^{23}.

4. A scintillation spectrum of the contaminant β-spectrum was measured by trapping an amount of active gas in the source volume, letting the He^6 decay for 10 seconds and then measuring the β-spectrum of the remaining activity with a 20 channel analyzer for about 20 sec. This procedure results in a spectrum of contaminants with $T_{1/2}$ longer than ~ 5 sec. In this way the end point of the contaminant β-spectrum was found to be in agreement with Schmidt's results for Ne^{23}. No other contaminants were found.

A chemical assay of the $Be(OH)_2$ indicated the presence of the following impurities: (all percentages relative to Be)

Na	1-5 per cent	Al	<5 per cent
Ni	.01 per cent	Fe	.1 per cent
Cu	.01 per cent	Si	5 per cent
Ti	.01 per cent	Mg	1-5 per cent
Ca	.1 per cent	Mn	.01 per cent

Upon neutron bombardment the only gaseous activities which should be formed are He^6, Ne^{23}, N^{16}, and possibly trace quantities of O^{19}. All but the He^6 and Ne^{23} are removed by the charcoal and calcium traps.

Effect of Impurities on He^6 Spectrum

Although the only contaminant activity detected in He^6 is the Ne^{23}, we shall discuss the effect on the spectrum shape of any possibly undetected contaminant activities.

The effect of impurity activities on the shape of the He^6 spectrum should be considered in light of the objectives of the experiment. In Chapter 6 it is shown that a precision measurement of the spectrum can, with the present techniques, only give an upper limit on the relative number of electrons at the lower energy end of the spectrum.

In discussing the effect of contaminants on the resultant spectrum shape we shall consider them in two groups: Those transitions which have $\epsilon_{max} > \epsilon_{max\ He^6}$ and those with $\epsilon_{max} < \epsilon_{max\ He^6}$

1. Contaminant transitions with $\epsilon_{max} > \epsilon_{max\ He^6}$

Since these transitions have their spectrum peaks at a higher energy than the peak of the He^6 spectrum, the effect of the addition of such a spectrum to the He^6 spectrum, is to result in a spectrum distorted, so as to give an apparantly greater number of electrons in the upper energy region of the He^6 spectrum, and a smaller relative number in the lower energy region. This type of contaminant would tend to invalidate the upper limit on excess electrons in the low energy region which we wish to get.

However, the presence of β-spectra with $\epsilon_{max} > \epsilon_{max\ He^6}$ is easily detectable and quantitative estimates of their intensities can be made. This is done by continuing the spectrum measurements

above the ϵ max. for He^6. In this region only contaminant radiations are seen, and by extrapolation of these spectra to the lower energy region, correction can be made for them. An extensive analysis of the effect of the Ne^{23} contamination the He^6 experimental results are discussed in Appendix C.

2. Contaminant transitions with $\epsilon_{max} < \epsilon_{max\ He^6}$

When a spectrum of lower ϵ_{max} is added to the He^6 spectrum, the result is a sum spectrum whose relative intensities are lower in the upper energy region and higher in the low energy region than from a pure He^6 spectrum. Although such a contaminant would increase the lower limit which we wish to set, and thus make the experimental results less valuable, it does not affect their validity.

V. THE SPECTROMETER - CONSTRUCTION AND PERFORMANCE

In this chapter we will be concerned with the use of our spectrometer for the purposes of obtaining a precise β - spectrum shape. The initial step in any experiment must be to determine the capabilities of the instrument to be used, and to ascertain the limits of precision obtainable with the instrument. For spectroscopy, it is most important to determine the possible distortions introduced into the spectrum by the instrument.[+] Unfortunately, the literature of β decay contains a relatively large number of experimental results which have been shown to be incorrect, mainly due to insufficient study of the instruments involved.

The root of the problem lies in the fact that there are no continuous β spectra whose shapes are accurately known.[++]

There are no β spectra which can be used to test the instrument to the degree of precision which we require. Other experimenters have often used a criterion of obtaining a linear Kurie plot of several allowed β-decays with different end points to check the performance of their spectrometers. It is clear from the nature of the Fierz-interference correction factor which is independent of ϵ_0, that such a procedure must be used with great care to test a spectrometer.

[+] The instrument refers here to spectrometer, source, and detector.

[++] No spectrum measurements where $P(\eta)d\eta$ is measured or known to better than ~ 1 percent over the range 200 kev $< \epsilon <$ 3.5 mev are reported.

Until some more satisfactory method can be found, the precision of a β spectrometer must be ascertained from both experimental evidence and theoretical considerations of the spectrometer system. We shall discuss these considerations in detail.

The Spectrometer

A scale drawing of the spectrometer baffle system, the source volume and the Geiger counter are shown in Fig. 6. The coil and vacuum tube were kindly lent to us by Dr. D. E. Alburger of Brookhaven National Laboratory. The spectrometer is designed according to the description of Hornyak, Lauritsen and Rasmussen.[35]

A new baffle system was designed for the spectrometer. Special consideration was given to the reduction of scattering in the baffle system.

The electron trajectories in a non-uniform field cannot be simply calculated. It is common practice to determine the trajectories empirically - either by photographic methods, or by empirical adjustment of baffles to obtain maximum transmission for a given resolution. The second method was used for determining the baffle positions for our spectrometer. The position and size of the ring focus baffle B and the entrance slit A were guided by the old baffle system, which was designed and empirically tested for best position by Alburger.

Small adjustments were made in the axial position of all 4 parts of these baffles to obtain a symmetric line shape and the desired resolution ($\frac{\Delta\eta}{\eta}$ = 2.8 per cent), where $\Delta\eta$ is the full width

at 1/2 maximum of an internal conversion line.

All other baffles are designed to reduce scattering and their positions were fixed such that they do not intercept any of the beam transmitted by A and B. Particular success was obtained with the rings D, E, F and G. in reducing scattering from the spectrometer tube. The lucite covered brass baffle plates are all sufficiently thick to stop 5 mev β particles, and all lucite parts are painted with aqua-dag to prevent charging.

Resolution Effects

In order to obtain a precise measurement of the shape of a spectrum it is essential that the efficiency or transmission of the spectrometer be a known function of the focussed momentum. Consider the equation:

$$S(H) = \int_0^\infty P(\eta)\, R(H,\eta)\, d\eta \qquad (5\text{-}1)$$

where

$P(\eta)$ - the true momentum distribution of the source; η is the momentum

H - the magnetic field at some arbitrary fixed point in the spectrometer

$S(H)$ - the measured electron distribution of the source as a function of the magnetic field in the spectrometer.

$R(H,\eta)$ - the S(H) for a source whose momentum distribution is $P(\eta_1) = \delta(\eta_1)$

$R(H,\eta)$- is the function describing the efficiency of the spectrometer. In this discussion we consider $R(H,\eta)$ to describe only the focussing properties of the magnetic field and the collimation (baffle) system. (It does not include scattering and other distorting effects which are not due to the field.)

It is only through the solution of the integral equation (5-1) that the true momentum distribution of the source can be obtained from the measured spectrum. One must know $R(H,\eta)$ for all H and for the total range of η covered by the spectrum in order to obtain $P(\eta)$ from a measurement of S(H).

For all magnetic spectrometers in which the <u>field shape is independent of the field magnitude,</u> (and in which the source, and counter, and baffle geometry is maintained constant as the field is varied) the response function

$$R(H,\eta) = f\left(\frac{\eta}{H}\right) \quad \dagger \qquad (5\text{-}2)$$

Thus a measurement of the response function for one value of η (for all H) is sufficient to determine it for all values of η for all H. Since the field of the air core lens spectrometer is produced by a rigidly supported current winding it is clear that the field produced by this coil conforms to the requirements set forth above. The field shape is independent of the field magnitude. From Maxwell's field equations it can be shown that the field at any point in the spectrometer is directly proportional to the current in the coils. Thus H = kI where I is the spectrometer current and k is a constant. It should be emphasized that the relation $R(H,\eta) = f\left(\frac{\eta}{H}\right)$

---

† See Appendix B

is not dependent upon the baffle arrangement. The form of the function f (and thus the transmission) may be determined by the baffle arrangement. One usually attempts to maximize $R(H,\eta)$ (ie. the transmission) for a chosen value of resolution, but even if the optimum positions are not found, for a constant field shape Eq. (5-2) is still true.

(The considerations of constancy of field shape must be amended because of external magnetic fields in the region of the spectrometer which are due to the earth's magnetic field and to the stray magnetic field of the cyclotron. These constant fields would add to the field due to the current and thus change the shape as a function of current. In order to minimize this effect two sets of Thompson coils are placed on two sides of the spectrometer. The current is adjusted to cancel all stray fields in the region of the center of the spectrometer with components perpendicular to the spectrometer symmetry axis. It is found that components parallel to the axis produce a negligible distortion of the spectrometer field.)

The Spectrometer Counter

The spectrometer counter is a home-made geiger counter with a .5 mgm/cm rubber hydrochloride window. The counter is filled with a 1/4 ethyl alcohol 3/4 argon gas mixture to a pressure of 12 cm Hg. Experiments on a similar counter (~4 cm in direction of electron beam) indicate that at this pressure, the counter efficiency should not be dependent upon incident electron energy. The counter has a plateau ~ 150 Volts wide.

Radioactive Gas Source Volume

For the spectroscopy of gaseous radioactive sources, the spectrometer was fitted with a source volume which is shown in Fig. 4. The 1 1/2 cu. inch brass container is lined with a lucite liner. The brass and lucite have a 1 cm. diameter hole which forms the virtual source for the spectrometer. The hole is covered with an .8 mgm/cm aluminized mylar film which forms a vacuum seal between the spectrometer vacuum and the evacuated source volume. The back of the source volume is covered with a large aluminized mylar film behind which another evacuated, lucite walled, volume is placed in order to prevent backscattering of electrons. Provision is made to evacuate all three volumes, (the spectrometer, the source volume and the rear vacuum space) simultaneously, since the films separating the volumes cannot support more than a few cm. Hg pressure.

The lucite liner of the source volume is designed so that no electron which scatters from it can enter a spectrometer trajectory which leads to the counter. The only surfaces in the region of the source volume from which electrons can scatter into the spectrometer beam, are the film backing of the source volume, the edge of the source aperture into the spectrometer, and the thin film across the source aperture.

Calibration

The calibration of the spectrometer for the current-momentum ratio was performed with a Bi^{207} source of internal conversion electrons.

This source has strong internal conversion lines at .9759 Mev and ..477 Mev[36]. The calibration constant was equal, to better than 1/2 per cent, for both lines, for both directions of current flow in the spectrometer winding, thus confirming the linearity of the system. The spectrometer current was measured using a Leeds and Northrup precision Shunt and type K Potentiometer.

The Bi^{207} source was electroplated on a 1" diameter, thin Cu disk and was placed in the median plane of the source volume. Tests were also made to insure that the calibration constant was the same for all parts of the gaseous source volume. These tests proved that the calibration was the same for all parts of the volume and was the same as for a source at the exit aperture (to within ~1/10 of the resolution width.)

VI. A STUDY OF THE EFFECT OF ELECTRON SCATTERING ON THE MEASURED β SPECTRUM

In all studies of the shapes of β spectra the problem of the scattering of electrons in the β- source, the spectrometer counter window, and the baffle system of the spectrometer must be considered very carefully. The efforts of many experimentors have been directed toward a study of the effects of scattering in the source and detector. For the purposes of a precise measurement of the He^6 spectrum, we also studied the scattering in the spectrometer baffle system extensively. This study was especially important for our measurements because of the unusually high maximum energy of the He^6 spectrum.

Let us consider qualitatively scattering effects from the various causes.

A. Scattering of Electrons in the Source:

The effect of source thickness on the shape of a β spectrum has been extensively investigated by direct techniques. Several spectra have been carefully measured as a function of source thickness. The effects of finite source thickness on spectral shape have been presented by Feldman and Wu.[37] They have shown that as the source thickness is increased, the Kurie plot begins to show an upward deviation beginning at an energy somewhat lower than that corresponding to the maximum intensity point of the spectrum. This upward deviation continues toward lower energy until finally the Kurie plot drops rather sharply at very low energies. The causes for these deviations are two-fold. Electrons lose energy upon scattering and thus become shifted to the low energy

region and also, the scattering effect is more pronounced for low energy electrons.

2. Scattering of Electrons in the Counter Window

The effect on β-spectral shape of the counter window thickness is always to cause a drop in the spectrum at low energies. The focusing properties of the spectrometer are such that electrons from the source, of the energy for which the magnetic field is adjusted, will pass through the annular opening called the ring focus. Ideally all electrons which pass through the ring focus should be detected in the Geiger counter. Because of the counter window thickness some of these electrons will not penetrate into the active region of the counter gas. Naturally, this effect becomes more pronounced at low energies where the counter window may be only semi-transparant. There have been several careful studies of the transmission of thin films for electrons of various energies which are summarized in the discussion of window absorption by Slätis[11].

3. Scattering of Electrons by the Spectrometer Baffle System

The effect of scattering of electrons from the baffle system is most difficult to investigate. No extensive study of this phenomenon has been reported in the literature. For the few spectra which have been carefully studied for their spectral shape, the effects of source thickness and counter window scattering are far more serious and difficult to overcome. However, for the He^6 β-spectrum, whose maximum

energy is very high (3.5 mev), baffle scattering is the most serious distorting influence. Furthermore, the effect of baffle scattering is probably very different for different spectrometer designs. It should be borne in mind that our study of this phenomenon in our spectrometer may give only a qualitative interpretation of this effect for some other spectrometer. The effect of baffle scattering on the spectrum shape can best be discussed by considering the scattering in the two regions of the spectrometer; near the source and near the detector. Every scattering of an electron reduces its energy. Therefore, scattering near the source can only increase the apparant number of low energy electrons in a β-spectrum. In the region near the counter it is possible for an electron of energy lower than that which the field is set to transmit, to scatter into the counter. However, in our spectrometer, a number of very efficient traps are provided to trap electrons of lower radius of curvature than the focused beam and therefore very few such electrons reach the detector. Of course in this region of the spectrometer it is possible for electrons of energy higher than the focused beam to be scattered into the counter. All the scattering effects in our spectrometer tend to raise the apparent electron distribution in the low energy region. In the region above ~.250 kev (we do not use any lower energy points in our analysis) our .5 mgm/cm^2 counter window is almost 100 per cent transparent. Therefore, the counter window will not introduce any effects which depress the low energy portion of the spectrum.

In our analysis we have attempted to set only a <u>lower</u> limit on the actual scattering effect in the low energy region of our spectrum.

After subtraction of this scattering "background" we obtain an upper limit on the upward deviation (from allowed shape) of the true He^6 spectrum in the low energy region.

A Quantitative Study of Scattering in the Spectrometer

A. Effect of Scattering at Zero and High Magnetic Field

Direct evidence which indicates the existence of scattering in the spectrometer is the observation of β particles reaching the detector from the source volume when the magnetic field of the spectrometer is zero, and also when it is set ~ 10 per cent above the end point of the β spectrum under investigation.

A study of the zero field counting rate, and the rate above the spectrum end point was performed with the following sources: He^6, A^{41}, Rh^{106}, P^{32} and O^{15}.

Since some of the sources used for these investigations also emit γ radiation it was necessary to determine the counting rate of the spectrometer counter due to γ radiation alone as a function of the magnetic field.[38] This was done by placing a 5 mc Co^{60} source centrally in the gas source volume. The small exit hole which usually forms the virtual β source for the gaseous activities was covered with a lucite cover which was sufficiently thick to stop all β rays coming from the Co^{60} source. Figure 7 shows the "spectrum" obtained from such a source. This curve exhibits the compton electron distribution which ends a little below the energy of the γ rays, and an almost constant background which is practically independent of field setting. The compton dis-

tribution is due to γ rays which produce electrons in the region of the source volume. The constant background is due to γ rays which scatter through the baffle system and produce compton electrons in or near the Geiger counter. These electrons give rise to the field independent background as is to be expected.

For all the β activities studied, it was found that the counting rate due to β activity of the source with the field set about four resolution width above the end point was essentially zero. The counting rate at zero field was directly proportional to the total activity of the spectrum. This result is in agreement with the interpretation that the scattered electrons which reach the counter are originated from electrons of initial energy higher than those focussed by the field.

On the basis of this evidence it was presumed that the background would be approximated by the following function:

$$B(\eta) = k \int_{\eta}^{\eta_{max}} P(\eta')d\eta' \qquad (6\text{-}1)$$

where $B(\eta)$ is the number of scattered electrons which reach the counter at a field setting corresponding to a focussed momentum η ; $P(\eta')d\eta'$ is the probability of emission of an electron by the source into the momentum interval η' to $\eta' + d\eta'$. The constant k should be dependent upon the baffle and spectrometer geometry and independent (within several per cent) of the shape of the spectrum measured. The constant k is found by measuring $B(0)$. $B(o)$ is the total counting rate at zero field (exclusive of γ ray background and room background). The value of k is then given by the equation:

$$k = \frac{B(0)}{\int_0^{\eta_{max}} P(\eta')\, d\eta'} \qquad (6\text{-}2)$$

It is clear that the assumptions from which formula (6-1) resulted are in agreement with the measured backgrounds at zero and at high field. For all the spectra we have measured, B(0) is just proportional to the total activity of the source and is independent of the end point of the spectrum. Also B($\eta > \eta_{max}$) is equal to zero by Eq. (6-1) and the measured counting rate is indeed never above zero. We have also attempted to justify experimentally the validity of Eq. (6-1) over the whole momentum region covered by the spectrum. For this purpose a scintillation spectrometer was used to replace the Geiger counter of the thin lens spectrometer. The actual energy distribution of electrons transmitted by the magnetic spectrometer at several different magnetic field was determined. By this method some of the electrons transmitted can be definitely identified as scattered electrons.

The scintillation spectrometer consisted of a 1" x 3/4" stilbene crystal mounted on a Du Mont No. 6292 phototube. A 2 mgm/cm^2 mica window replaced the normal Geiger counter window on the spectrometer so that the crystal and phototube could remain outside the vacuum chamber. The crystal face was covered with a 0.2 mgm aluminum light reflector and was placed almost in contact with the mica window. By increasing the voltage between the 1st. dynode and

the photocathode of the multiplier to about 300 v, and by surrounding the phototube with a 1/16" commercial μ-metal shield it was possible to make the tube gain almost independent of the magnetic field up to the fields used to focus ~ 1.4 mev β-particles.

For the purposes of this study a source of Rh^{106} was placed in the median plane of the gas source volume. The end point of the complex spectrum of Rh^{106} is close to that of He^6. In order to subtract the small effect upon the scintillation crystal spectra of the γ rays from Rh^{106}, a lucite absorber thick enough to stop all Rh^{106} β rays from the source, could be placed over the virtual source hole.

Scintillation spectra of the transmitted beam of the lens spectrometer at four different field settings corresponding to focused energies 0, .2, .5 and 1.1 mev. were measured with the use of an Atomic 20 channel pulse height analyzer. At each setting of field a spectrum was taken also with the lucite absorber covering the source. The curves with absorber were subtracted from those without it and the resultant spectra are shown in Fig. 8.

Curve (a) shows the spectrum of scattered electrons arriving at the detector at zero field. Qualitatively this shows a spectrum similar to the source spectrum but depressed in energy about 1 Mev. The rise at low energy is probably not real but due to the backscattering in the scintillator.

As the spectrometer field is increased one sees a sharp electron line in the curves of Fig(8 b, c and d) which is due to the focused electron beam of the spectrometer. The region below the energy of the focused beam

is difficult to interpret because of the possibility of scattering some of the electrons in the intense focused beam out of the crystal, giving rise to small pulses. The similarity in the qualitative shape and maximum energy of the spectra at different field settings above the energy of the focused peak should be noted.

We wish to compare the results of these experiments with the proposed background shape of Eq. (6-1). Ideally, $\beta(\eta)$ of Eq. (6-1) should be compared with the integral of the entire spectrum obtained with the Stilbene crystal at a given field setting(corresponding to η) exclusive of the area under the focused peak. Due to the rather poor resolution and the very serious effects of backscattering out of the scintillation spectrometer an exact evaluation of this integral is not possible.

On the basis of the general shape of the scintillation spectrum obtained at zero field (where there is no focused beam) we have extrapolated the continuous scattered electron curve to zero field as indicated by the dotted lines in fig 8b,c,d. The area of the shaded portion of each of these curves is measured and plotted versus the focused momentum on Fig. 8E . The proposed curve of Eq. (6-1) is normalized to the results of the scintillation data and is plotted as the solid curve on the same figure (8e).

It seems that actually at low field, the background is somewhat higher than at zero field[+].

[+] A qualitative explanation for the rise in background at low fields is as follows: $\beta(\eta)$ as assumed may be considered as the available

However, since we are only attempting to determine a small correction to the He^6 spectrum the experimental points can be said to justify quite well, the use of Eq. (6-1) in correcting the He^6 spectrum.

Although the scintillation data indicates that the background is somewhat higher in the very low energy portion of the spectrum than that indicated by Eq. (6-1) we use (6-1) to correct the He^6 spectrum. This decision is in agreement with the assumption that we wish to find the minimum scattered background at low fields and will therefore tend to undercorrect slightly in this region.

---

number of electrons for scattering in the region near the source. $\beta(\eta)$ changes very little at low field settings. The scattering probability for electrons favors small angle scattering and electrons that have scattered only through very small angle cannot reach the detector. As the field is increased the whole space in the spectrometer becomes "curved" for electrons and the baffle will transmit electrons which have scattered through a smaller angle. Thus the increase in scattering at low fields, until the effect of the drop of $\beta(\eta)$ becomes the predominant effect.

VII. THE He^6 SPECTRUM MEASUREMENTS AND CORRECTIONS

Monitor Counter

Due to rather rapid fluctuations in both the cyclotron beam current, the beam position on the target, as well as changes in the pumping speeds of the He^6 purifying system, the activity delivered to the spectrometer source volume was not constant. In order to correct the β-spectrum for variations in source strength it was necessary to monitor the total source activity.

A 2" long, 1/4" copper tube was connected to the source volume (see Fig. 4) of the spectrometer and was sealed at the other end. At the very low gas pressures in the source volume, equilibrium is quickly established between the activity in the tube and source volume. A commercial end-window Geiger counter was placed about 1/4" from the end of the blind tube. This served as a monitor for the source activity. It was determined experimentally that the monitor efficiency was not a function of the spectrometer field. The monitor counting rate is proportional to the total decay rate in the source. No data on the He^6 spectrum was accepted for analysis if the average monitor rate for the individual counting interval deviated by more than $\pm$ 50 per cent of the average monitor rate for the whole spectrum.

Background of Counters

Both the spectrometer counter and the monitor counter detect background radiation due to cosmic rays, general contamination of the cyclotron experimental area, and also some leakage of radiation through

the sheilding wall between the experimental area and the cyclotron. The first two sources of background are constant over the period of a single He^6 run: (approximately 8 hrs.) The background due to the cyclotron is mainly due to the high neutron flux in the cyclotron vault which leaks through the 6 foot shielding wall. Attempts were made to shield both the monitor and spectrometer counters from this radiation, however, it was not possible to reduce this background below ~1/2 of the natural background when 50 μ A of deuteron beam was focused on the Be target. Care must be taken in subtracting this background from the spectrometer counter rate. It may be as much as 6-7 per cent of the spectrometer count when one is investigating the low ends of the β-spectrum. It is also correlated in intensity with the intensity of the He^6 source since both vary with the cyclotron beam current.

To properly account for variations in this background another monitor Geiger counter was placed next to the spectrometer counter inside its lead shield. This counter was completely shielded from any electrons inside the spectrometer.

The procedure used to calculate the spectrum as a function of energy is demonstrated by the following formula:

$$S'(I) = \frac{\left(\frac{N(I)}{T} - \mathscr{L}_{NB}\right) - K\left(\frac{M_c}{T} - \mathscr{M}_{CNB}\right)}{\frac{M_A}{T} - \mathscr{M}_{AB}} \qquad (7\text{-}1)$$

$S'(I)$ = Relative count of the spectrum corrected for all external background and normalized to unit source activity.

$N(I)$ = Total count of spectrometer counter for time T (at field H) corresponding to current I)

T =Time required to accumulate count

$\mathscr{S}_{NB}$ = Rate of backgrounds due to cosmic rays and room contamination-- determined by counting with cyclotron beam turned off-- No He^6 activity in spectrometer source volume.

M_c = Background monitor count taken at the same time as S

$\mathscr{M}_{cnb}$ = Background of background monitor due to cosmic rays and room contamination -- taken with cyclotron off.

k = Constant relating efficiency of background counter and spectrometer counter for cyclotron background -- determined under the following conditions -- cyclotron running; He^6 flowing into experimental area, but not into spectrometer source volume; under these conditions the Eq.

$$\frac{N}{T} - \mathscr{S}_{NB} - k\left(\frac{M_c}{T} - \mathscr{M}_{CNB}\right) = 0 \qquad (7\text{-}2)$$

determines the constant k.

Ma = Total count of activity monitor taken at the same time as S.

$\mathscr{M}_{ab}$ = Background of activity monitor -- determined under same conditions used to determine k. ($\frac{\mathscr{M}_{AB}}{M_A}$ is of the order of 1 per cent. Since it was possible to shield this counter quite effectively from the cyclotron background no account is made of variations of Mab with cyclotron beam current.)

Small Dead time corrections are applied to both S and Ma before entry into Eq. (7-1).

Values of N(I) were obtained for 35 field values corresponding to the range W = 0 to W = 4.7 Mev. Six complete runs of the spectrum were taken on different days over a period of about two months. The values of all the constants in (7-1) were determined separately for each run. A large part of the experimental equipment including the electronic apparatus, all the counters, and part of the cyclotron shielding wall had to be dismantled between these runs.

Care was taken each time to reproduce the positions of the spectrometer counter and the activity monitor. The values of the constants in Eq. (7-1) may differ by as much as 50 per cent from run to run. In spite of these variations, the $\sum_I N(I)$ corresponding to the integral of the measured spectra obtained from each of the runs were in agreement to within several per cent for all the runs, attesting to the reliability of the spectrometer counter and activity monitor and the validity of the Eq. (7-1).

A total of more than 6000 counts was obtained for N for each value of I in the region of the He^6 spectrum.

After normalizing the data from the six runs, the six sets of values of S'(I) were averaged. The plot of S'(I) VS I is shown in Fig. 9 .

Correction for Scattering of Electrons in Baffle System of the Spectrometer

S'(I) must now be corrected for the effects of electron scattering in the spectrometer. This correction has been extensively discussed in Chapter 6. The correction

$$B(\eta) = k \int_{\eta}^{\eta_{max}} P(\eta')\, d\eta'$$

must be subtracted from S'(I). [The identification is simply made between S'(I) and S'(η) through the calibration]. It should be recalled that P(η') is the relative probability of emission of an electron in the energy range $\eta' + \eta' + d\eta'$. k is an experimentally determined constant.

For the determination of k and B(η) it is sufficiently accurate to approximate P(η') by $\frac{S'(\eta)}{\eta}$.

Now the Eq:

$$S'(0) = B(0) = k \int_{0}^{\eta_{MAX}} \frac{S'(\eta)}{\eta}\, d\eta = k \int_{0}^{I_{MAX}} \frac{S'(I)}{I}\, dI$$

determines k.

All the integrals are performed graphically using the measured S'(I). We then set $S(I) = S'(I) - B(I) = S'(I) - k \int_{I}^{I_{MAX}} \frac{S'(I')dI'}{I'}$.

Resolution Correction

S(I) is now the spectrum corrected for electron scattering in the spectrometer. The resolution correction has been discussed in Chapter 5. According to Eq. (5-1) we must solve the integral equation:

$$S(H) = \int_0^\infty P(\eta)\, R(H,\eta)\, d\eta \qquad (7\text{-}3)$$

for $P(\eta)$ given $S(H)$ and $R(H,\eta)$. This solution may be performed according to the expansion of Eq. 3, Appendix B. However, since the resolution used in this experiment is very good (2.8 per cent), the resolution correction is extremely small and a simpler method may be used to estimate the effect on the spectrum. We note that according to Eq. 7 and 9 of Appendix B:

$$\int_0^\infty R(H,\eta_1)\, d\eta_1 = k H_1$$

thus

$$\frac{S(H)}{H} \approx \frac{\int_0^\infty R(\eta,H)\, P(\eta)\, d\eta}{\int_0^\infty R(H,\eta)\, d\eta} = P(\eta) + \text{small terms} \qquad (7\text{-}4)$$

we now define

$$C(\eta) = \frac{S(H_\eta)}{H_\eta\, P(\eta)} = \frac{1}{P(\eta)} \frac{\int_0^\infty P(\eta)\, R(H,\eta)\, d\eta}{\int_0^\infty R(H,\eta)\, d\eta}$$

Except in the immediate region of the spectrum end point $C(\eta)$ differs from one by terms of order <.02 as can be seen from Eq. 1B, Appendix B. We have calculated $C(\eta)$ from Eq. (7-4) by considering $P(\eta)$ to be a theoretical allowed spectrum (no coulomb effect) ie. $P(\eta) = (\epsilon_0 - \epsilon)^2 \eta^2$ and using the measured $R(H,\eta)$ for the conversion line (expanded in η so that its full width at half maximum is $\frac{\Delta\eta}{\eta} = 2.8$ 2.8 per cent ie, the exact $R(H,\eta)$). From these

numerical integrations we have found that $.999<C(\eta)<1.001$ for all but three points in the neighborhood of the end point of He^6. Fig. 10 shows a plot of $(C(\eta)-1)$ vs $(\epsilon_0-\epsilon)$ for $\epsilon_0 \sim 7.83$. Since the resolution correction in the region of the end-point is not too certain, we have removed from the final He^6 analysis the three points for which the correction is greater than 0.1 per cent. The other points are not corrected.

We therefore have

$$P'(\eta) = \frac{S(H_\eta)}{H_\eta} \approx \frac{S(I)}{I}$$

as the probability of electron emission by the source per unit momentum interval. A plot of $P'(\eta)$ vs η is shown in Fig. 11. The presence of a small Ne^{23} contaminant is evidenced by the tail of the spectrum beyond the He^6 end-point.

Correction for Ne^{23} Contaminant

In the previous section we have shown the derivation of $P'(\eta)$ the spectrometer measurements. $P'(\eta)$ is the momentum distribution of electrons. It was indicated in Chapter 4 that the source contains a small contaminant of Ne^{23} activity. Before the momentum distribution of He^6 can be obtained, the spectrum of Ne^{23} contaminant must be subtracted from $P'(\eta)$.

The decay scheme of Ne^{23} has been measured as shown in Fig. 5. Since the end point of the He^6 spectrum is lower than that of the two upper energy groups of Ne^{23}, the distribution $P'(\eta)$ contains electrons only from Ne^{23} at the high energy end. A Kurie plot of the upper end

of the distribution $P'(\eta)$ is shown in Fig. 12. The line drawn on this curve corresponds to a normalized theoretical composite Kurie plot of the two upper groups of Ne^{23} with the relative intensities and end points as given in Penning and Schmidts decay scheme. It is clear that, within statistics, the distribution $P'(\eta)$ corresponds to the expected distribution from Ne^{23} above the He^6 end point energy. From this analysis, and the extrapolation of the two Ne^{23} groups to lower energy, it is possible to state that the contaminant Ne^{23} accounts for 5.4 ± 1.0 per cent of the total decays of the source.

We shall correct for the Ne^{23} contaminant activity by the following Equation

$$P(\eta) \equiv P'(\eta) - Q\,G(\eta) \quad . \tag{7-5}$$

$P(\eta)$ is the He^6 momentum distribution, and $G(\eta)$ is the Ne^{23} momentum distribution calculated on the basis of the decay scheme of fig. 5, and normalized to total intensity equal to that of $P'(\eta)$. (We have assumed allowed shape for the two Ne^{23} upper energy groups, and have not included the 2.4 Mev group of Ne^{23} on the basis of the discussion of effects of impurities with $\epsilon_{max} < \epsilon_{max\ He^6}$). on the He^6 spectrum shape (see Chap. IV)). Q is a constant which is the relative intensity of Ne^{23} to (Ne^{23} + He^6) in $P'(\eta)$. In this section we shall set $Q = 5.4$ per cent. In Appendix C it will be shown that the limits on Fierz interference or Pseudoscalar interaction to be set from $P(\eta)$ are insensitive to Q for 2.4 per cent $< Q <$ 8.4 per cent which surely includes any possible error in the experimental determination of $Q = 5.4 \pm 1.0$ per cent described in the

preceding paragraph.

A plot of $P(\eta)$ ($Q = .054$) is shown in Fig. 13 . We wish to reemphasize that this measured momentum distribution of the He^6 spectrum still contains certain instrumental distortions which are, however, known to cause only a relative increase in low energy electrons i.e. the spectrum at low energies represents only a relative maximum for the true He^6 $P(\eta)$.

A conventional Kurie plot of $\sqrt{\frac{P(\eta)}{\eta^3 F}}$ vs. ϵ is shown in Fig. 14 .

VIII. COMPARISON OF THE MEASURED SPECTRUM WITH THE THEORETICALLY EXPECTED SHAPE OF THE He^6 SPECTRUM

The theoretically expected shape of the spectrum of He^6 is given in Eq. (2-15).

We rewrite that formula with a new notation which will be useful in the comparison between the theoretically predicted and the experimentally measured spectra.

$$T(\eta,\alpha,\beta) = \left\{K\eta^2(\epsilon_0-\epsilon)^2 F(Z=3,\eta)\right\}\left[1+\frac{\alpha}{\epsilon}-\beta\left(2\epsilon-\epsilon_0-\frac{1}{\epsilon}\right)\right] I(\epsilon_0,\epsilon)\, R(\epsilon_0,\epsilon) \quad (8\text{-}1)$$

$T(\eta, \alpha, \beta) \longrightarrow$ theoretical distribution of electrons per unit momentum interval.

$\{\ \} \longrightarrow$ "Allowed shape" factor including coulomb correction factor as calculated by Feister[7] or Rose.[8] K is an arbitrary normalization constant independent of η .

$$\alpha \equiv b_{GT} + \frac{\epsilon_0}{3M}\frac{Re(C_A C_P^* + C_A' C_P'^*)}{\Sigma_{GT}} \quad ; \quad \beta \equiv +\frac{1}{3M}\frac{Re(C_P C_T^* + C_P' C_T'^*)}{\Sigma_{GT}} \quad (8\text{-}2)$$

$I(\epsilon_0,\epsilon) \rightarrow$ the Inner Bremsstrahlung correction factor of Eq. (2-8)

$R(\epsilon_0,\epsilon) \rightarrow$ the correction factor for finite recoil energy given in Eq.(2-10).

Since the correction factor $.999 < R(\epsilon_0, \epsilon) < 1.001$ over the whole range of the measured spectrum, detection of the effect

of $R(\epsilon_0, \epsilon)$ is not possible with the present data.

It can also be shown that the correction factor

$I(\epsilon_0, \epsilon) \approx \mathcal{H}\left(\frac{\epsilon_0' - \epsilon}{\epsilon_0 - \epsilon}\right)^2$ to within ± 0.15% where $\epsilon_0' - \epsilon_0 \approx .014 mc^2 = .007 Mev.$

for He^6. Reference to Eq. (8-1) will show that because of this identity it is outside of the range of experimental accuracy to determine any effect of $I(\epsilon_0, \epsilon)$ upon the spectrum shape. $I(\epsilon_0, \epsilon)$ tends only to change the end point of the spectrum by a minute quantity.

For these reasons we have set $I(\epsilon_0, \epsilon) = R(\epsilon_0, \epsilon) = 1$ in the analysis. (The constant $\mathcal{H}$ is absorbed in k of Eq. (8-1)). The explicit form for the theoretical spectrum with which we now wish to compare the experimental spectrum which is denoted by $P(\eta)$ is thus

$$T(\eta, \alpha, \beta) = k \eta^2 (\epsilon_0 - \epsilon)^2 F(Z=3, \eta) \left[1 + \frac{\alpha}{\epsilon} - \beta\left(2\epsilon - \epsilon_0 - \frac{1}{\epsilon}\right)\right] \quad (8-3)$$

In the comparison of $T(\eta)$ with $P(\eta)$ (the measured distribution) there are 4 unknown constants which must be determined. They are $k, \epsilon_0, \alpha + \beta$. It can be shown that any fit of $T(\eta)$ to $P(\eta)$ to determine the four unknown constants cannot, without very much more precise data than is obtainable at this time, determine discrete values for both α and β. If a fit is made to $T(\eta)$ of $P(\eta)$ only correlated ranges of α and β can be obtained. This is due to the fact that various combinations of Fierz interference and pseudo-scalar correction factors can give experimentally indistinguishable spectra for many combinations of α and β.

We have therefore analyzed separately for each of the individual quantities α and β under the assumption that the other was identically zero.

Analysis of He^6 Spectrum Assuming $\beta = 0$

Under the assumption $\beta = 0$, the theoretical spectrum is given by

$$T'(\eta, \alpha, 0) = K\eta^2(\epsilon_0 - \epsilon)^2 F(z=3, \eta)\left[1 + \frac{\alpha}{\epsilon}\right] \tag{8-4}$$

The comparison with the experimental data was performed by use of the following reduction. Let

$$t'(\eta) \equiv \frac{T'(\eta, \alpha, 0)}{\eta^2(\epsilon_0 - \epsilon)^2 F(z=3, \eta)} = K\left[1 + \alpha/\epsilon\right] \tag{8-5}$$

We also define the quantity:

$$p(\eta) \equiv \frac{P(\eta)}{\eta^2(\epsilon_0 - \epsilon)^2 F(z=3, \eta)} \quad \text{which is assumed to differ} \tag{8-6}$$

from $t'(\eta)$ only by the random statistical errors in $P(\eta)$ which is the measured momentum distribution of electrons.

Now $t'(\eta) = a + bx$ where

$$a \equiv K \qquad b \equiv \alpha K \qquad x \equiv \frac{1}{\epsilon} \quad ; \quad \frac{b}{a} = \alpha \tag{8-7}$$

A least square fit of $p(\eta)$ vs. $\frac{1}{\epsilon}$ to a straight line can be performed to determine the constants a and b.

We wish to note now that $p(\eta)$ depends upon the choice of ϵ_0 which is essentially an unknown. A first approximation can be obtained for ϵ_0 by performing a linear extrapolation of the usual Kurie plot of $P(\eta)$. Such a plot is shown in figure 14. From this we obtain $\epsilon_0 = 7.845mc^2$ as the first approximation. With the use of the computing facilities of the Watson Laboratories we have performed least square fits of $p(\eta)$ to the straight line $t'(\eta)$ for five different values of ϵ_0 (used to calculate five sets of $p(\eta)$), namely $\epsilon_0 = 7.765$; 7.815; 7.845; 7.875, and 7.925. For each value of ϵ_0 a "least square" value for $\frac{b}{a} = \alpha$ is obtained. Figure 15a is a plot of b/a VS ϵ_0.

We now note that unless ϵ_0 is the true end point of the spectrum $p(\eta)$ VS $\frac{1}{\epsilon} = \chi$ should not be a straight line, and in fact should deviate significantly from straightness in the region of ϵ_0. (This is independent of α). For each ϵ_0 mentioned above, we have calculated the errors:

$$\delta\left(\frac{b}{a}\right) = \frac{b}{a}\frac{.67}{\sqrt{M}}\sqrt{\frac{\Sigma X_i^2}{a^2} + \frac{n}{b^2}}\left[\sqrt{D}\right] = \text{Probable error in } \frac{b}{a} \qquad (8\text{-}8)$$

where $M = n\Sigma X_i^2 - (\Sigma X)^2$ (8-9) n = no. of points included in the fit

$D = \dfrac{\Sigma \delta_i^2(x)}{n-2}$ for internal error where δ_i is the deviation of the point from the line,

i.e., $\delta_i = p_i - (a + bx_i)$. (8-10)

$D = \Sigma \delta_i'^2(x)$ (8-11) for external error where δ'_i is the probable error in $p_i(\eta)$ due to statistics.

The probable errors (both internal and external) are plotted in figure 15b. The internal errors give a measure of the goodness of fit of the experimental data to a straight line, and the external error gives the expected internal error if the theoretical assumptions are correct. The external "errors" are essentially independent of the choice of ϵ_0. The minimum of the internal probable error curve determines the best value of ϵ_0 and thereby the best value of b/a.

The results of this analysis are that $\frac{b}{a} = +.055 \pm .020$ where the error is twice the external error and 1.6 times the internal error and is based qualitatively upon the error in fit due to choice of ϵ_0.

In this analysis $\frac{b}{a} = \alpha = .055 \pm .020$. However, we wish to re-emphasize that the limitations of the experiment only permit the setting of an upper limit on α (see Chapter VI). Thus the non-zero value obtained for $\frac{b}{a}$ is not to be interpreted as evidence that α is not zero. The conclusion to be drawn is that if $\beta = 0$ then $\alpha < .080$ (8-12)

Figure 16a is a plot of $p(\eta)$ vs ϵ ($p(\eta)$ normalized to $t(\eta)$ at the high energy region) with $\epsilon_0 = 7.845$. One line drawn is the theoretical $t(\eta)$ for $\alpha = +.08$. The plot indicates that the experimental points lie below $t'(\eta)$ in the low energy region.

Since unknown scattering phenomenon which require and allow us to set only an <u>upper</u> limit on α are likely to occur only in the lower energy region of the He^6 spectrum, we have attempted to set a lower negative limit on α by considering the spectrum shape only above $W = 1.5$ Mev; $\epsilon = 3\ mc^2$. The limit that can be set from this region is, of course,

large. It is based upon the comparison of $p(\eta)$ with the curve of $t'(\eta)$ with $\alpha = -.20$. Thus we conclude that $\alpha \geq -.20$ (8-13)

Analysis of He^6 Spectrum Assuming $\alpha = 0$

If we assume $\alpha = 0$ the theoretical spectrum is then given by

$$T''(\eta) = K\eta^2(\epsilon_0-\epsilon)^2 F(Z=3,\eta)\left[1-\beta\left(2\epsilon-\epsilon_0-\frac{1}{\epsilon}\right)\right] \quad (8\text{-}14)$$

The comparison with the experimental data was performed in a similar manner to that used for the Fierz interference fit. We set

$$t'' = \frac{T''(\eta)}{\eta^2(\epsilon_0-\epsilon)^2 F(Z=3,\eta)} = K\left[1-\beta\left(2\epsilon-\epsilon_0-\frac{1}{\epsilon}\right)\right] \quad (8\text{-}15)$$

$$p(\eta) = \frac{P(\eta)}{\eta^2(\epsilon_0-\epsilon)^2 F(Z=3,\eta)} \quad (8\text{-}16)$$

which is assumed to differ from $t''(\eta)$ only by random statistical errors in $P(\eta)$.

Now $t''(\eta) = c + dy$ where $C \equiv K$ $d \equiv -\beta K$ (8-17)

$$\beta \equiv -\frac{d}{c} \qquad y \equiv \left(2\epsilon-\epsilon_0-\frac{1}{\epsilon}\right) \quad (8\text{-}18)$$

We note that the correction factor itself and also y is a relatively insensitive function of ϵ_0. An approximation $\epsilon_0 = 7.845\ mc^2$. is made for calculation of y vs ϵ and y is then considered independent of ϵ_0. $p(\eta)$ is, however, quite sensitive to ϵ_0 and therefore least square fits of $p(\eta)$ to $t''(\eta)$ were performed for several values of ϵ_0. For each value of ϵ_0 a "least square" value of $\frac{d}{c}$ was obtained. Figure 17a is a plot of $\frac{d}{c}$ vs ϵ_0.

$\delta\left(\frac{d}{c}\right)$ was calculated according to the formulas (8-8) to (8-11)

where $b \longrightarrow d$, $a \longrightarrow c$ $\qquad \chi \rightarrow y$

The probable errors are plotted in figure 17b. The minimum value of the internal probable error curve determined the best value of $\frac{d}{c}$.

The results of this analysis are that $\frac{d}{c} = -.0035 \pm .0010$.

In view of the discussion given regarding the interpretation of the limits on α, which apply also to the pseudoscalar results, only upper limit can be set on β.

This limit is given by $\beta < .0045$.

A limit can be set on negative values of β from analysis of the spectrum above $\sim$1.5 Mev. This results in a low limit $-.01 < \beta$.

Figure 16b shows a curve of $p(\eta)$ vs ϵ ($\epsilon_0 = 7.845$.) The lines drawn represent the normalized pseudoscalar correction factor for the limits set above, i.e. $\beta = -.01$, and $\beta = +.0045$

Combined Limits for $\alpha + \beta$

In the previous paragraphs we have considered analysis of the He^6 spectrum under the assumption that either $\alpha = 0$ or $\beta = 0$. If neither is 0 then the correction factor is

$$t(\eta) = K\left[1 + \frac{\alpha}{\epsilon} - \beta\left(2\epsilon - \epsilon_0 - \tfrac{1}{\epsilon}\right)\right.$$

The spectrum measurement is not sufficiently refined to distinguish between the correction factors for the two different energy dependences of the $\alpha + \beta$ terms if both α and β are small.

If the correction factor $t(\eta)$ is compared with the experimental

correction factor p(η) for any two values of η it is seen that

$$\frac{t(\eta_1)}{t(\eta_2)} \approx 1 + \alpha\left[\frac{1}{\epsilon_1} + \frac{1}{\epsilon_2}\right] - \beta\left[2\epsilon_1 - \frac{1}{\epsilon_1} - 2\epsilon_2 + \frac{1}{\epsilon_2}\right]$$

in the limit of small α and β .

Also $\frac{t(\eta_1)}{t(\eta_2)} = \frac{p(\eta_1)}{p(\eta_2)}$ within statistical errors.

Thus for any two points on the spectrum, a linear relationship is obtained between α and β . The co-efficients α and β in linear relationship depends upon the points η_1 and η_2 chosen. However, in the limit of the refinement of the experiment, i.e. when the two correction factors are experimentally indistinguishable, approximately the same linear relationship will hold for any two chosen points on the spectrum.

On this basis we have assumed that in the region of small α and β, the limits on these quantities are related in a linear fashion.

The range of values of α and β consistent with the measured He^6 spectrum are thus shown by the shaded area of the graph of figure 18. The upper and lower bounds are given by straight lines determined by the limits obtained on the assumption that either $\alpha = 0$ or $\beta = 0$.

This analysis is valid in the region $-.4 < \alpha < .4$ and $-.03 < \beta < +.03$. Outside this region the separate correction factors are sufficiently different to distinguish the two co-efficients of α and β in t(η). Therefore we have placed the completely unqualified limits

$$-.4 < \alpha < .4 \quad \text{and} \quad -.03 < \beta < +.03$$

IX. INTERPRETATION OF RESULTS IN TERMS OF COUPLING CONSTANTS OF β-DECAY AND COMPARISON WITH OTHER EXPERIMENTS

The limits upon the coupling constants that can be set from our investigation of the He^6 spectrum are presented in the graph of figure 18. We recall the definitions of the quantities α and β in terms of the decay coupling constants as presented in eq. (8-2):

$$\alpha \equiv \frac{2\,Re\left[C_A C_T^* + C_A' C_T'^* + \frac{\epsilon_0}{3M}\left(C_P^* C_A + C_P' C_A'^*\right)\right]}{|C_A|^2 + |C_T|^2 + |C_A'|^2 + |C_T'|^2} \quad ; \quad \beta \equiv \frac{1}{3M}\frac{Re\left(C_P C_T^* + C_P' C_T'^*\right)}{|C_T|^2 + |C_A|^2 + |C_T'|^2 + |C_A'|^2}$$

$$\frac{\epsilon_0}{3M} = 1.42 \times 10^{-3} \quad ; \quad \frac{1}{3M} = 1.82 \times 10^{-4}$$

The graph of figure 18 shows the combinations of values of α and β which are consistent with our He^6 measurements. The interpretation of these results in terms of the ratios of individual coupling constants will be attempted in terms of the invariance requirements presented in table I of chapter I.

Previous experiments to determine the relative magnitudes of pseudoscalar, axial vector, and tensor coupling were interpreted only under the assumptions of the old theory of β-decay (assumptions (a) of table I). We can, however, compare our results with the results of other experimenters without concerning ourselves with the detailed invariance assumptions.

All shape measurements to determine the extent of interference in allowed β-decay have been a measure of the co-efficient of the $\frac{1}{\epsilon}$ term in the spectral shape, i.e. the quantity we have defined as "α". (The measurements of K capture to positron branching ratio are also a measure

of α.) The experimental as well as the theoretical papers which have considered the magnitude of Fierz interference in allowed β-spectra usually assume that this effect is the only one which may possibly contribute to a deviation of an allowed spectrum from allowed shape. If the pseudoscalar coupling constant is not actually much larger than the other coupling constants, this point of view seems quite justified. However, no a priori or firm experimental evidence for this fact is at present available. Therefore, in attempts to set very small limits on the Fierz interference, care should be taken in neglecting the effect of the pseudoscalar interaction when analyzing for Fierz interference.

For the comparison of our results with those of other experiments we must therefore assume that the co-efficient β is equal to zero. We repeat that if $\beta = 0$ the He^6 spectrum indicates that

$$-.20 \leq \alpha \leq +.08 \quad .$$

The most significant analyses of the shapes of allowed spectra for Fierz interference in the Gamow-Teller interaction are presented in table IIa. There is, of course, no disagreement between any of the results. The most careful work of Pohm et al. as well as the analysis of Davidson and Peaslee in which the P^{32} spectrum is the most heavily weighted are somewhat difficult to interpret in terms of the β-decay coupling constants. The ft value of the β decay of P^{32} is $\sim 10^8$ sec. The decay is retarded approximately one thousand fold from the usual allowed β- decays and more than a factor of 10^5 from the superallowed transition of He^6. The assumption of both the above mentioned authors that the shape of the spectrum may be analyzed as a pure allowed spectrum with no consideration of

Table IIa

Reference	Limits on	Spectra Analyzed
Mahmoud and Konopinski [39]	$-.2 < \alpha < +.2$	Cu^{64} β^+ and β^-, and S^{35}
Davidson and Peaslee [40]	$-.08 < \alpha < +.08$	P^{32}, He^6 (old Columbia spectrum), Cu^{64} β^+ and β^-
Pohm, Waddel, Jensen [41]	$-.04 < \alpha < +.04$	P^{32}
He^6 present results	$-.20 < \alpha < .08$	He^6

Table IIb

Sherr and Miller [12]	$-.04 < \alpha < +.02$	Na^{22}
Driver, Moljk, Scobie [42]	$-.04 < \alpha < +.05$	F^{18}

the effect of forbidden matrix elements and energy dependent shape factors seems most tenuous. Estimates of the pseudoscalar matrix element in the decay of P^{32} by Brysk,[43] for example, indicate that if the pseudoscalar coupling constant is equal to the tensor coupling constant, the pseudoscalar interaction would contribute about 8% to the decay probability of P^{32}. Other nuclear relativistic effects may contribute in like manner to this decay.

Other measurements of Fierz interference have been performed by measuring K capture to positron branching ratios. Since the nuclear matrix elements are equal for both processes, they drop out in the calculation of the branching ratios for a particular decay. The ratio depends upon the coupling constant ratio and the associated shape factors. It also depends upon the energy available for decay, the K binding energy, the Coulomb function and certain properties of the K electron wave function. The latter quantities are theoretically well known. The results of these experiments can be presented in terms of the co-efficient α of the $\frac{1}{\epsilon}$ dependence of the positron spectrum. These results are shown in table IIb. The same remarks in the above paragraph, which refer to the neglect of any higher order effects of β-decay in the shape measurements, also apply to these measurements. Again we mention that the ft value of the Na^{22} β - decay is anomolously large ($\log ft = 7.4$), which makes interpretation more tenuous. The $\log ft = 4.0$ for the F^{18} decay and the limits on Fierz interference from this experiment are probably the most indicative of the assumption that $Re(G_A G_T^*) \approx 0$.

There have been several previous attempts at setting a limit on the pseudoscalar coupling in β decay. Fujita and Yamada[14] have compared the spectra of He^6 and B^{12} (old Columbia data) with predictions based upon the correction factor given in eq. (2-1). They have neglected all effects due to the axial vector interaction. In terms of our co-efficient β their results may be expressed in the following manner:

$-.013 < \beta < .027$ from old He^6 data

$-.010 < \beta < .0035$ from Be^9

A similar analysis by Alaga, Kofoed-Hansen and Winther[15] of the same He^6 data resulted in the limits

$-.018 < \beta < +.018$

If our He^6 data are analyzed on the same basis, i.e. assuming that $C_A = C_A' = 0$ we obtain

$-.010 < \beta < .0043$

Other estimates of the strength of the pseudoscalar interaction in β decay have been made by Brysk.[13] He considered the two ℓ-forbidden decays of C^{14} and P^{32}. In both these cases the Gamow-Teller matrix element is apparently very small. Brysk[13] approximates a lower limit for the pseudoscalar matrix element for these decays, assumes that the total decay goes completely by the pseudoscalar interaction, and thus obtains an upper limit for the pseudoscalar coupling constant.

In the notation of Chapter I his results may be expressed as follows:

$$\frac{|C_P|^2+|C_P'|^2}{|C_A|^2+|C_T|^2+|C_A'|^2+|C_T'|^2} \leqslant 16 \qquad \text{from } C^{14} \text{ decay}$$

$$\frac{|C_p|^2+|C_p'|^2}{|C_A|^2+|C_T|^2+|C_A'|^2+|C_T'|^2} \leq 4 \qquad \text{from } P^{32} \text{ decay}$$

Conclusions Regarding the Limits Obtainable from He^6 Results

We shall now attempt to express the limits set upon α and β in our experiment as limits on the individual coupling constants, in terms of some of the limitations on the coupling constants due to the invariance requirements as presented in table I.

All the presently available experimental evidence is consistent with the two component theory for the neutrino. The results of the experiments of Wu et.al.[4] also indicate that $C_i = C_i'$ within ~ 30 o/o. This theory is particularly attractive as an explanation of parity non-conservation in interactions involving neutrinos. We shall therefore attempt to interpret our results in terms of the two component theory both with and without invariance under time reversal, i.e. cases 4 and 5 of table I. Actually if the two component theory is not assumed it is rather difficult to determine any further relationships between the coupling constants other than those presented in terms of α and β in the previous section.

Interpretation in Terms of the Two Component Neutrino Theory

On the basis of the two component theory we have the relationships

$$C_T = \pm C_T' \qquad C_A = \pm C_A' \qquad \text{and} \quad C_p = \pm C_p' \tag{9-1}$$

according to cases 4 and 5 of table I.

With the use of eqs.(9-1), the quantities α and β reduce to:

$$\alpha = \frac{2\,\mathrm{Re}(C_A C_T^* + \frac{\epsilon_0}{3M} C_A C_P^*)}{|C_A|^2 + |C_T|^2} \tag{9-2}$$

$$\beta = \frac{1}{3M} \frac{\mathrm{Re}(C_P C_T^*)}{|C_A|^2 + |C_T|^2} \tag{9-3}$$

Since only the relative phases between the coupling constants are observable we may redefine the coupling constants in the following manner:

$$C_T \equiv G_T \quad ; \quad C_A \equiv G_A e^{i\theta_{AT}} \quad ; \quad C_P \equiv G_P e^{i\theta_{PT}} \tag{9-4}$$

where all the G_i are taken as real numbers, and the θ_{iT} are the phases relative to the tensor phase.

By substitution of eqs. (9-4) in eos. (9-2) and (9-3) we find that

$$\alpha = 2\frac{G_A}{G_T}\left[\cos\theta_{AT} + \frac{\epsilon_0}{3M}\frac{G_P}{G_T}\cos(\theta_{AT} - \theta_{PT})\right]\left(1 + \frac{G_A^2}{G_T^2}\right)^{-1} \tag{9-5}$$

and

$$\beta = \frac{1}{3M}\frac{G_P}{G_T}\cos\theta_{PT}\left(1 + \frac{G_A^2}{G_T^2}\right)^{-1} \tag{9-6}$$

The β-ν angular correlation measurements[34] on He^6 indicate that

$$\frac{G_A^2}{G_T^2} \leq \frac{1}{3} \tag{9-7}$$

By substitution of this limit and of the numerical values of ϵ_0 and M into the forms of eqs. (9-5) and (9-6) we obtain correlated experimental limits on the quantities

$$\gamma \equiv \frac{G_A}{G_T}\left[\cos\theta_{AT} + .0014\frac{G_P}{G_T}\cos(\theta_{AT} - \theta_{PT})\right] \tag{9-8}$$

and

$$\delta \equiv \frac{G_P}{G_T}\cos\theta_{PT} \tag{9-9}$$

given in graph of figure 19.

Interpretation in Terms of Two Component Theory and Invariance under Time Reversal

If the Hamiltonian of β decay is invariant under time reversal then the phase angles of eqs. (9-5) and (9-6) may all be taken as equal to zero (the C_i however may differ in sign).

In this case α and β reduce to:

$$\alpha = 2\frac{G_A}{G_T}\left[1+\frac{\epsilon_0}{3M}\frac{G_P}{G_T}\right]\left(1+\frac{G_A^2}{G_T^2}\right)^{-1} \quad ; \quad \beta = \frac{1}{3M}\frac{G_P}{G_T}\left(1+\frac{G_A^2}{G_T^2}\right)^{-1}$$

By the use of an iteration procedure which starts with the maximum values of $|\alpha|$ and $|\beta|$ permissible according to the graph of figure 18 and the assumption that $\frac{G_A^2}{G_T^2} \leqslant \frac{1}{3}$ we obtain the graph of figure 20 which gives the correlated limits on $\frac{G_A}{G_T}$ and $\frac{G_P}{G_T}$ consistent with the He^6 spectral shape and the assumption that the β decay Hamiltonian is invariant under time reversal.

Appendix A

We here demonstrate the derivation of eq. (1-14) from the eqs. (1-2), (1-5) and (1-10). Since the mathematical techniques are similar for all the terms arrising in eq. (1-14) we shall demonstrate the derivation only for the parity conserving tensor interaction and for the Fierz interference term between the tensor and axial vector interactions.

Combining eqs. (1-2), (1-5), and (1-10) we have

$$P(\epsilon)d\epsilon = k\eta\epsilon(\epsilon_0-\epsilon)^2 d\epsilon\, \Omega^2 \int d\omega_e \int d\omega_\nu \sum_e \sum_\nu \sum_{m_f} \left| S_j \left(\psi_e^+ O_j [C_j + C_j'\gamma_5]\psi_\nu\right)\left(\int \psi_f O_j \psi_i d\tau_k\right)\right|^2 \quad \text{(A-1)}$$

We now set all C_i and $C_i' = 0$ except for C_T. Eq. (A-1) reduces to the following;

$$P(\epsilon)d\epsilon = k\eta\epsilon(\epsilon_0-\epsilon)^2 d\epsilon\, \Omega^2 \int d\omega_e \int d\omega_\nu \sum_e \sum_\nu \sum_{m_f} \left| C_T C_T^* \sum_k \left(\psi_e^+ \beta\vec{\sigma}\psi_\nu\right)\int \psi_f \beta\vec{\sigma}\psi_i d\tau_k\right|^2 \quad \text{(A-2)}$$

Consider now the term

$$\sum_e \sum_\nu \left| C_T C_T^* \left(\psi_e^+ \beta\vec{\sigma}\psi_\nu\right) \sum_k \int \psi_f \beta\vec{\sigma}\psi_i d\tau_k \right|^2 \quad \text{(A-3)}$$

and denote

$$\sum_k \int \psi_f \beta\vec{\sigma}\psi_i d\tau_k \equiv \langle \beta\vec{\sigma}\rangle \quad \text{(A-4)}$$

The (A-3) is equal to

$$|C_T|^2 \sum_{ij} \sum_{e\nu} \langle \beta\sigma_j\rangle^* \psi_e \beta\sigma_j \psi_\nu \psi_\nu^+ \beta\sigma_i \psi_e \langle \beta\vec{\sigma}_i\rangle \quad \text{(A-5)}$$

where σ_j denotes the j^{th} component of the Dirac vector operator $\vec{\sigma}$.

The $\sum_e \sum_\nu$ denotes summation over the <u>two</u> possible spin states of the electron and neutrino.

The wave functions ψ_e of the electron are the two positive energy solutions of the Dirac equation

$$-(\vec{\alpha}\cdot\vec{\eta}+\beta)\psi_e = E\psi_e \qquad (A\text{-}6)$$

corresponding to the two possible electron spin states. The wave functions ψ_ν are the two negative energy solutions of the Dirac equation

$$-(\vec{\alpha}\cdot\vec{q})\psi_\nu = q\psi_\nu \; . \qquad (A\text{-}7)$$

(ψ_e & ψ_ν are normalized to one over the volume Ω and we set $\Omega=1$ in the following discussion.)

We define the projection operators Λ_e and Λ_ν as follows:

$$2\Lambda_e \equiv -\frac{(\vec{\alpha}\cdot\vec{\eta}+\beta)}{E} + 1 \; , \qquad (A\text{-}8)$$

$$2\Lambda_\nu \equiv -\frac{\vec{\alpha}\cdot\vec{q}}{q} + 1 \; . \qquad (A\text{-}9)$$

It is clear that

$$\Lambda_e\psi_e = \begin{cases} \psi_e & \text{for positive energy states} \\ 0 & \text{for negative energy states} \end{cases} \quad \text{and} \quad \Lambda_\nu\psi_\nu = \begin{cases} 0 & \text{for positive energy} \\ \psi_\nu & \text{for negative energy} \end{cases}$$

Thus (A-5) reduces to

$$|C|^2 \sum_{ij}^{3} \sum_{e\nu}^{4} \langle \beta\sigma_j \rangle^* \psi_e^+ \beta\sigma_j \Lambda_\nu \psi_\nu \psi_\nu^+ \beta\sigma_i \Lambda_e \psi_e \langle \beta\sigma_i \rangle \; . \qquad (A\text{-}10)$$

The spin summation can now be carried over the four possible spin and energy states of the electron and neutrino.

Summation over e and ν states reduces (A-10) to

$$|G|^2 \sum_{ij}^{3} \langle \beta\sigma_j \rangle \langle \beta\sigma_i \rangle \left[\text{Trace}\left(\beta\sigma_j \Lambda_\nu \beta\sigma_i \Lambda_e\right)\right] . \qquad \text{(A-11)}$$

We now demonstrate te evaluation of the trace $(\beta\sigma_j \Lambda_\nu \beta\sigma_i \Lambda_e)$.

$$\text{Tr}\left(\beta\sigma_j \Lambda_\nu \beta\sigma_i \Lambda_e\right) = \frac{\text{Tr}}{4Eq} \left(\beta\sigma_j(-\vec{\alpha}\cdot\vec{\eta} - \beta + E)\beta\sigma_i(-\vec{\alpha}\cdot\vec{q} + q)\right)$$

$$= \frac{1}{4Eq} \text{Tr}\left[\beta\sigma_j\beta\sigma_i Eq - \beta\sigma_j\sigma_i q - \beta\sigma_j(\vec{\alpha}\cdot\vec{\eta})\beta\sigma_i q - \beta\sigma_j\beta\sigma_i(\vec{\alpha}\cdot\vec{q})E + \beta\sigma_j(\vec{\alpha}\cdot\vec{\eta})\beta\sigma_i(\vec{\alpha}\cdot\vec{q}) + \beta\sigma_j\sigma_i(\vec{\alpha}\cdot\vec{q})E\right]$$

In order to evaluate the traces in expression (A-11) it is useful to note some of the properties of the 4x4 Dirac matrices and the traces of products of Dirac matrices as given below .

A. $\vec{\alpha} = \rho\vec{\sigma}$ $\qquad \rho = \begin{pmatrix} 0 & 1 \\ 1 & 0 \end{pmatrix}$

B. $\rho^2 = 1$

C. $\alpha_i^2 = \beta^2 = 1$

D. $\rho\beta + \beta\rho = 0$; $\rho\alpha_i = \alpha_i\rho$

$\alpha_i\alpha_j + \alpha_j\alpha_i = 2\delta_{ij}$; $\alpha_i\beta + \beta\alpha_i = 0$

E. $(\vec{\alpha}\cdot\vec{B})(\vec{\alpha}\cdot\vec{C}) = (\vec{B}\cdot\vec{C}) + i\rho\vec{\alpha}\cdot(\vec{B}\times\vec{C})$

F. $\text{Tr}(\alpha_i) = 0$

$\text{Tr}(\beta) = 0$ $\qquad \text{Tr}(\rho\alpha_i) = 0 \qquad \text{Tr}(\beta\rho\alpha_i) = 0$

$\text{Tr}(\alpha_i\alpha_j) = 4\delta_{ij}$; $\text{Tr}(\alpha\beta) = 0$

$\text{Tr}(\alpha_i\alpha_j\beta) = 0$ for all i, j

$\text{Tr}(\alpha_i\alpha_j\alpha_k) = 0$ for all i, j, k

Thus,

$$Tr(\beta\sigma_j\beta\sigma_i Eq) = Eq\,Tr(\beta\rho\alpha_j\beta\rho\alpha_i) = Eq\,Tr(-\beta\alpha_j\beta\alpha_i) = Eq\,Tr(\alpha_j\alpha_i) = 4Eq\,\delta_{ij}$$

$$Tr(\beta\sigma_j\sigma_i q) = q\,Tr(\beta\rho\alpha_j\rho\alpha_i) = q\,Tr(\beta\alpha_j\alpha_i) = 0$$

$$Tr(\beta\sigma_j(\vec{\alpha}\cdot\vec{\eta})\beta\sigma_i q) = q\,Tr(\beta\rho\alpha_j(\vec{\alpha}\cdot\vec{\eta})\beta\rho\alpha_i) = q\,Tr(-\beta\alpha_j(\vec{\alpha}\cdot\vec{\eta})\beta\alpha_i) = q\,Tr(-\alpha_j(\vec{\alpha}\cdot\vec{\eta})\alpha_i) = 0$$

$$Tr(\beta\sigma_j\beta\sigma_i(\vec{\alpha}\cdot\vec{q})E) = E\,Tr(\beta\rho\alpha_j\beta\rho\alpha_i(\vec{\alpha}\cdot\vec{q})) = -E\,Tr(\beta\alpha_j\beta\alpha_i(\vec{\alpha}\cdot\vec{q})) = E\,Tr(\alpha_j\alpha_i(\vec{\alpha}\cdot\vec{q})) = 0$$

$$Tr(\beta\sigma_j\sigma_i(\vec{\alpha}\cdot\vec{q})E) = E\,Tr(\beta\rho\alpha_j\rho\alpha_i(\vec{\alpha}\cdot\vec{q})) = E\,Tr(\beta\alpha_j\alpha_i(\vec{\alpha}\cdot\vec{q}) = -E\,Tr(\alpha_j\alpha_i(\vec{\alpha}\cdot\vec{q})\beta) = 0$$

$$Tr(\beta\sigma_j(\vec{\alpha}\cdot\vec{\eta})\beta\sigma_i(\vec{\alpha}\cdot\vec{q})) = Tr(\beta\rho\alpha_j(\alpha\cdot\eta)\beta\rho\alpha_i(\vec{\alpha}\cdot\vec{q}) = -Tr(\beta\alpha_j(\vec{\alpha}\cdot\vec{\eta})\beta\alpha_i(\vec{\alpha}\cdot\vec{q})) = -Tr(\alpha_j(\vec{\alpha}\cdot\vec{\eta})\alpha_i(\vec{\alpha}\cdot\vec{q}))$$

Now $\alpha_i = \vec{\alpha}\cdot\hat{\imath}$.

Thus

$$-Tr(\alpha_j(\vec{\alpha}\cdot\vec{\eta})\alpha_i(\vec{\alpha}\cdot\vec{q})) = -Tr[(\hat{\jmath}\cdot\vec{\eta}) + i\rho\vec{\alpha}\cdot(\hat{\jmath}\times\vec{\eta})][(\hat{\imath}\cdot\vec{q}) + i\rho\vec{\alpha}\cdot(\hat{\imath}\times\vec{q})] =$$

$$= -Tr\{(\hat{\jmath}\cdot\vec{\eta})(\hat{\imath}\cdot\vec{q}) - [\vec{\alpha}\cdot(\hat{\jmath}\times\vec{\eta})][\vec{\alpha}\cdot(\hat{\imath}\times\vec{q})] + (\hat{\jmath}\cdot\vec{\eta})i\rho\vec{\alpha}\cdot(\hat{\imath}\times\vec{q}) + [i\rho\vec{\alpha}\cdot(\hat{\jmath}\times\vec{\eta})](\hat{\imath}\cdot\vec{q})$$

$$= -4(\hat{\jmath}\cdot\vec{\eta})(\hat{\imath}\cdot\vec{q}) + Tr([\vec{\alpha}\cdot(\hat{\jmath}\times\vec{\eta})][\vec{\alpha}\cdot(\hat{\imath}\times\vec{q})]) .$$

$$Tr([\vec{\alpha}\cdot(\hat{\jmath}\times\vec{\eta})][\vec{\alpha}\cdot(\hat{\imath}\times\vec{q})]) = Tr((\hat{\jmath}\times\vec{\eta})\cdot(\hat{\imath}\times\vec{q}) + i\rho\vec{\alpha}\cdot[(\hat{\jmath}\times\vec{\eta})\times(\hat{\imath}\times\vec{q})]) = 4(\hat{\jmath}\times\vec{\eta})\cdot(\hat{\imath}\times\vec{q})$$

$$= 4((\hat{\imath}\cdot\hat{\jmath})(\vec{q}\cdot\vec{\eta}) - (\vec{\eta}\cdot\hat{\imath})(\vec{q}\cdot\hat{\jmath})) = 4\vec{\eta}\cdot\vec{q}\,\delta_{ij} - 4\eta_i q_j .$$

Thus collecting terms we have

$$Tr(\beta\sigma_j(\vec{\alpha}\cdot\vec{\eta})\beta\sigma_i(\vec{\alpha}\cdot\vec{q})) = 4(\vec{\eta}\cdot\vec{q})\delta_{ij} - 8\eta_i q_j$$

and

$$Tr(\beta\sigma_j\Lambda_-\beta\sigma_i\Lambda_e) = \delta_{ij} + \frac{1}{Eq}(\vec{\eta}\cdot\vec{q}\,\delta_{ij} - 2\eta_i q_j)$$

Expression (A-11) reduces to

$$|C_T|^2 \sum_{ij} \left[\delta_{ij} + \frac{1}{Eq} \left(\vec{\eta} \cdot \vec{q} \, \delta_{ij} - 2 \eta_i q_j \right) \right] \langle \beta \vec{v}_j \rangle^* \langle \beta \vec{v}_i \rangle$$

$$= |C_T|^2 \left[|\langle \beta \vec{v} \rangle|^2 + \frac{1}{Eq} \left(|\langle \beta \vec{v} \rangle|^2 \vec{\eta} \cdot \vec{q} - 2 \left[\vec{\eta} \cdot \langle \beta \vec{v} \rangle^* \right] \left[q \cdot \langle \beta \vec{v} \rangle \right] \right) \right].$$

Equation (A-2) can now be written as follows:

$$P(\epsilon) d\epsilon = k \eta \epsilon (\epsilon_0 - \epsilon)^2 d\epsilon \int d\omega_e \int d\omega_\nu |C_T|^2 \sum_{m_f} \left[|\langle \beta \vec{v} \rangle|^2 + \frac{1}{Eq} \left(|\langle \beta \vec{v} \rangle|^2 \vec{\eta} \cdot \vec{q} - 2 (\vec{\eta} \cdot \langle \beta \vec{v} \rangle^*)(\vec{q} \cdot \langle \beta \vec{v} \rangle) \right) \right]$$

The evaluation of the last term of the bracket of the above summation on [44] is discussed from the classical point of view by Blatt and Weiskopf. The quantum mechanical evaluation of the sum is given in very general form by Wigner [45]. In both cases the results of the summation are:

$$\sum_{m_f} (\vec{\eta} \cdot \langle \beta \vec{v} \rangle^*)(\vec{q} \cdot \langle \beta \vec{v} \rangle) = \frac{1}{3} \vec{\eta} \cdot \vec{q} \sum_{m_f} |\langle \beta \vec{v} \rangle|^2$$

$$P(\epsilon) d\epsilon = k \eta \epsilon (\epsilon_0 - \epsilon)^2 d\epsilon \int d\omega_e \int d\omega_\nu |C_T|^2 \left(1 + \frac{1}{3} \frac{\vec{\eta} \cdot \vec{q}}{qE} \right) \sum_{m_f} |\langle \beta \vec{v} \rangle|^2$$

This form contains all the terms of equation (1-14) with co-efficients $|C_T|^2$.

We now consider the interference term between the tensor and axial vector interactions (parity conserving terms only). From the form of eq. (A-1) , the interference term is given by:

$$\left| \sum_{m_f} \sum_{e} \sum C_T C_A^* \, \psi_e^+ \beta \vec{\sigma} \psi_\nu \, \psi_\nu^+ \vec{\sigma} \psi_e \langle \beta \vec{\sigma} \rangle^* \langle \vec{\sigma} \rangle + \text{Complex Conj.} \right| . \qquad \text{(A-12)}$$

We now note that according to Eq. (1-12)

$$\langle \beta \vec{\sigma} \rangle = - \langle \vec{\sigma} \rangle .$$

Thus the expression (A-12) reduces to

$$\left| \left(C_A^* C_T + C_A C_T^* \right) \sum_{m_f} \sum_{e}^{2} \sum_{\nu}^{2} \sum_{ij}^{3} \psi_e^+ (\beta \sigma_i) \psi_\nu \psi_\nu^+ \sigma_i \psi_e \langle \beta \vec{\sigma} \rangle_i \langle \beta \vec{\sigma} \rangle_j^* \right|$$

$$= \sum_{m_f} \sum_{ij}^{3} \langle \beta \sigma_i \rangle \langle \beta \sigma_j \rangle^* \left[\text{Trace} \left(\beta \sigma_i \Lambda_\nu \sigma_j \Lambda_e \right) \right] \qquad \text{(A-13)}$$

according to the same method used to obtain expression (A-11).

We now evaluate the Trace in expression (A-13).

$$\text{Trace} \left(\beta \sigma_i \Lambda_\nu \sigma_j \Lambda_e \right) = \frac{\text{Tr}}{4 E q} \left(\beta \sigma_i \left(-\vec{\alpha} \cdot \vec{\eta} - \beta + \epsilon \right) \sigma_j \left(-\vec{\alpha} \cdot \vec{q} + q \right) \right)$$

$$= \frac{1}{4Eq} \Big[\text{Tr} \Big(\beta \sigma_i \sigma_j \epsilon q - \beta \sigma_i (\vec{\alpha} \cdot \vec{\eta}) \sigma_j q + \beta \sigma_i (\vec{\alpha} \cdot \vec{\eta}) \sigma_j (\vec{\alpha} \cdot \vec{q}) + \beta \sigma_i \beta \sigma_j (\vec{\alpha} \cdot \vec{q})$$

$$- \beta \sigma_i \beta \sigma_j q - \beta \sigma_i \sigma_j (\vec{\alpha} \cdot \vec{q}) \epsilon \Big) \Big]$$

By the methods outlined above it is simple to show that all the terms have zero trace except for $\beta \sigma_i \beta \sigma_j q$.

$$Tr(\beta\sigma_i \beta\sigma_j) = Tr(\beta\rho\alpha_i \beta\rho\alpha_j) = -Tr(\beta\alpha_i\beta\alpha_j) = Tr\,\alpha_i\alpha_j = 4\delta_{ij}$$

Thus

$$Tr(\beta\sigma_i \Lambda_v \sigma_j \Lambda_c) = -\frac{1}{E}\delta_{ij} \quad .$$

Therefore the expression (A-12) reduces to

$$(C_A^* C_T + C_A C_T^*)\sum_{m_f}\sum_{ij} \langle\beta\sigma_i\rangle\langle\beta\sigma_j\rangle^* \delta_{ij} = |C_A^* C_T + C_T C_A^*|\;\Big|\sum_{m_f}\langle\beta\hat{\vec{\sigma}}\rangle\Big|^2 .$$

This is just the interference term between the parity conserving tensor and axial vector interactions in eq (1-14).

By using the notation developed above it can be shown that

$$\frac{H_1'}{H_1} = \frac{\int_{X_0-\Delta}^{X_0+\Delta} \frac{F(x)}{X^3}\,dx}{\int_{X_0-\Delta}^{X_0+\Delta} \frac{F(x)}{X^2}\,dx} \cdot \frac{\int_{X_0-\Delta}^{X_0+\Delta} x\,F(x)\,dx}{\int_{X_0-\Delta}^{X_0+\Delta} F(x)\,dx} \qquad \text{(B-20)}$$

By obtaining upper and lower bounds on the integrals in (B-24)(see footnote 2) it can be shown that

$$1-3\lambda^2 < \frac{H_1'}{H_1} < 1+3\lambda^2 \quad .$$

Footnote 2: The maximum and minimum of integrals of the form

$$\int_a^b X^n F(x)\,dx$$

is easily obtained due to the special nature of the function F and the limits of integration.

The conditions

$$F(x) \geq 0 \quad ; \quad b > a \geq 0$$

lead to the following maxima and minima;

$$0 \leq \int_a^b X^n F(x)\,dx \leq \begin{cases} b^n \int_a^b F(x)\,dx & n \geq 0 \\ a^n \int_a^b F(x)\,dx & n \leq 0 \end{cases}$$

APPENDIX B

The equation governing the connection between the spectrum measured by the spectrometer (as a function of magnetic field strength H at some point in the spectrometer) and the momentum distribution of electrons emitted by the source is:

$$S(H) = \int_0^\infty R(H,\eta)\, P(\eta)\, d\eta \qquad \text{(B-1)}$$

where

η = electron momentum

H = magnetic field

S(H) = measured spectrum

$R(H,\eta)$ = response function of the spectrometer

$P(\eta)$ = momentum distribution of the source

$R(H,\eta_1)$ is defined operationally as the response of the spectrometer for a source whose spectrum $P(\eta_1) = \delta(\eta_1)$; for this $P(\eta)$, $R(H,\eta) = S(H)$. The function $R(H,\eta_1)$ can thus be determined experimentally by investigating the spectrum of an internal conversion line of momentum η_1 . $R(H,\eta_1)$ is the measured spectrum of such a source. However, in order to determine $P(\eta)$ from S(H) for a continuous spectrum it is necessary to know $R(H,\eta)$ for all η . If we consider a spectrometer and source arrangement conforming to the following conditions:

A. The magnetic field shape is independent of field magnitude,

B. The geometry of the collimating or baffle system is unchanged when the field is varied,

C. The angular distribution of electrons from the source is not a function of momentum,

D. Scattering effects are neglected in $R(H,\eta)$,

then the function $R(H,\eta)$ has the simple property that

$$R(H,\eta) = F\left(\frac{\eta}{H}\right) \quad . \tag{B-2}$$

We shall attempt to indicate the physical reasons for this relationship. It follows from a consideration of the motion of electrons in magnetic fields and other purely geometric considerations:

1. It can be shown that an electron of momentum $\vec{\eta}$ at $\vec{r} = 0$ has a trajectory in an arbitrary magnetic field $H(x,y,z)$ which is identical in space to the trajectory of an electron of momentum $k\vec{\eta}$ at $\vec{r} = 0$ in a field $kH(x,y,z)$ where k is a constant. This identity of trajectories is true for relativistic electrons if radiation can be neglected (as is the case for beta-ray spectrometer trajectories).

2. Because of (1) any small (infinitesimal) bundle of possible electron trajectories which pass through the collimating or baffle system corresponds to a fixed spread of values of $\frac{\eta}{H}$ and a fixed solid angle at the source. From the operational definition for $R(H,\eta)$ in terms of the $S(H)$ of a δ function source relation (2) then follows directly.

We shall attempt to prove that for all magnetic spectrometers, which conform to the conditions A to D mentioned above, the equation

$$P(\eta) = \frac{kS(H)}{H} \tag{B-3}$$

where k is a constant,

is an excellent approximation for the correct solution of the integral equation (B-1) in the momentum region below several resolution widths from the end point of a continuous spectrum.

We shall show that the approximation given in eq. (B-3) is valid under very general conditions which hold for all presently used variable magnetic field spectrometers. These conditions are

A. The function $R(H,\eta) = F\left(\frac{\eta}{H}\right)$ as discussed above.

B. The function $R(H,\eta)$ has a value zero except in a small range of values of η/H, i.e. the full width of the function $R(H,\eta)$ is only several per cent in H for a given η. Eq. (B-3) is a good approximation independent of the detailed shape of the function $R(H,\eta)$.

We shall demonstrate the validity of eq. (B-3) by calculating the function $G(\eta) = \frac{S(H)}{k\,H\,P(\eta)}$ in terms of the full fractional width $2r$ of the resolution function $R(H,\eta)$ by the use of eq. (B-1) (the exact equation). We shall show that $G(\eta)$ differs from one by a quantity significantly smaller than r (except in the region of the end point).

It should be emphasized that much smaller limits can be set on the deviation of $G(\eta)$ from the one we set here if certain more specific assumptions are made regarding the detailed nature of the function $R(H,\eta)$, for example its symmetry properties.

(We have shown by numerical integration (see Chapter VII) that for the particular resolution function of our thin lens spectrometer, if $P(\eta)$ is a simple allowed β-spectrum, that below several resolution widths from the spectrum end point

$$.999 < G(\eta) < 1.001 \quad .)$$

Let us now consider the relation between S(H) for a continuous spectrum $P(\eta)$. Perform a Taylor series expansion for $P(\eta)$ about η_1.

$$P(\eta) = P(\eta_1) + \left.\frac{dP}{d\eta}\right]_{\eta_1}(\eta-\eta_1) + \frac{1}{2}\left.\frac{d^2P}{d\eta^2}\right]_{\eta_1}(\eta-\eta_1)^2 + \sum_{n=3}^{\infty}\frac{1}{n!}\frac{d^nP}{d\eta^n}(\eta-\eta_1)^n \qquad \text{(B-4)}$$

We substitute Eq (B-4) into Eq. B-1

$$S(H) = P(\eta_1)\int_0^\infty R(H,\eta)d\eta + \left.\frac{dP}{d\eta}\right]_{\eta_1}\int_0^\infty(\eta-\eta_1)R(H,\eta)d\eta + \frac{1}{2}\frac{d^2P}{d\eta^2}\int_0^\infty(\eta-\eta_1)^2R(H,\eta)d\eta$$
$$+\sum_{n=3}^{\infty}\frac{1}{n!}\frac{d^nP}{d\eta^n}\int_0^\infty(\eta-\eta_1)^nR(H,\eta)d\eta \qquad \text{(B-5)}$$

We now make use of the property of the function $R(H,\eta)$ as evidenced by Eq. (B-2) and also change variables according to the definition;

$$\chi \equiv \eta/H$$

$$S(H) = HP(\eta_1)\int_0^\infty F(x)dx + H\left.\frac{dP}{d\eta}\right]_{\eta_1}\int_0^\infty(Hx-\eta_1)F(x)dx + \frac{H}{2}\left.\frac{d^2P}{d\eta^2}\right]_{\eta_1}\int_0^\infty(Hx-\eta_1)^2F(x)dx$$
$$+H\sum_{n=3}^{\infty}\frac{1}{n!}\left.\frac{d^nP}{d\eta^n}\right]_{\eta_1}\int_0^\infty(Hx-\eta_1)^nF(x)dx \qquad \text{(B-6)}$$

The identification can now be made between H and η in terms of the following equation which defines H, corresponding to η_1 (thus defining the spectrometer calibration constant).

We set

$$\int_0^\infty(H_1x-\eta_1)F(x)dx = 0 \quad = \quad \left[\int_0^\infty(\eta-\eta_1)R(H_1,\eta)d\eta\right] \qquad \text{(B-7)}$$

(see footnote 1 at end of appendix B.

Then Eq. (B-6) reduces to

$$S(H_1) = H_1 P(\eta_1)\int_0^\infty F(x)dx + \frac{H_1}{2}\frac{d^2P}{d\eta^2}\Big]_{\eta_1}\int_0^\infty (H_1x-\eta_1)^2F(x)dx + H_1\sum_{n=3}^{\infty}\frac{1}{n!}\frac{d^nP}{d\eta}\Big]_{\eta_1}\int_0^\infty (H_1x-\eta_1)^nF(x)dx \qquad \text{(B-8)}$$

We define the constant K according to

$$K \equiv \int_0^\infty F(x)dx \qquad \text{(B-9)}$$

then

$$\frac{S(H_1)}{H_1K} = P(\eta_1)\left[1 + \frac{1}{2KP(\eta_1)}\frac{d^2P}{d\eta^2}\Big]_{\eta_1}\int_0^\infty (H_1x-\eta_1)^2F(x)dx + \frac{1}{KP(\eta_1)}\sum_{n=3}^{\infty}\frac{1}{n!}\frac{d^nP}{d\eta^n}\Big]_{\eta_1}\int_0^\infty (H_1x-\eta_1)^nF(x)dx\right] \qquad \text{(B-10)}$$

Let us define the bracket of Eq. (B-10) as $G(\eta_1)$. Then

$$\frac{S(H_1)}{K H_1} = G(\eta_1)\,P(\eta_1)$$

We now consider the function $G(\eta)$. We shall show that if $P(\eta_1)$ represents a continuous spectrum, if the resolution is good, and if we consider values of η at least several resolution widths from the end point of the spectrum, that

$$G(\eta_1) \approx 1$$

and therefore that

$$\frac{S(H_1)}{K H_1} = P(\eta_1) \qquad \text{(B-12)}$$

is an excellent approximation to the true solution of the integral equation (B-1).

By good resolution we imply that

$$F(x) \neq 0 \qquad x_0 - \Delta \leq x \leq x_0 + \Delta$$

$$F(x) = 0 \qquad x > x_0 + \Delta \quad x < x_0 - \Delta \qquad \text{(B-13)}$$

where $\frac{\Delta}{x_0} \equiv \rho \approx$ several per cent

Now, by the Remainder theorem for the Taylor expansion we may cut off the sum of eq. (B-10) at $n = 2$ so that now

$$G(\eta_1) = 1 + \frac{1}{2K P(\eta_1)} \left.\frac{d^2P}{d\eta^2}\right]_{\eta_1'} \int_{x_0-\Delta}^{x_0+\Delta} (H_1 x - \eta_1)^2 F(x)\, dx \qquad \text{(B-14)}$$

where

$$\eta_1(1-\rho) < \eta_1' < \eta_1(1+\rho) \,. \qquad \text{(B-15)}$$

Equation (B-14) is exact as long as we are sufficiently removed from the end point of the spectrum $P(\eta)$ where $P(\eta)$ is no longer analytic..

Now by the use of eq.(B-7) to relate H_1 to η_1 we find:

$$\frac{1}{2K} \int_{x_0-\Delta}^{x_0+\Delta} (H_1 x - \eta_1)^2 F(x)\, dx = \eta_1^2 \left[\frac{\int_{x_0-\Delta}^{x_0+\Delta} F(x)\, dx \int_{x_0-\Delta}^{x_0+\Delta} x^2 F(x)\, dx}{\left(\int_{x_0-\Delta}^{x_0+\Delta} x F(x)\, dx\right)^2} - \right] \qquad \text{(B-16)}$$

Now since $F(x) \geq 0$, it can be shown that: (see footnote 2 at end of appendix B)

$$\left| \frac{\int_{x_0-\Delta}^{x_0+\Delta} F(x)\,dx \int_{x_0-\Delta}^{x_0+\Delta} x^2 F(x)\,dx}{\left[\int_{x_0-\Delta}^{x_0+\Delta} x\,F(x)\,dx\right]^2} - 1 \right| < \rho^2 \qquad \text{(B-17)}$$

Thus $G(\eta)$ is given by

$$|G(\eta) - 1| < \left| \rho^2 \left[\frac{1}{2P(\eta)} \frac{d^2P}{d\eta^2} \right]_{\eta'} \eta^2 \right| \qquad \text{(B-18)}$$

If $P(\eta)$ is of the form $P(\eta) = \eta^2(\epsilon_0 - \epsilon)^2$ then, except within ~10% of the momentum corresponding to η, the bracket of equation (B-18) is less than 20. Thus it is seen that in this energy range, and for a resolution of 2%, $G(\eta)$ differs from one by less than 0.8%

Footnote 1; For the purposes of mathematical simplicity we have defined the relation between H and η according to eq. (B-7). In practice the identification is made by the use of a mathematically similar relation but, a physically totally different equation. That equation is

$$\int_0^\infty (H - H_1')\, F\left(\frac{\eta}{H}\right) dH = 0 \qquad \text{(B-19)}$$

rather than

$$\int_0^\infty (\eta - \eta_1)\, F\left(\frac{\eta}{H_1}\right) d\eta \qquad \text{(B-7)}$$

It can, however, be shown that in the limit of good resolution H_1 differs from H_1' by terms of order ρ^2

APPENDIX C

Effect of Neon Contaminant on Limits of α and β

The Ne^{23} contaminant of the He^6 is discussed in Chapter IV. The spectrum of Ne^{23} is subtracted from the gross spectrum of $He^6 + Ne^{23}$ according to eq. (7-5). The value of Q in that equation is the percentage of Ne^{23} subtracted from the gross spectrum. It is shown in that section, that analysis of the upper end of the gross spectrum provides a value of $Q = 5.4 \pm 1.0$ o/o.

The analysis of the resulting spectrum with $Q = 5.4$ o/o for limits on Fierz interference and pseudoscalar coupling is discussed in Chapter VIII. We have performed identical least squares analyses to determine both α and β, using the He^6 spectra resulting from eq. (7-5) with $Q = 2.4$ o/o, 4.4 o/o, 5.4 o/o, 6.4 o/o, and 8.4 o/o.

Analysis for α (assuming $\beta = 0$)

Curves similar to these shown in figure 15 are given in figures 21a and 21b for different values of Q. Figure 22 shows a curve of $\delta(\frac{b}{a})$ vs $\frac{b}{a}$ where $\frac{b}{a}$ is that value obtained from the least square fit with the appropriate parameters ϵ_o and Q. $\delta(\frac{b}{a})$ is given in eq. (8-8) and is calculated for each of the 25 least square fits. The points are plotted independently of the parameters used and are coded according to the values of the parameter Q. in Fig. 22.

The results of these calculations shown in the figure 22 are to be interpreted as follows.

1. The "best fit" for each value of Q determines the parameter ϵ_o slightly differently for each Q.

2. The value of b/a and the quantity $\delta(\frac{b}{a})$ obtained for the best fit for each Q are essentially identical and independent of Q in the range considered. This is evidenced by the fact that the minimum of the curve of $\delta(\frac{b}{a})$ vs b/a of figure 22 is independent of the value of Q.

This result can be explained in the following manner. The subtraction of several per cent of the Ne^{23} β spectrum from the He^6 β spectrum affects the He^6 spectrum shape in the regions of sensitivity to the $1/\epsilon$ correction factor by essentially multiplying the He^6 spectrum by a function very similar to $\left(\frac{\epsilon_o' - \epsilon}{\epsilon_o - \epsilon}\right)^2$ where ϵ_o is the true end point energy of the He^6 spectrum and ϵ_o' is slightly different from ϵ_o and depends upon the percentage of Ne^{23}. Examination of eq. (8-1) will show that multiplication of a β-spectrum by $\left(\frac{\epsilon_o' - \epsilon}{\epsilon_o - \epsilon}\right)^2$ effects only the end point but not the "shape."

Analysis for β (assuming $\alpha = 0$)

Curves similar to these shown in figure 17 are given in figure 23 for three values of Q = 4.4, 5.4 and 6.4 o/o. Figure 24 shows a curve of $\delta(\frac{d}{e})$ vs $\frac{d}{c}$. As in figure 22, in this figure all values of parameter Q and ϵ_o are again included and coded according to the parameter Q.

As in the analysis for α, it is seen that good fits of the experimental to the theoretical correction factor can be obtained only

for a small region of $\cdot \frac{c}{d}$ independent of Q.

The envelope of points on this plot is almost identical to that obtained for Q = 5.4 e/e and the fit is thus insensitive to Q.

The critical regions in the fit for the pseudoscalar interaction correction factor are sufficiently different from those for the $1/\epsilon$ dependence so that contrary to the analysis for α , some values of Q cannot lead to a good fit for β no matter what value of ϵ_0 is chosen. This results from the qualitative fact that the $1/\epsilon$ dependence for large values of α cannot significantly affect the shape of the upper end of the spectrum whereas the pseudoscalar correction factor has an effect upon the upper energy region. The upper energy region is the most seriously affected part of the spectrum as the value of Q is varied.

Conclusion

From this analysis we conclude that the uncertainty in the experimental determination of Q (from the Ne^{23} Kurie plot in the region $\epsilon > \epsilon_{max\ He^6}$ produces an uncertainty in the value of ϵ_0 for the He^6 spectrum of order 0.02 mc^2 (.01$\frac{1}{2}$ Mev) but produces essentially no uncertainty in the limits of α and β. This conclusion is drawn from the fact that no matter what value of Q is chosen for the particular least squares fit, the best fit is always obtained with the same value of either α or β.

REFERENCES

1. Fermi, Zeit. fur Physik 88, 161 (1934).
2. Schiff, Quantum Mechanics, McGraw-Hill Book Co., New York (1949), p. 312.
3. Yang and Tiomno, Phys. Rev. 79, 495 (1950).
4. Wu, Ambler, Hayward, Hoppes and Hudson, Phys. Rev. 105, 1413 (1957).
5. Lee and Yang, Phys. Rev. 104. 254 (1955), and several articles in press.
6. Tolhoek and DeGroot, Physica XVI, 456 (1950).
7. Tables for the Analysis of β-Spectra, National Bureau of Standards Applied Mathematics Series 13, USGPO, Washington, D. C. (1952).
8. Rose, Dismuke, Perry and Bell, Oak Ridge National Laboratory Report No. 1222; also see reference 11.
9. M. E. Rose, Phys. Rev. 49, 727 (1936).
10. J. R. Reitz, Phys. Rev. 77, 10 (1950).
11. Siegbahn, β and γ Ray Spectroscopy, North Holland Publishing Co. (1955).
12. Sherr and Miller, Phys. Rev. 93, 1076 (1953).
13. Garwin, Lederman and Weinrich, Phys. Rev. 105, 1415 (1957).
14. Fujita and Yamada, Prog. Theor. Physics 10, 518 (1953).
15. Alaga, Kofoed-Hansen and Winther, Dan. Mat. Fys. Medd. 28, no. 3 (1953).
16. Ruderman, Phys. Rev. 89, 1227 (1953).
17. Knipp and Uhlenbeck, Physica 3, 425 (1936).
18. Siegbahn, β and γ Ray Spectroscopy (1955), Chapter XX by C. S. Wu.
19. Kofoed-Hansen, Phil. Mag 42, 1411 (1951).
20. Winther and Kofoed-Hansen, Dan. Mat. Fys. Medd. 27, no. 14 (1953).
21. Ajzenberg and Lauritsen, Rev. Mod. Phys. 27, 73 (1955).
22. Rustad and Ruby, Phys. Rev. 89, 880 (195); W. J. Knox, Phys. Rev. 74, 1192 (1948).

23. Ajzenberg and Lauritsen, Rev. Mod. Phys. 27, 73 (1955).

24. Zaffarano and Kline, Phys. Rev. 96, 1620 (1954).

25. Allen, Almquist, Dewan and Pepper, Phys. Rev. 96, 684 (1954).

26. Curran, Angus and Cockroft, Phil. Mag. 40, 53 (1949).

27. Hanna and Pontecorvo, Phys. Rev. 75, 983 (1949).

28. Li, Whaling, Fowler and Lauritsen, Phys. Rev. 83, 512 (1951).

29. Collins, McKenzie and Raum, Proc. Royal Soc. (London) A216, 242 (1953).

30. Perez-Mendez and Brown, Phys. Rev. 77, 404 (1950).

31. Wu, Rustad, Perez-Mendez and Lidofsky, Phys. Rev. 87, 1140 (1952).

32. A. I. Baz, Izvest. Akad. Nauk SSSR Ser. Fiz. 19, 363 (1955).

33. Kofoed-Hansen and Winther, Physica 18, 1079 (1952), Dan. Mat. Fys. Medd. 27, no. 14 (1953); and private communication.

34. Rustad and Ruby, Phys. Rev. 97, 991 (1955).

35. Hornyak, Lauritsen and Rasmussen, Phys. Rev. 76, 731 (1949).

36. D. E. Alburger, Phys. Rev. 92, 1257 (1953).

37. Feldman and Wu, Phys. Rev. 76, 697 (1949).

38. Schwarzschild, Rustad and Wu, Phys. Rev. 103, 1796 (1956).

39. Mahmoud and Konopinski, Phys. Rev. 88, 1266 (1952).

40. Davidson and Peaslee, Phys. Rev. 91, 1232 (1953).

41. Pohm, Waddel and Jensen, Phys. Rev. 101, 1315 (1956).

42. Driver, Moljk and Scobie, Phil. Mag. Vol. 1 eighth ser. 10, 942 (1956).

43. Brysk, Phys. Rev. 94, 1794 (1954).

44. Blatt and Weisskopf, Theoretical Nuclear Physics, John Wiley and Sons, New York (1952).

45. Wigner, Gruppentheorie und ihre Anwendung auf die Quantenmechanik der Atomspektren, Friedr. Vieweg und Sohn, Braunscweig (1931).

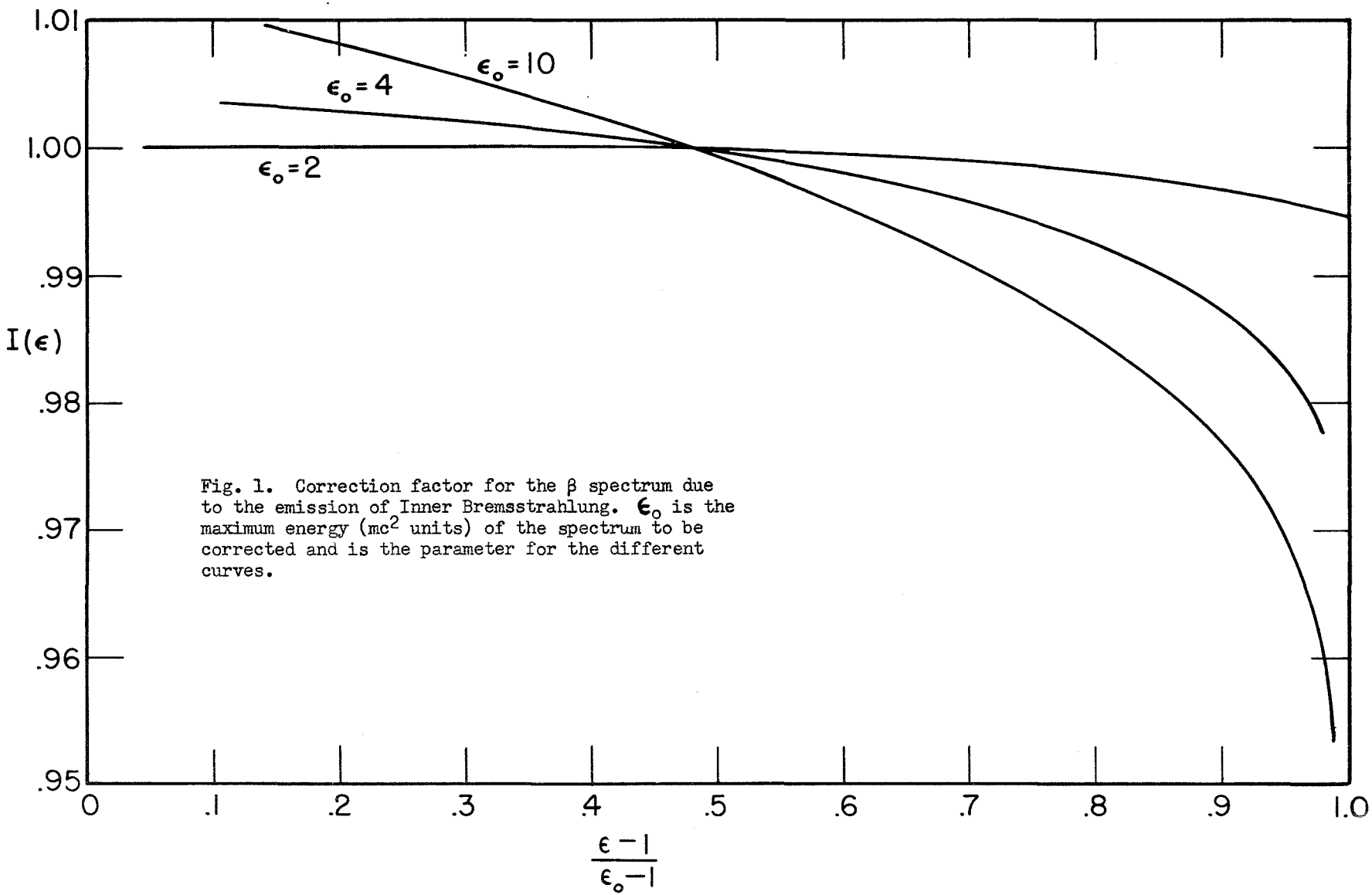

Fig. 1. Correction factor for the β spectrum due to the emission of Inner Bremsstrahlung. ϵ_0 is the maximum energy (mc^2 units) of the spectrum to be corrected and is the parameter for the different curves.

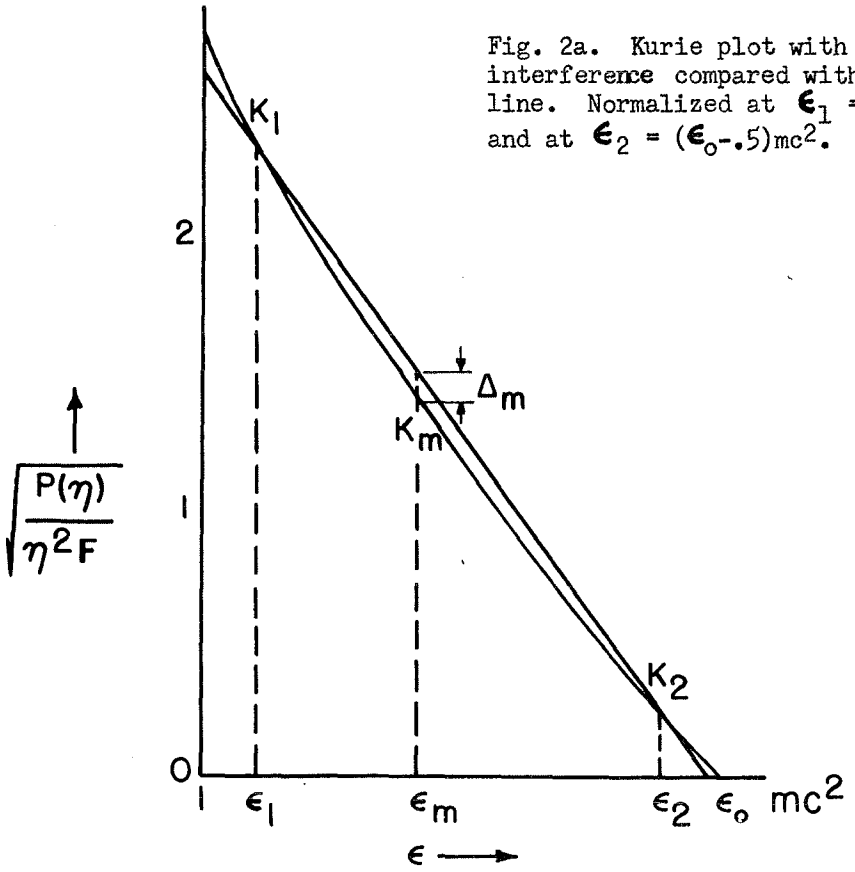

Fig. 2a. Kurie plot with Fierz interference compared with straight line. Normalized at $\epsilon_1 = 1.5\ mc^2$ and at $\epsilon_2 = (\epsilon_o - .5)mc^2$.

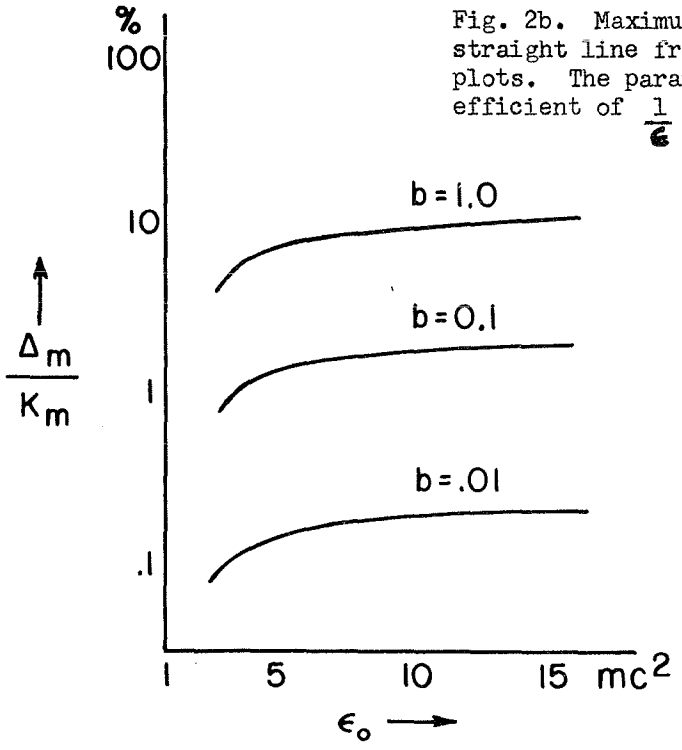

Fig. 2b. Maximum deviation of the straight line from the curved Kurie plots. The parameter b is the coefficient of $\frac{1}{\epsilon}$ term in curved plot.

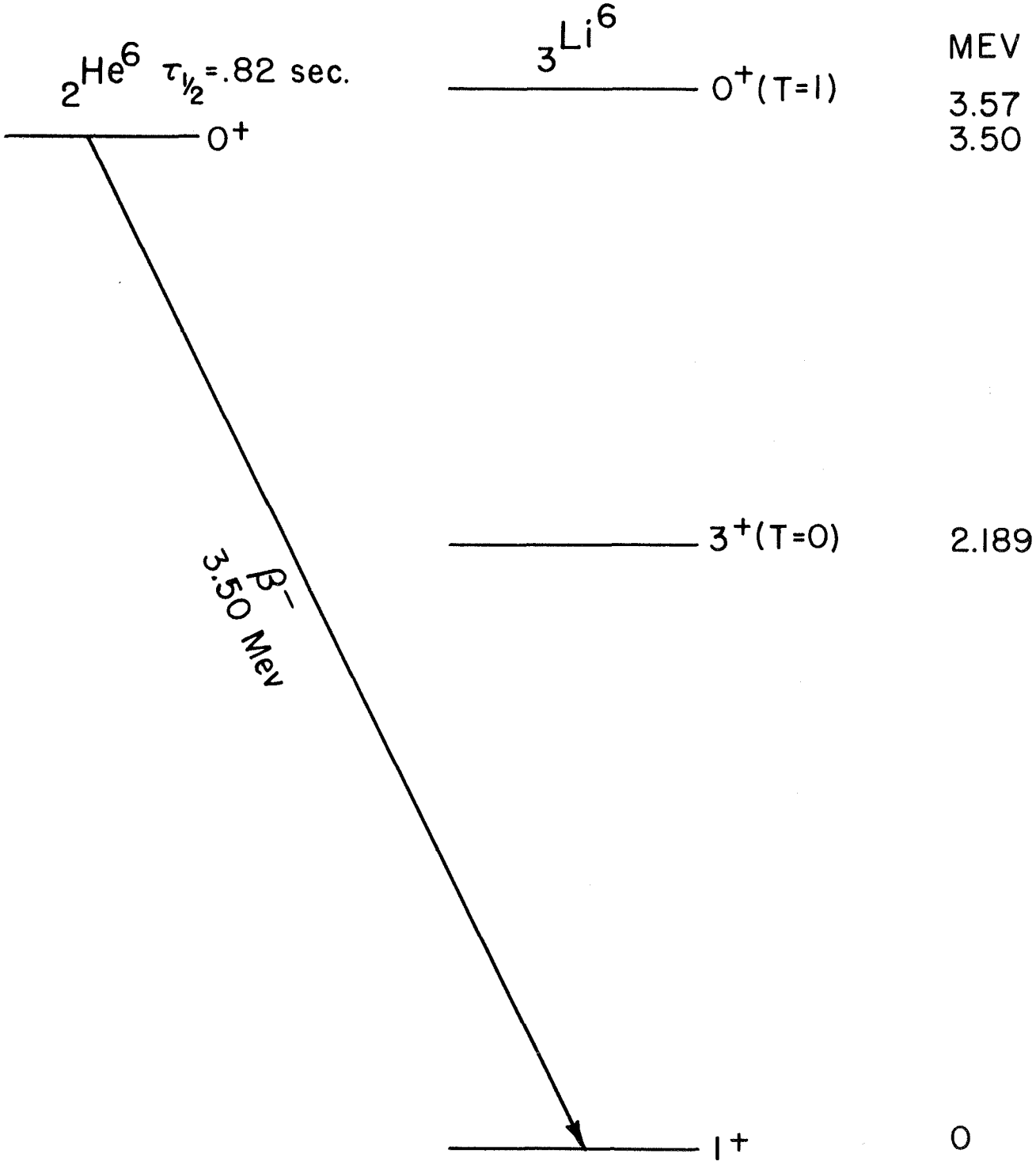

Fig. 3. Decay scheme of He^6 and levels of Li^6.

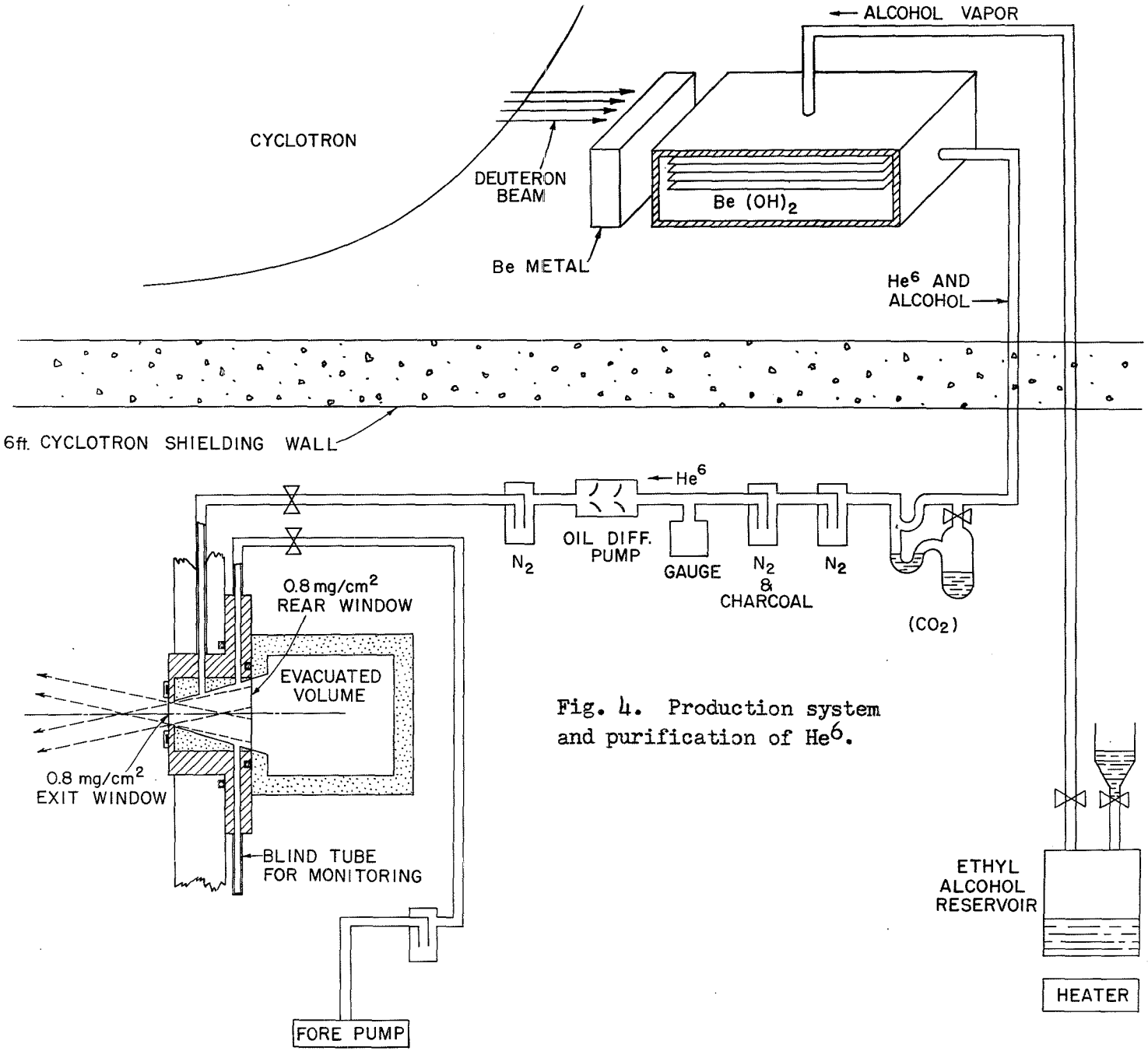

Fig. 4. Production system and purification of He^6.

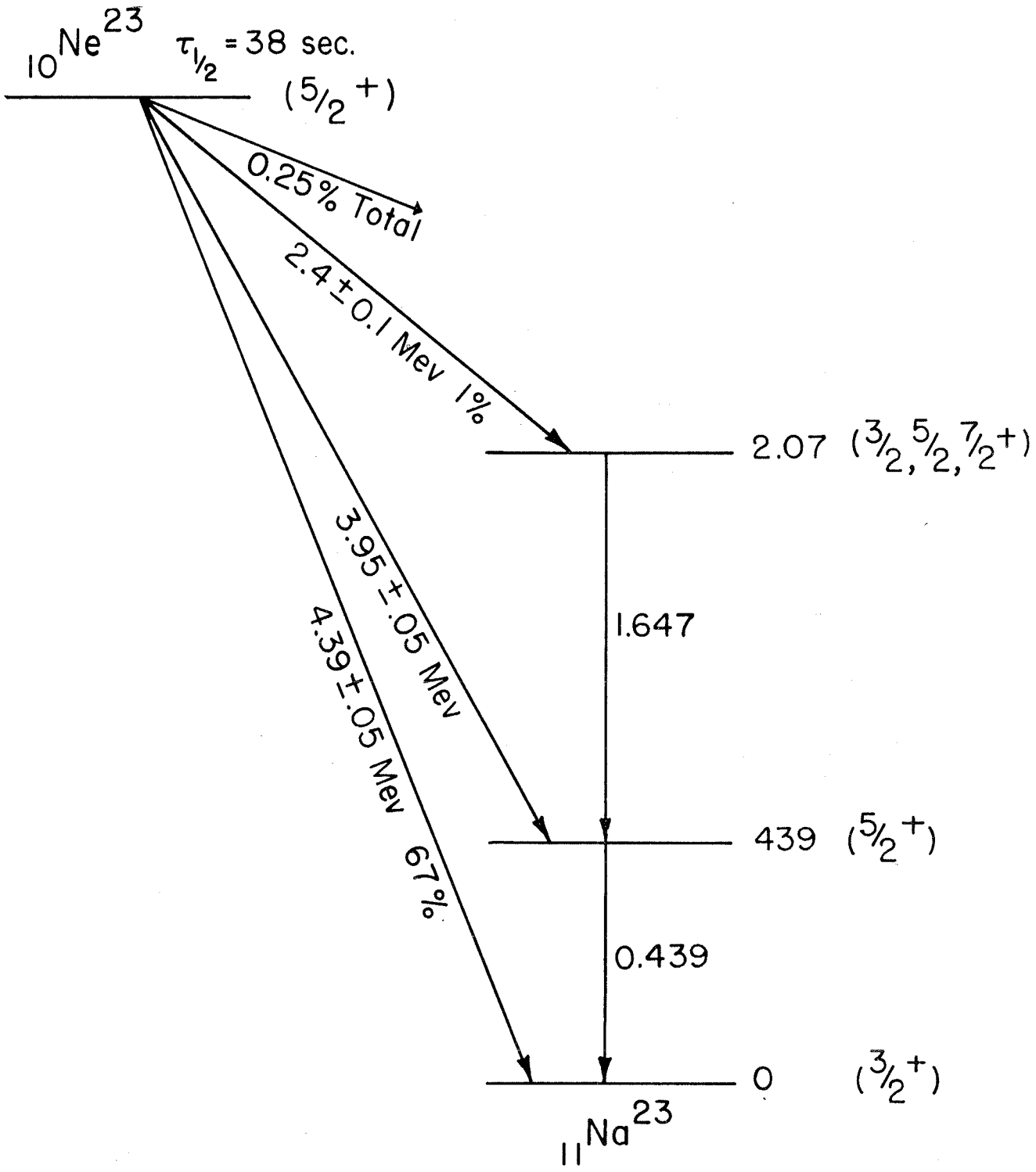

FIG. 5

DECAY SCHEME OF Ne^{23}

PENNING & SCHMIDT, PHYS. REV. 105, 650 (1957)

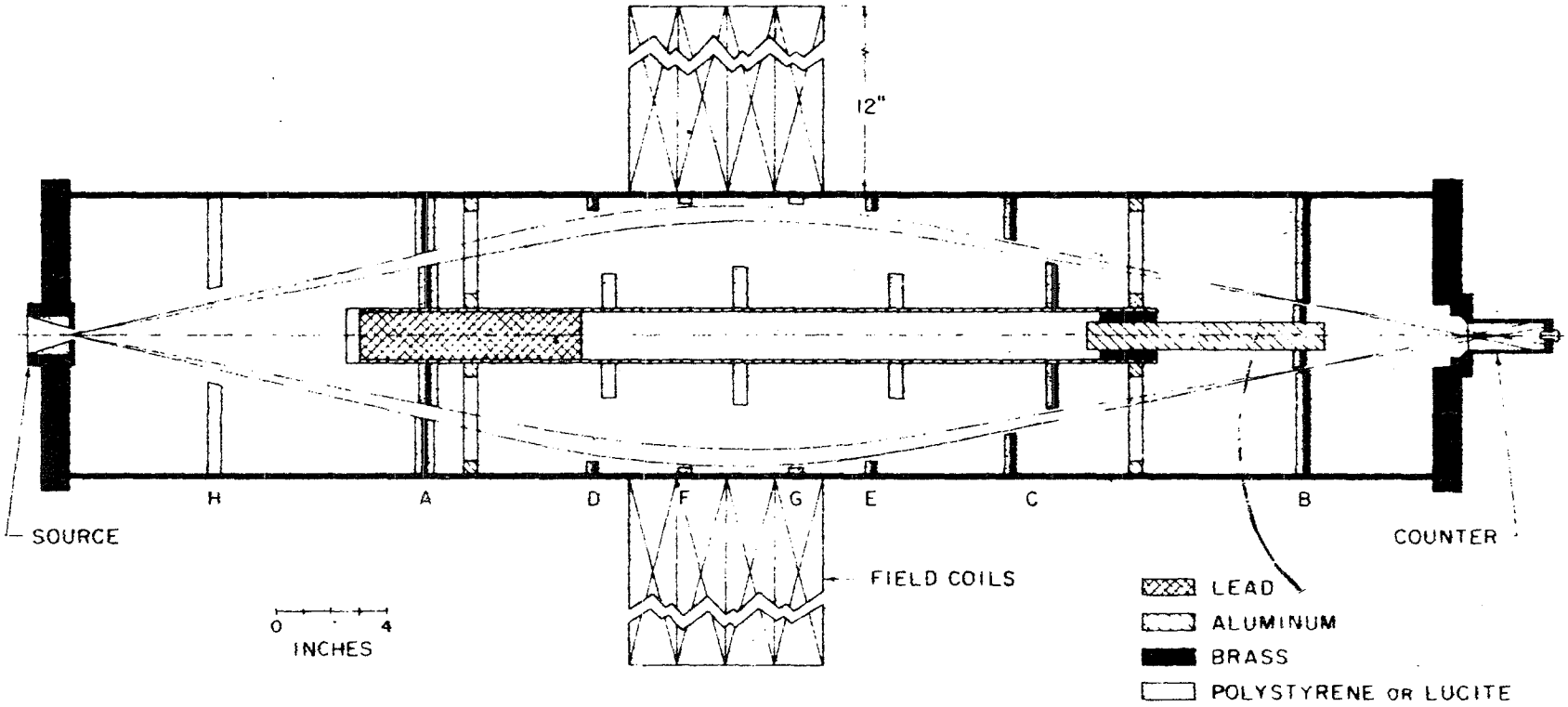

Fig. 6. Thin lens spectrometer

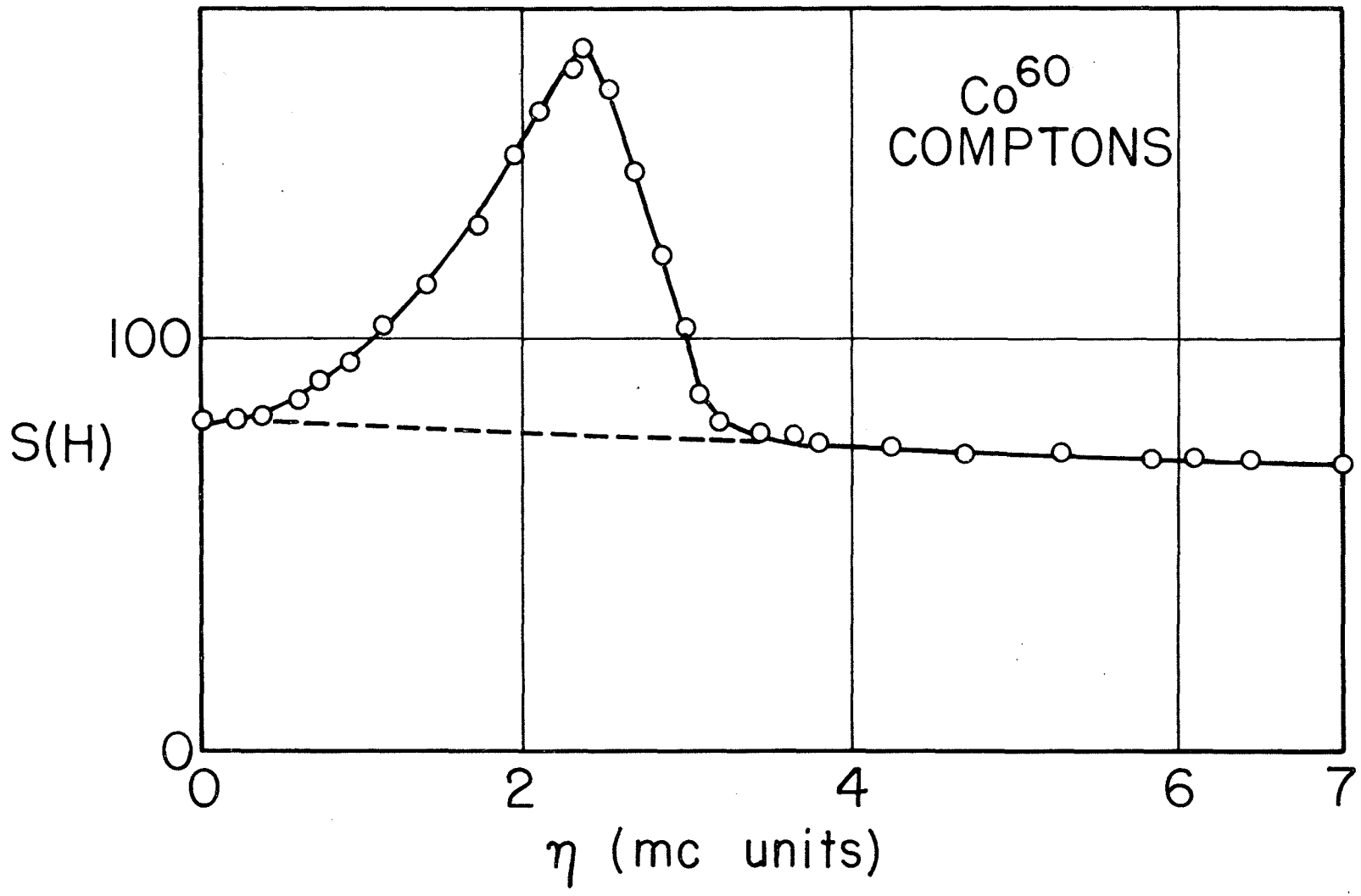

Fig. 7. Distribution of electrons reaching the lens spectrometer detector from a gamma ray source in the source volume.

SCINTILLATION SPECTRA OF ELECTRONS TRANSMITTED BY THIN LENS SPECTROMETER

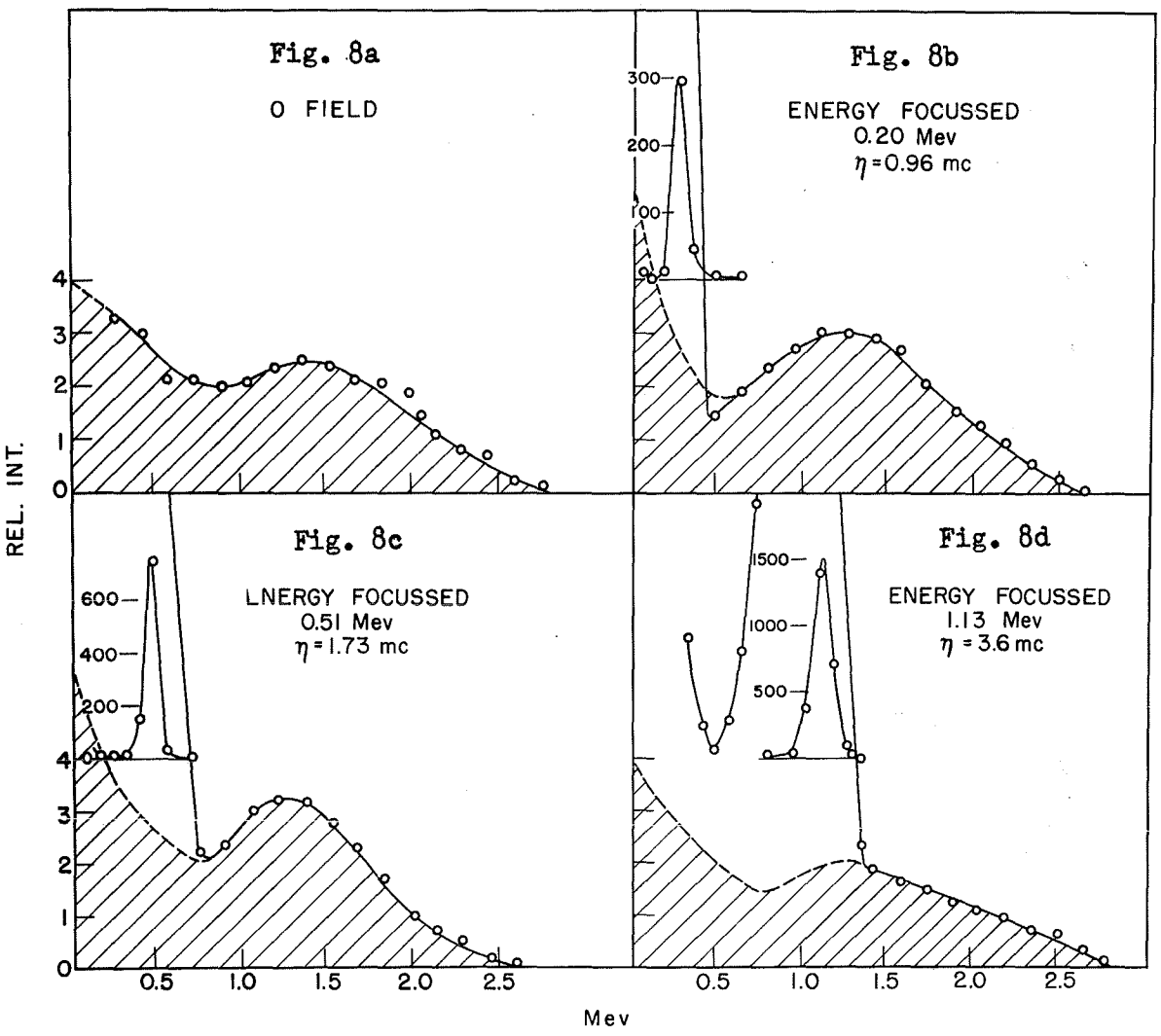

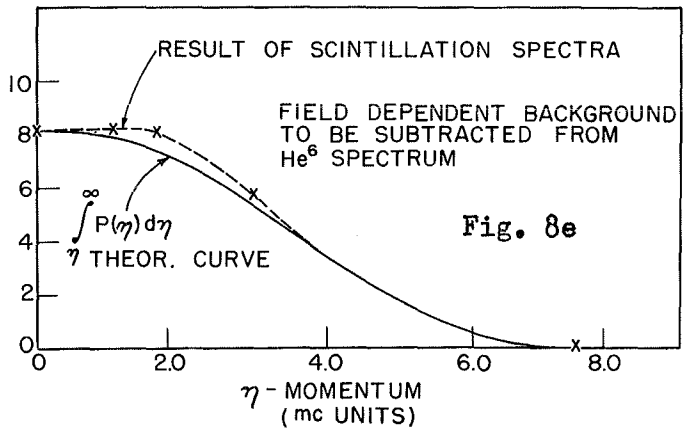

Fig. 8e

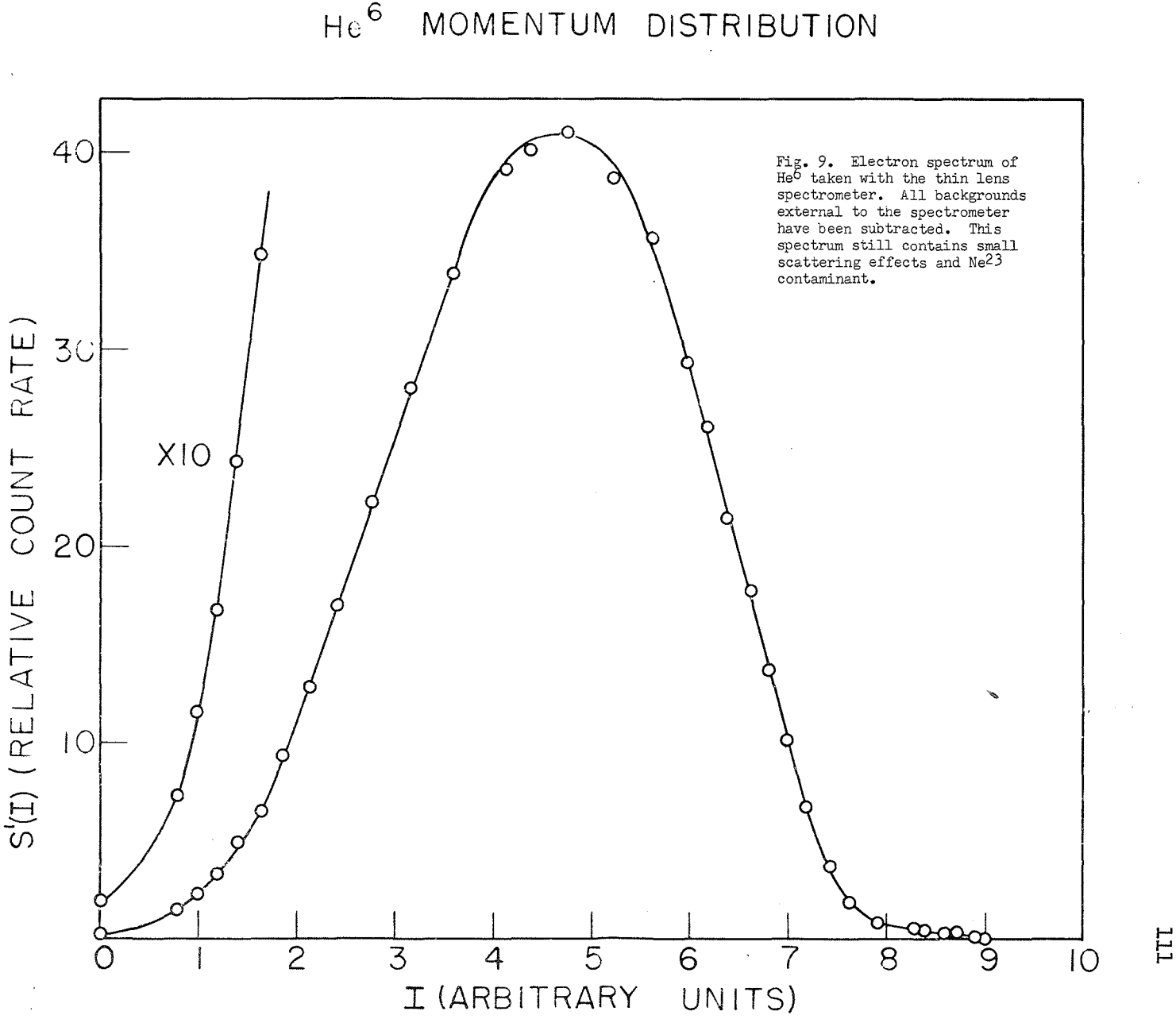

Fig. 9. Electron spectrum of He^6 taken with the thin lens spectrometer. All backgrounds external to the spectrometer have been subtracted. This spectrum still contains small scattering effects and Ne^{23} contaminant.

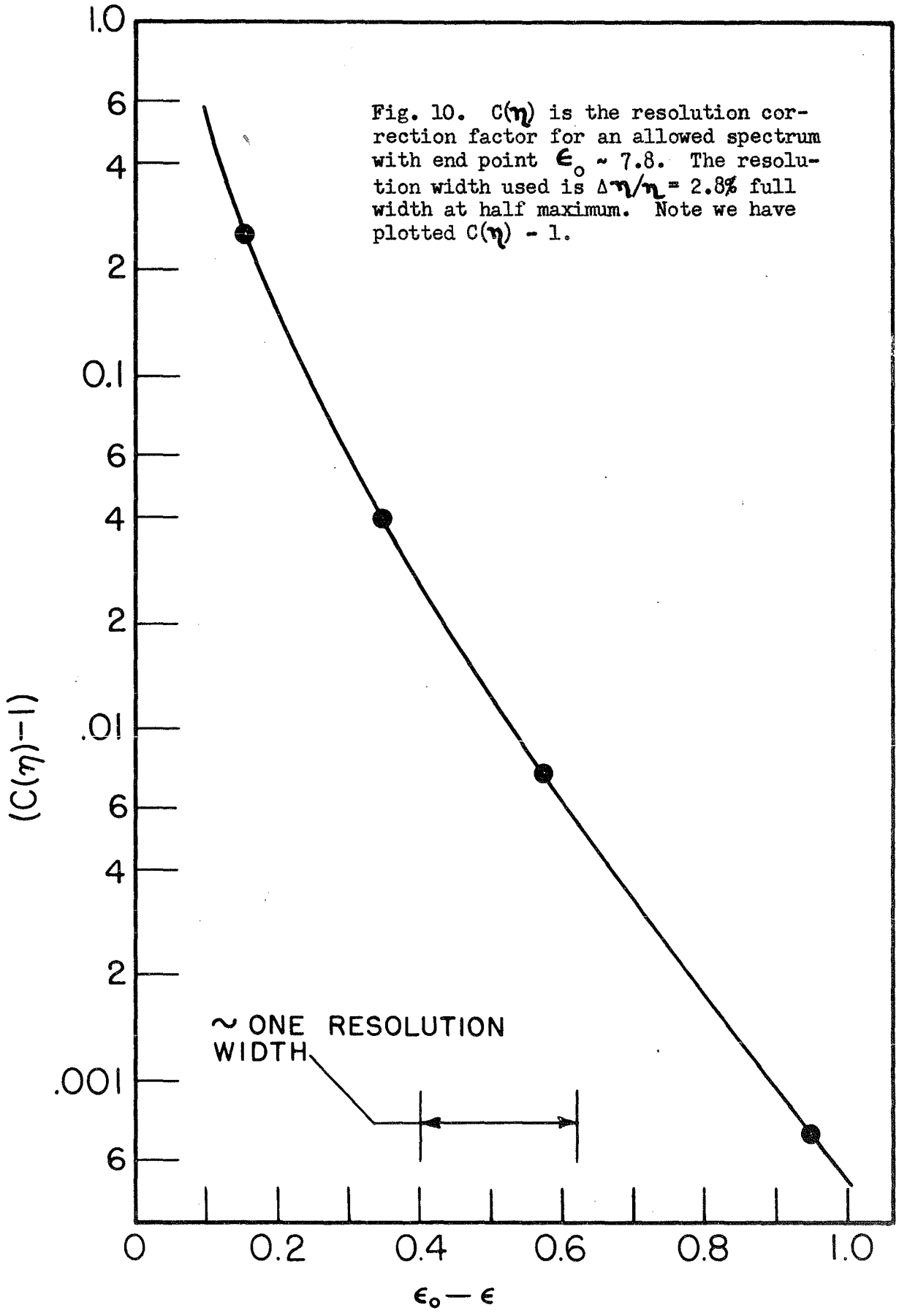

Fig. 10. $C(\eta)$ is the resolution correction factor for an allowed spectrum with end point $\epsilon_0 \sim 7.8$. The resolution width used is $\Delta\eta/\eta = 2.8\%$ full width at half maximum. Note we have plotted $C(\eta) - 1$.

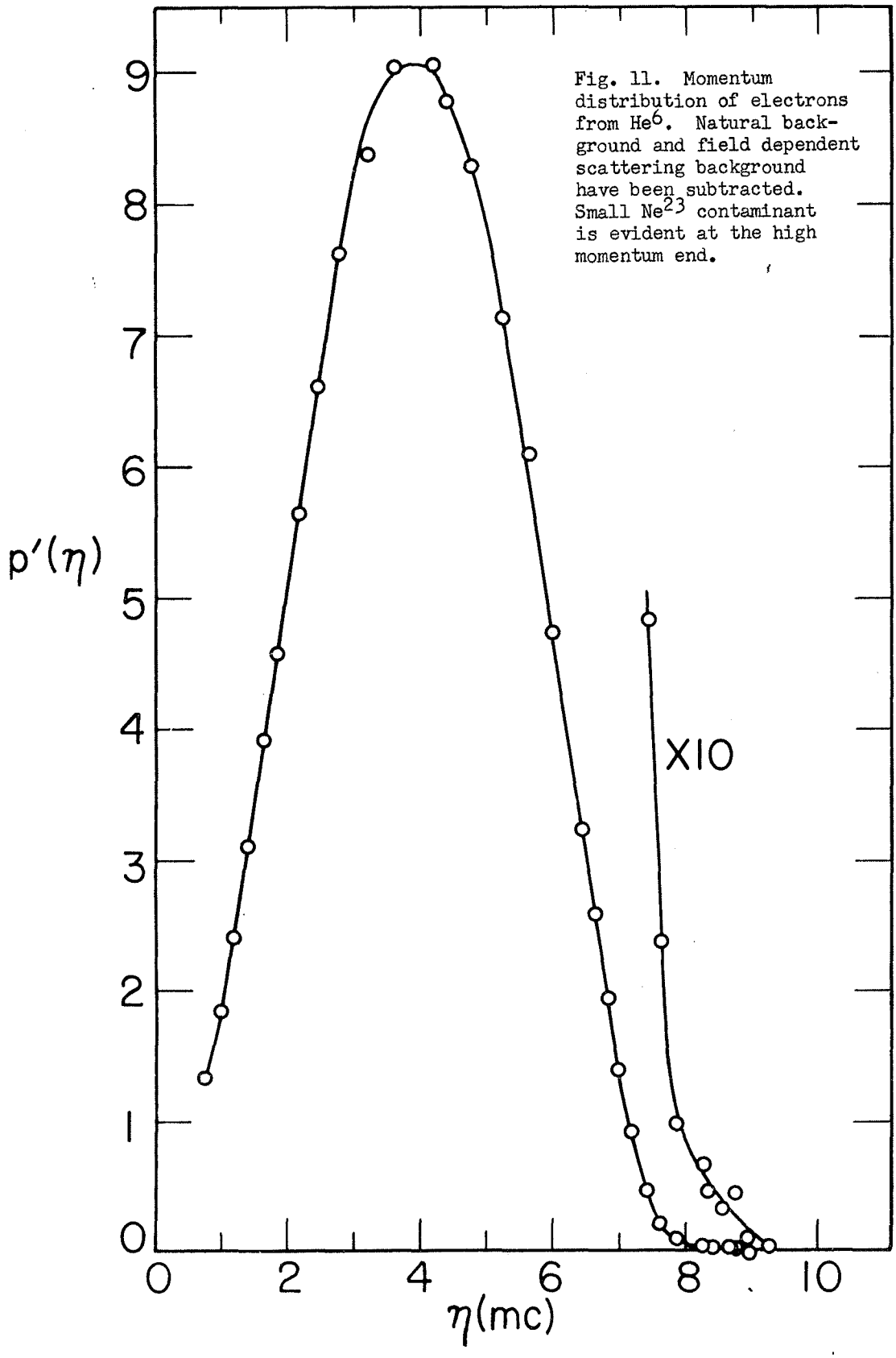

Fig. 11. Momentum distribution of electrons from He^6. Natural background and field dependent scattering background have been subtracted. Small Ne^{23} contaminant is evident at the high momentum end.

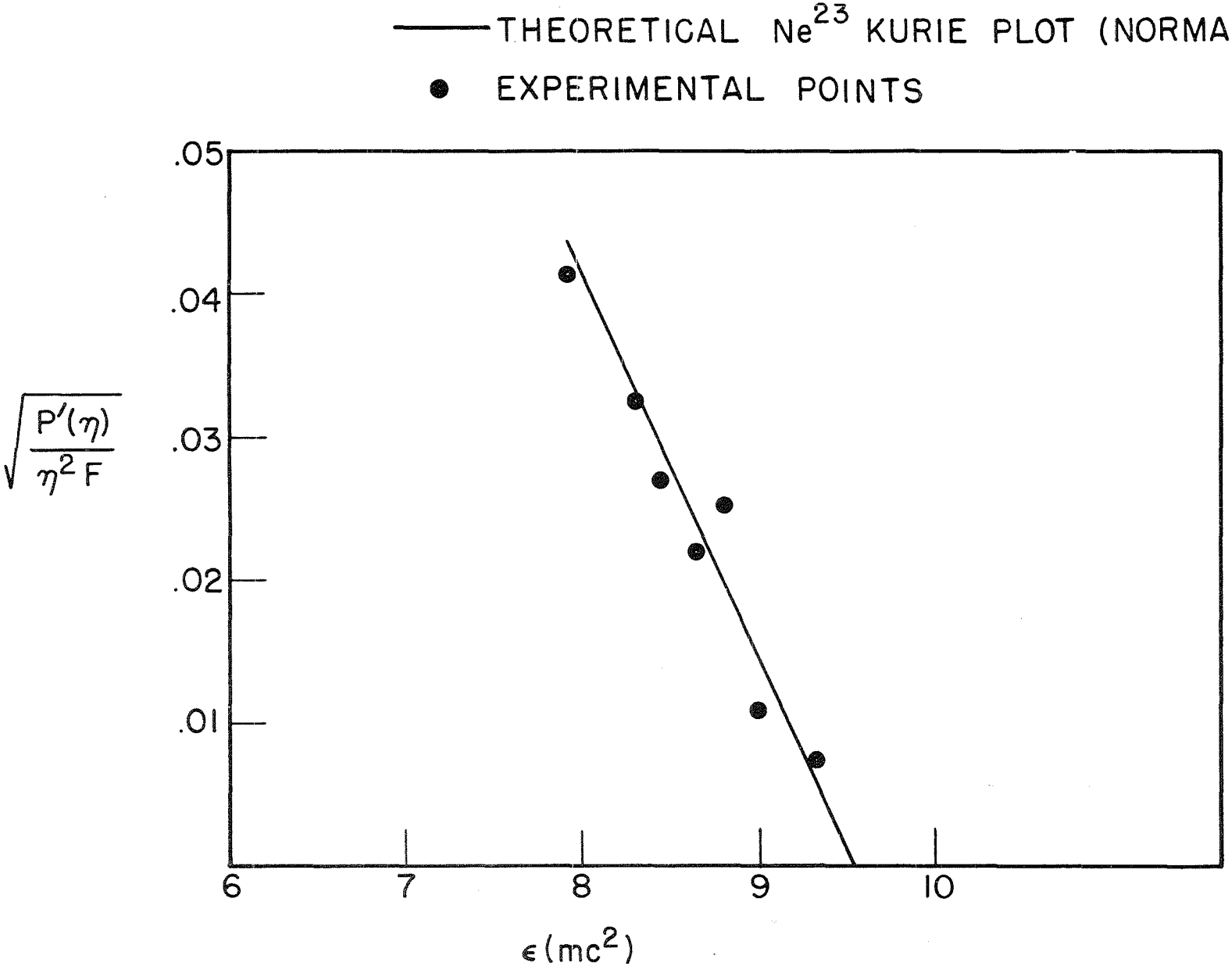

Fig. 12. Kurie plot of the measured spectrum in the region of energy about the end point of He^6.

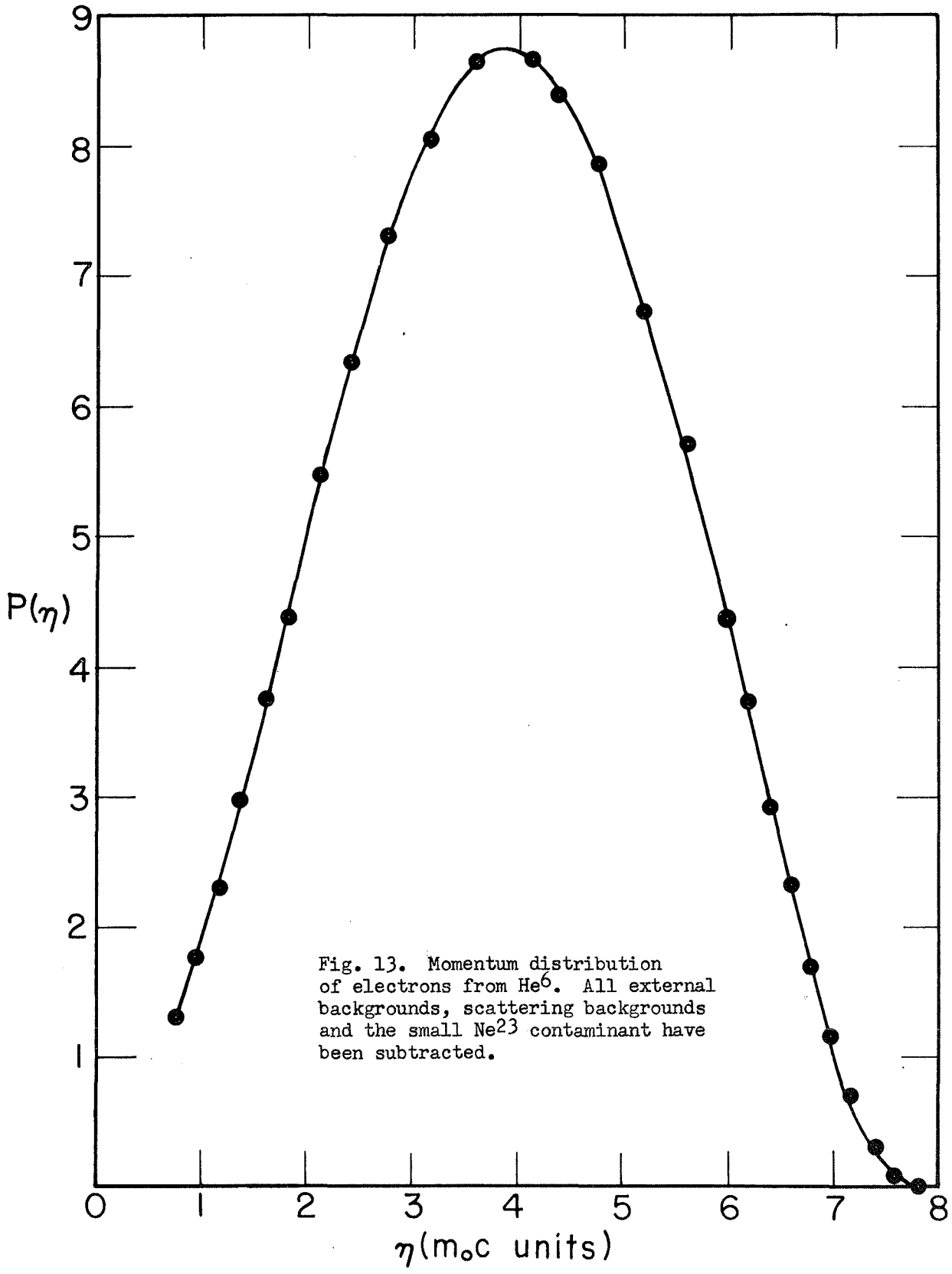

Fig. 13. Momentum distribution of electrons from He^6. All external backgrounds, scattering backgrounds and the small Ne^{23} contaminant have been subtracted.

KURIE PLOT He^6 SPECTRUM

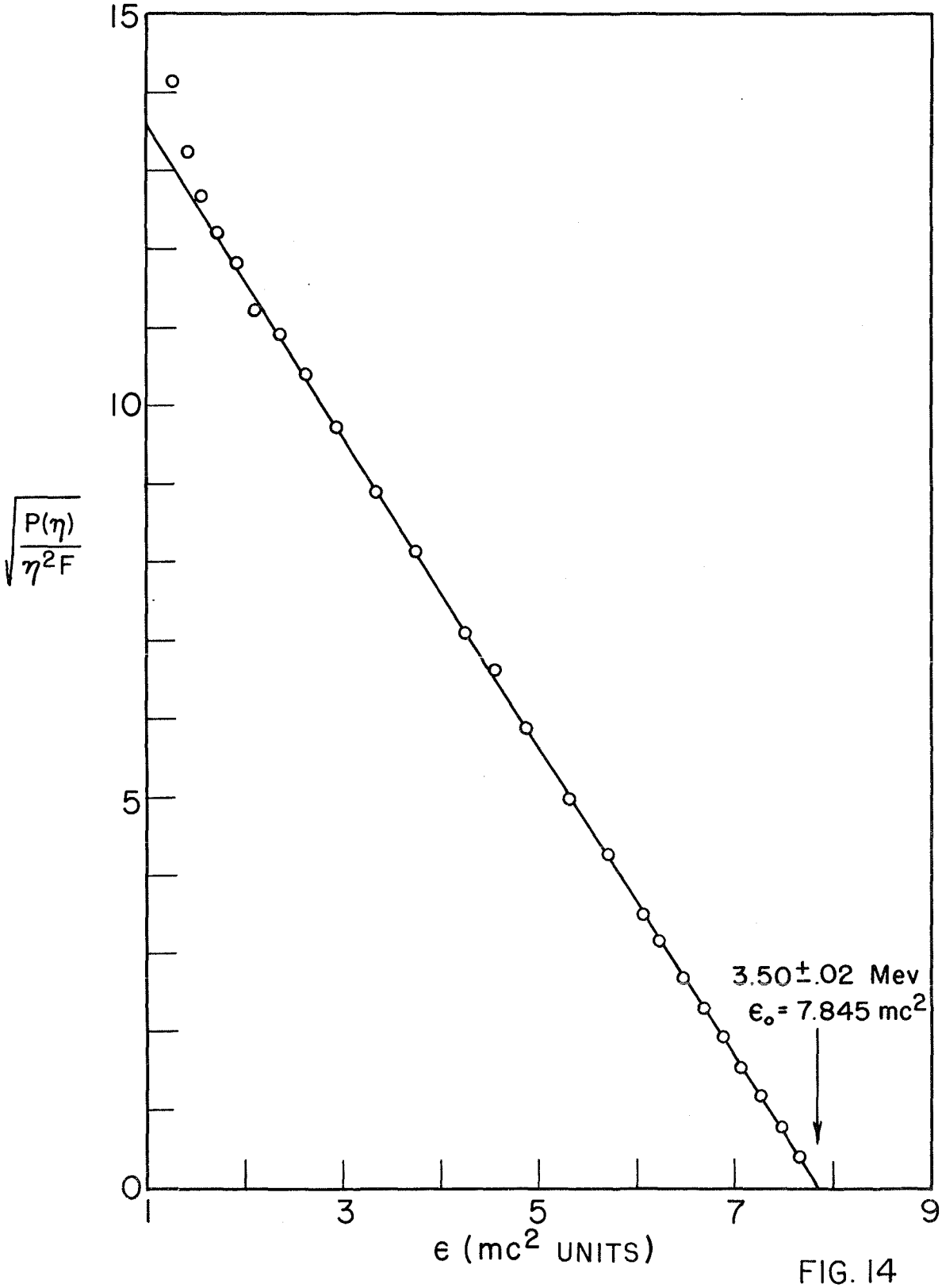

FIG. 14

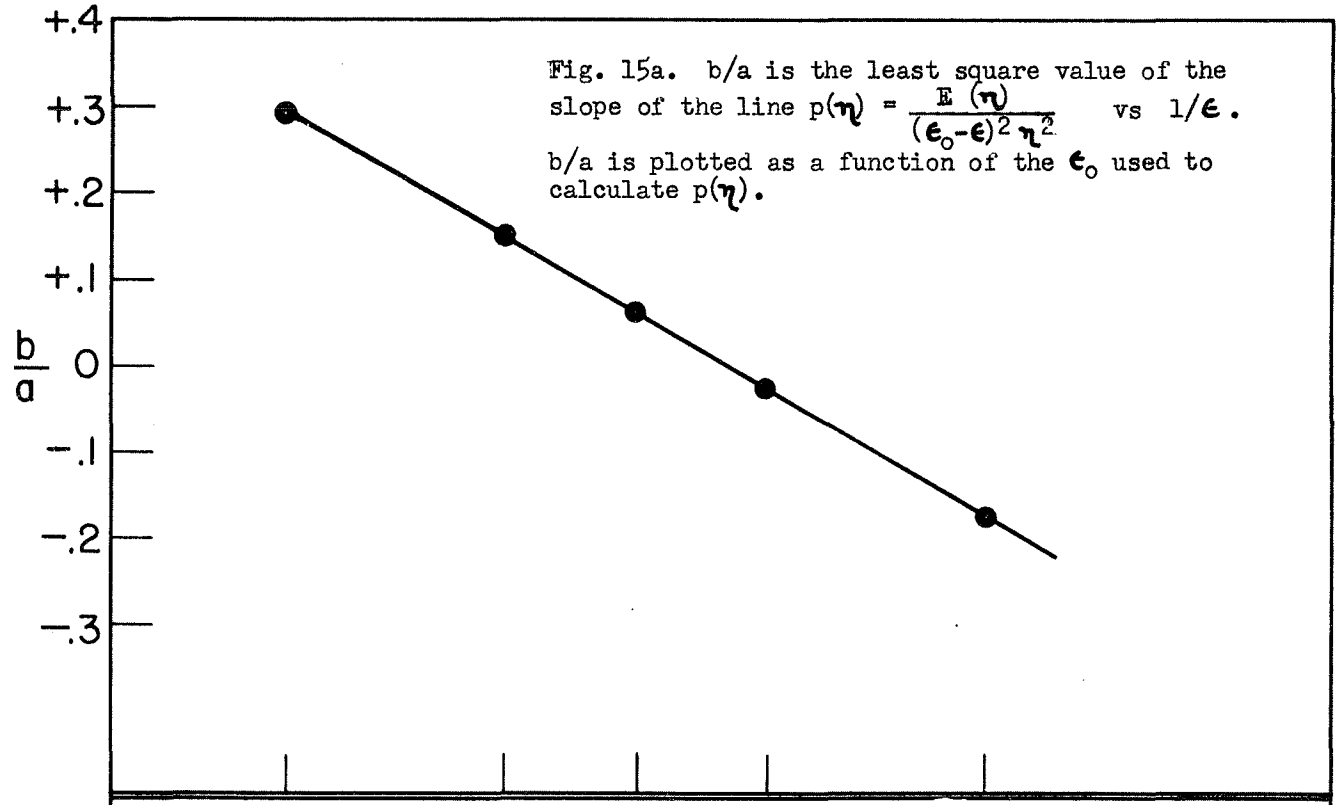

Fig. 15a. b/a is the least square value of the slope of the line $p(\eta) = \frac{E(\eta)}{(\epsilon_o - \epsilon)^2 \eta^2}$ vs $1/\epsilon$. b/a is plotted as a function of the ϵ_o used to calculate $p(\eta)$.

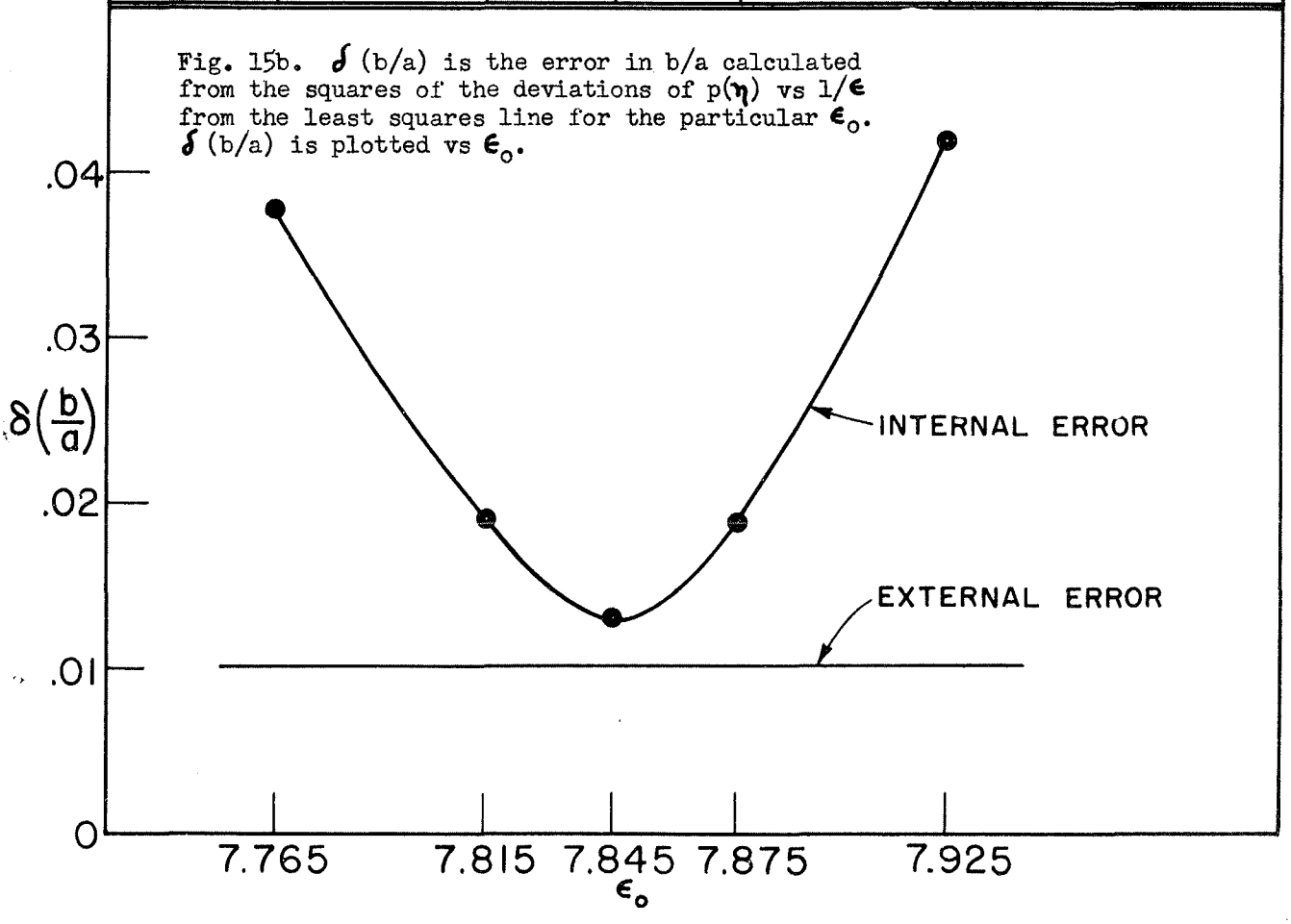

Fig. 15b. δ (b/a) is the error in b/a calculated from the squares of the deviations of $p(\eta)$ vs $1/\epsilon$ from the least squares line for the particular ϵ_o. δ (b/a) is plotted vs ϵ_o.

Fig. 16a and 16b. The function $p(\eta) = \frac{P(\eta)}{(\epsilon_o - \epsilon)^2 \eta^2 F}$ where $P(\eta)$ is the momentum distribution of electrons from He^6, and $\epsilon_o = 7.845\ mc^2$. The lines are the theoretical correction factors denoting the limits on α and β consistent with the experiment.

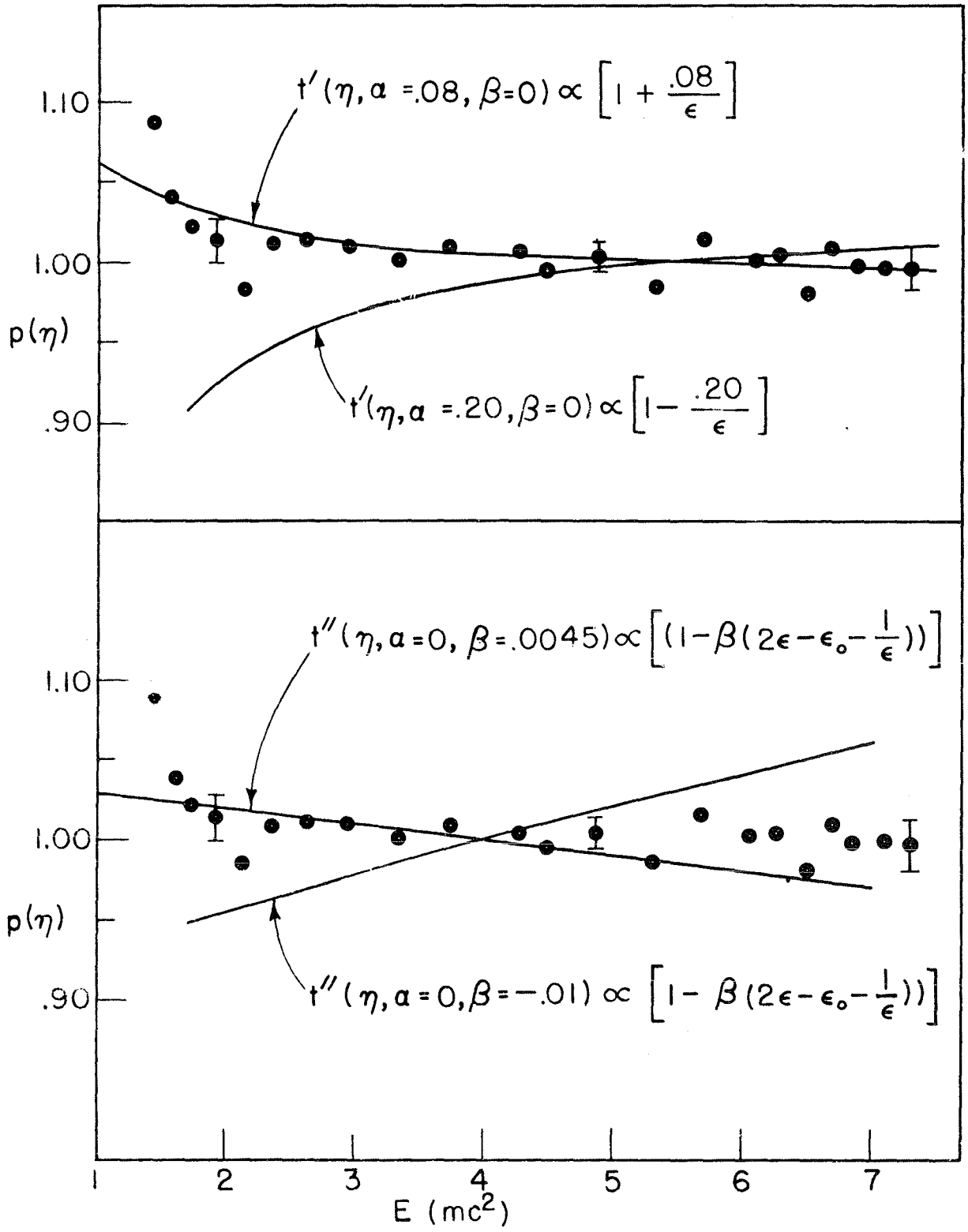

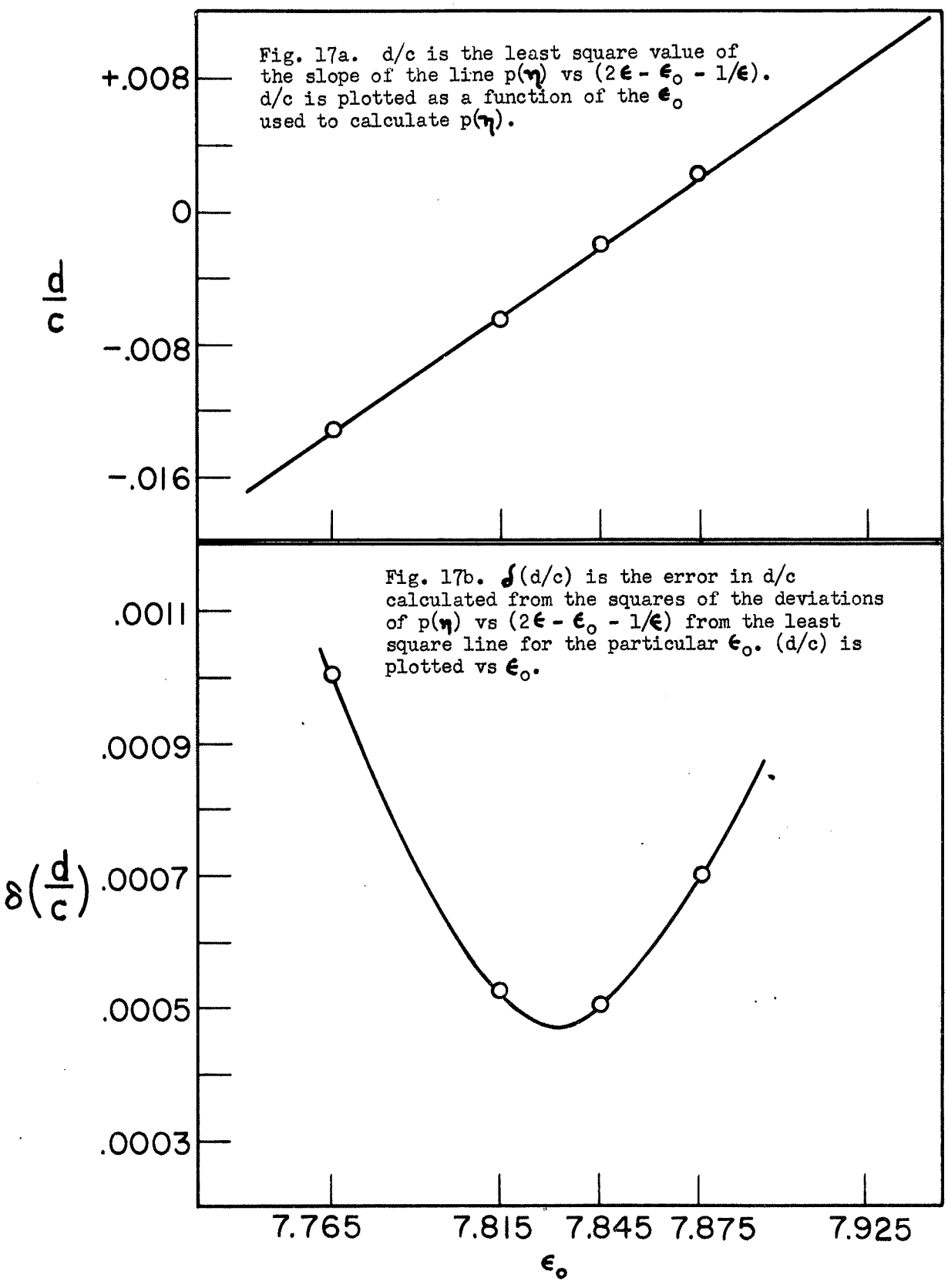

Fig. 17a. d/c is the least square value of the slope of the line $p(\eta)$ vs $(2\epsilon - \epsilon_0 - 1/\epsilon)$. d/c is plotted as a function of the ϵ_0 used to calculate $p(\eta)$.

Fig. 17b. $\delta(d/c)$ is the error in d/c calculated from the squares of the deviations of $p(\eta)$ vs $(2\epsilon - \epsilon_0 - 1/\epsilon)$ from the least square line for the particular ϵ_0. (d/c) is plotted vs ϵ_0.

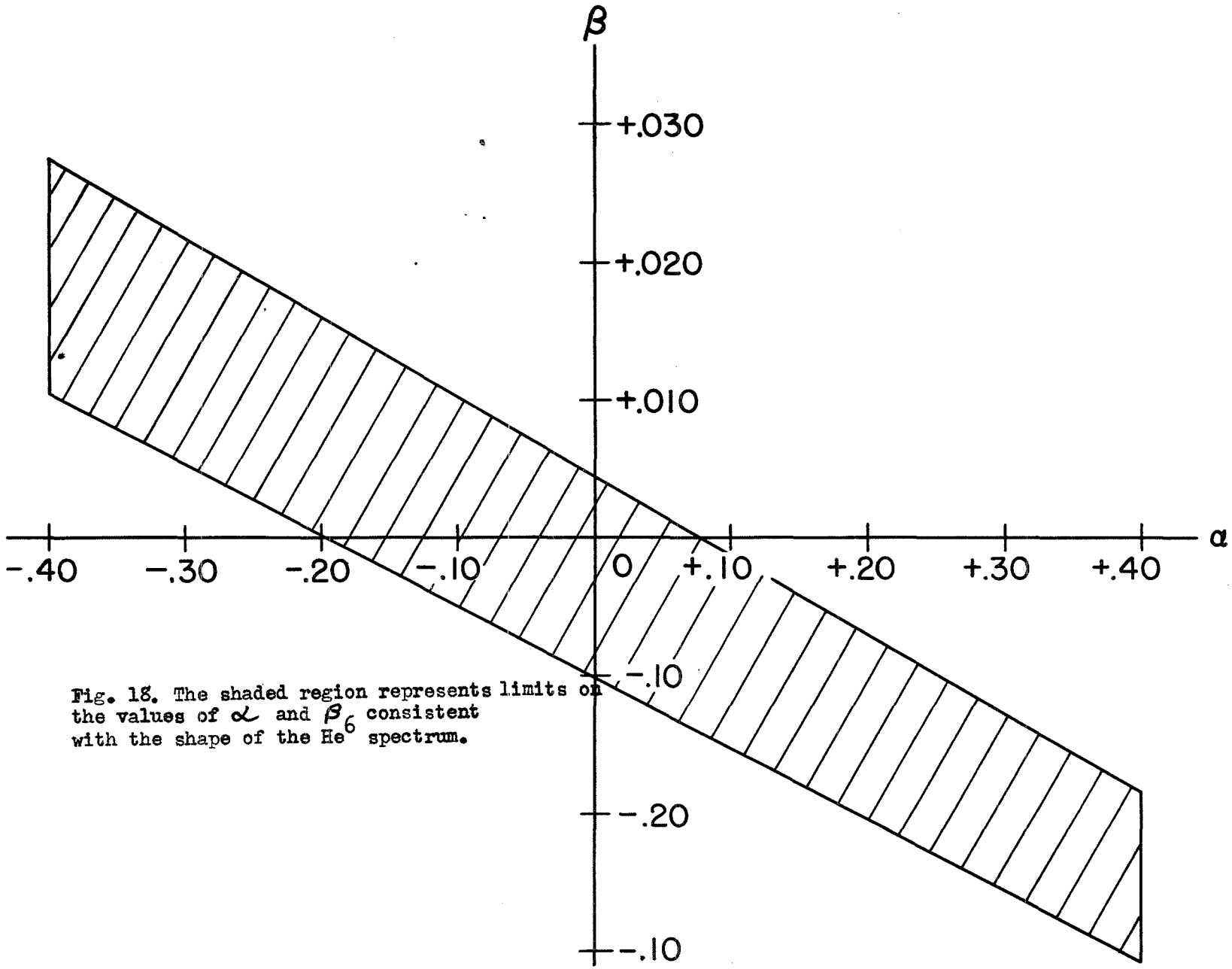

Fig. 18. The shaded region represents limits on the values of α and β_6 consistent with the shape of the He^6 spectrum.

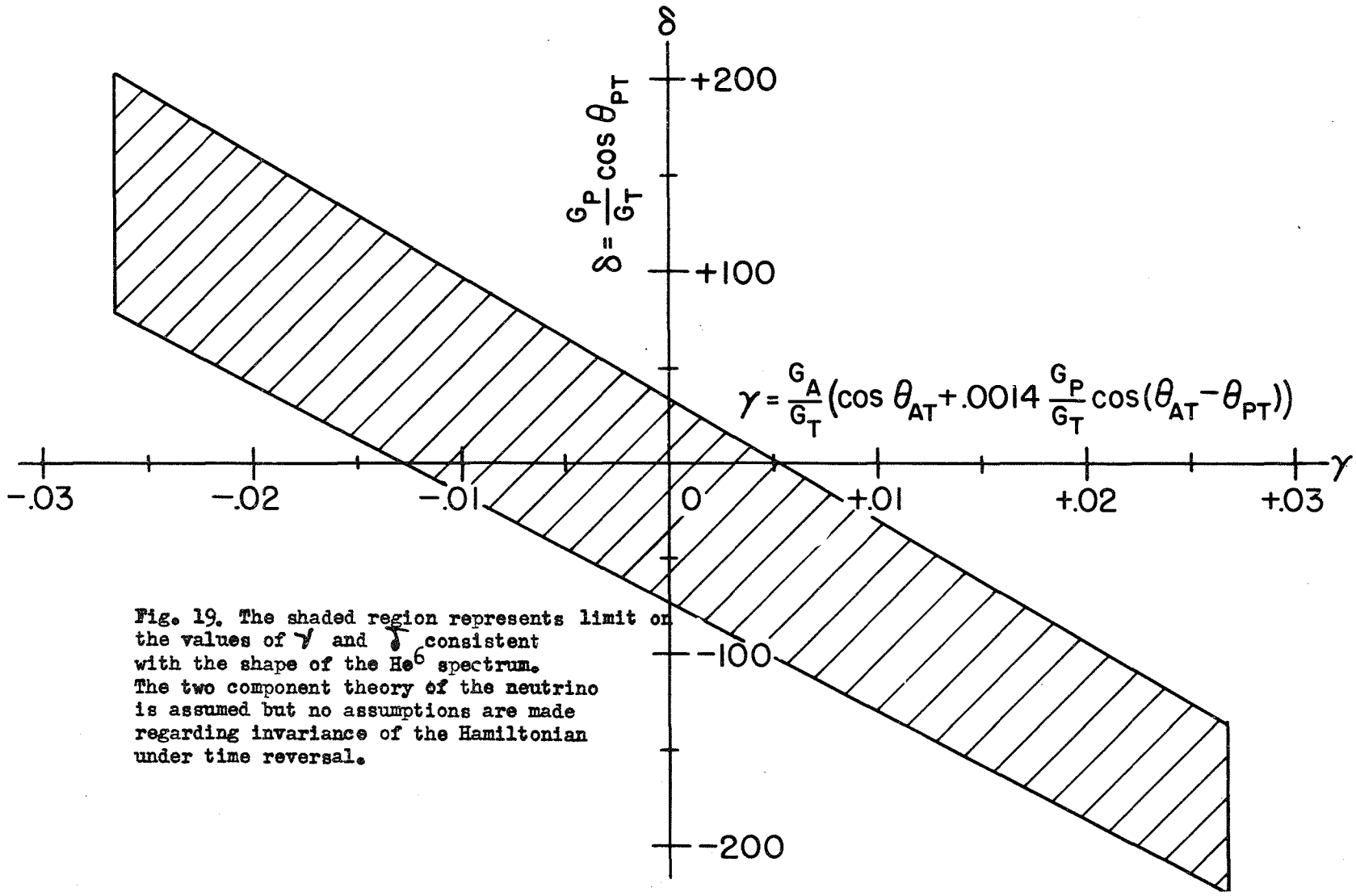

Fig. 19. The shaded region represents limit on the values of γ and δ consistent with the shape of the He^6 spectrum. The two component theory of the neutrino is assumed but no assumptions are made regarding invariance of the Hamiltonian under time reversal.

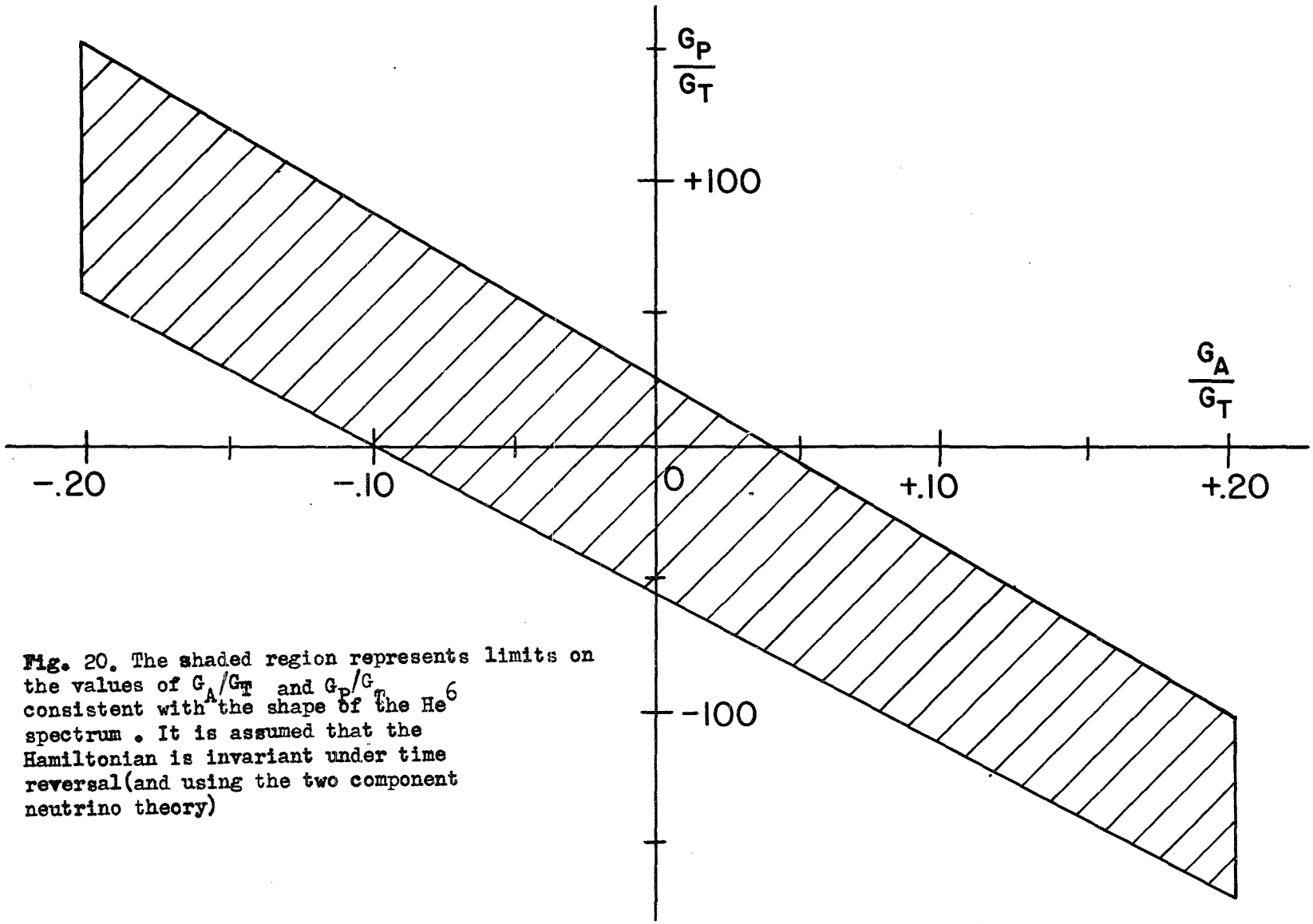

Fig. 20. The shaded region represents limits on the values of G_A/G_T and G_P/G_T consistent with the shape of the He^6 spectrum . It is assumed that the Hamiltonian is invariant under time reversal(and using the two component neutrino theory)

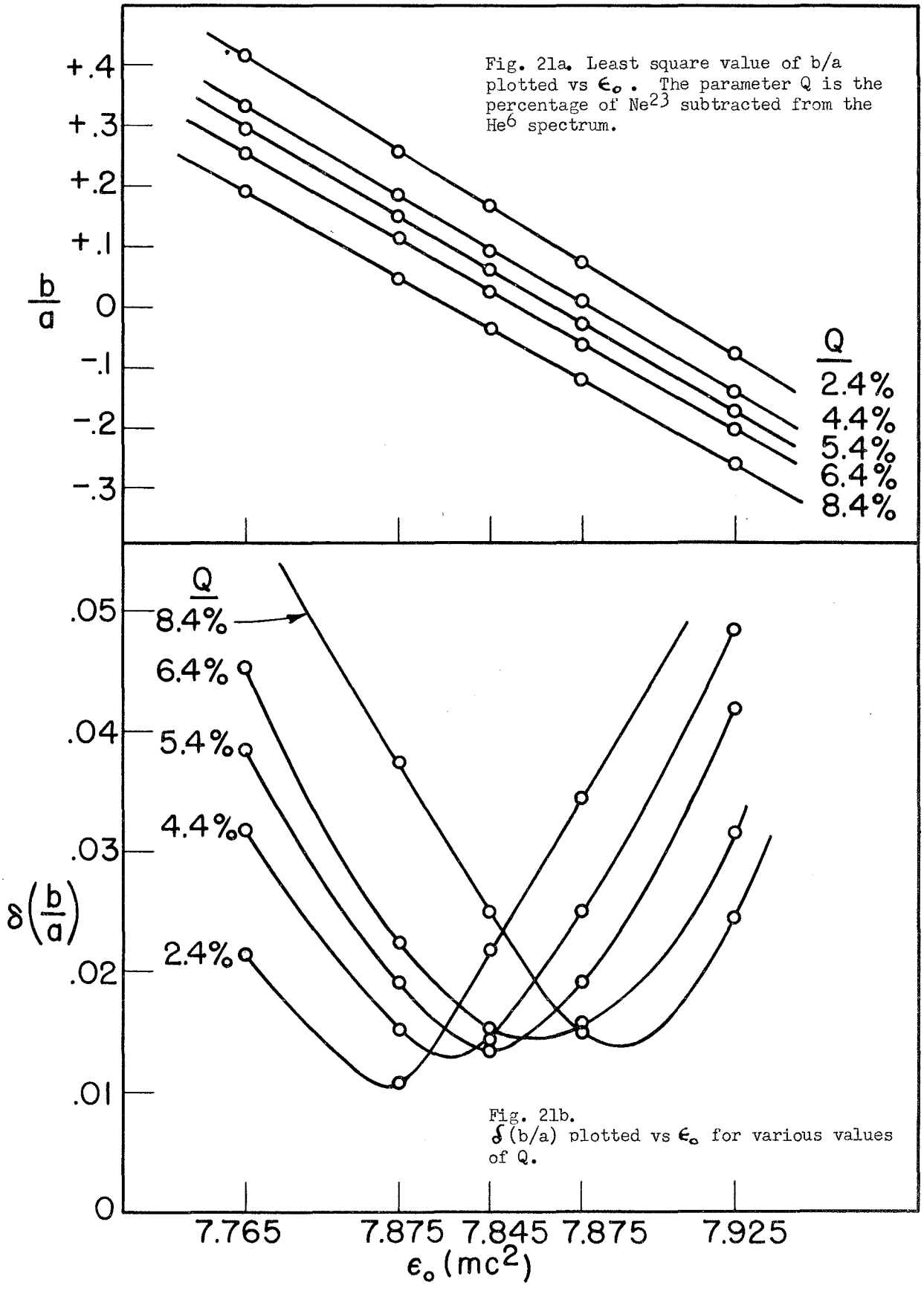

Fig. 21a. Least square value of b/a plotted vs ϵ_o. The parameter Q is the percentage of Ne^{23} subtracted from the He^6 spectrum.

Fig. 21b. δ(b/a) plotted vs ϵ_o for various values of Q.

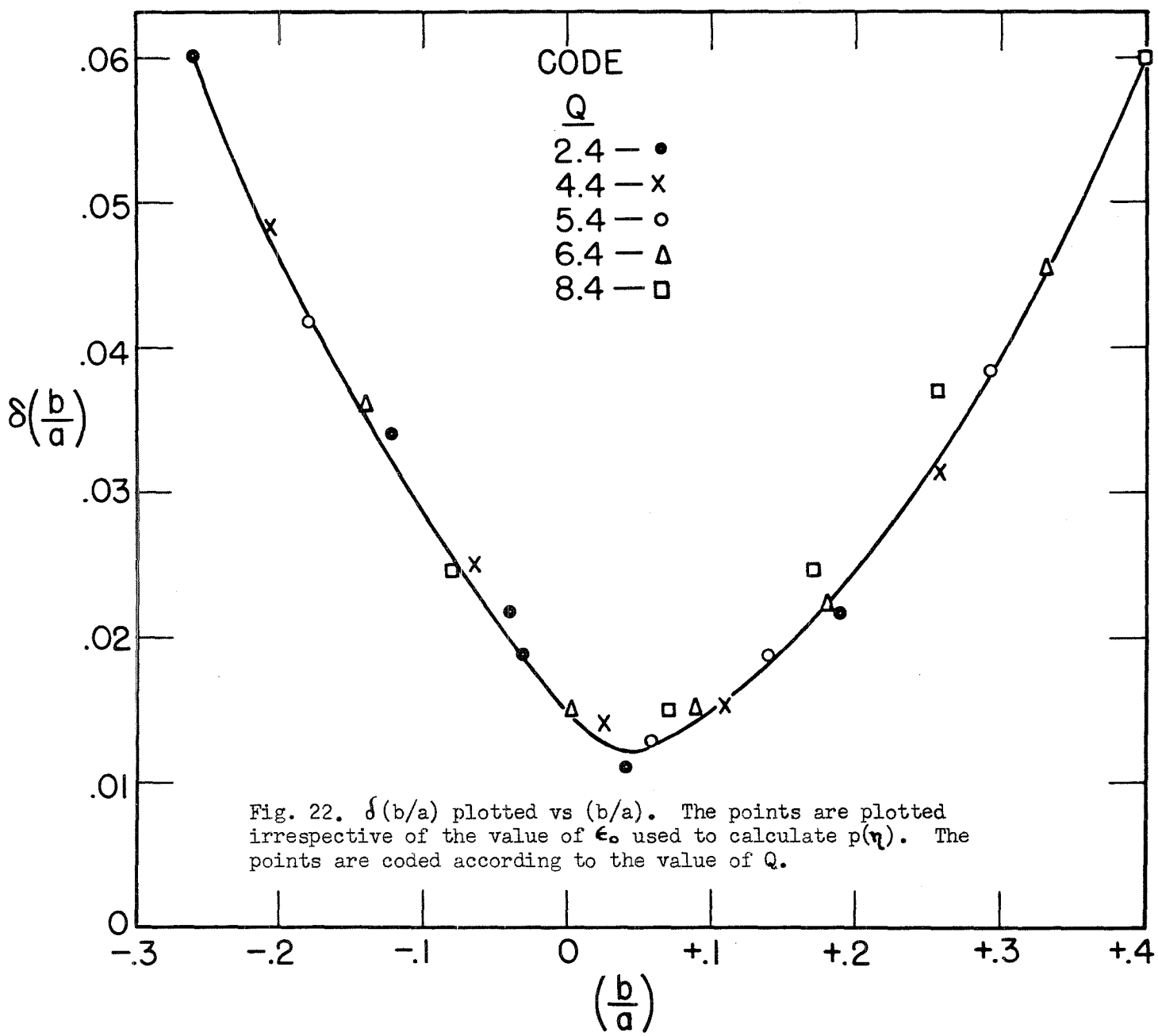

Fig. 22. $\delta(b/a)$ plotted vs (b/a). The points are plotted irrespective of the value of ϵ_o used to calculate $p(\eta)$. The points are coded according to the value of Q.

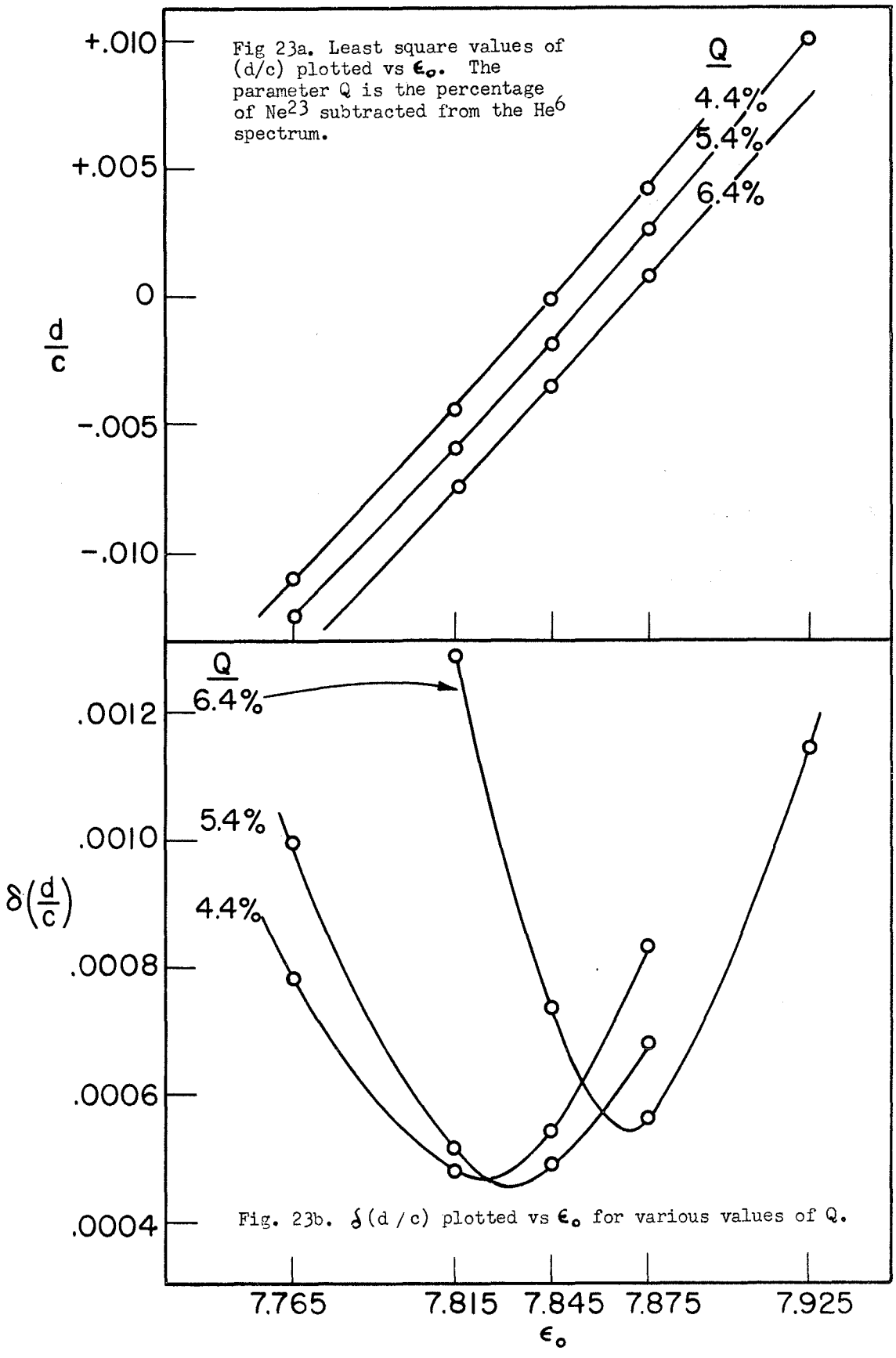

Fig 23a. Least square values of (d/c) plotted vs ϵ_o. The parameter Q is the percentage of Ne^{23} subtracted from the He^6 spectrum.

Fig. 23b. $\delta(d/c)$ plotted vs ϵ_o for various values of Q.

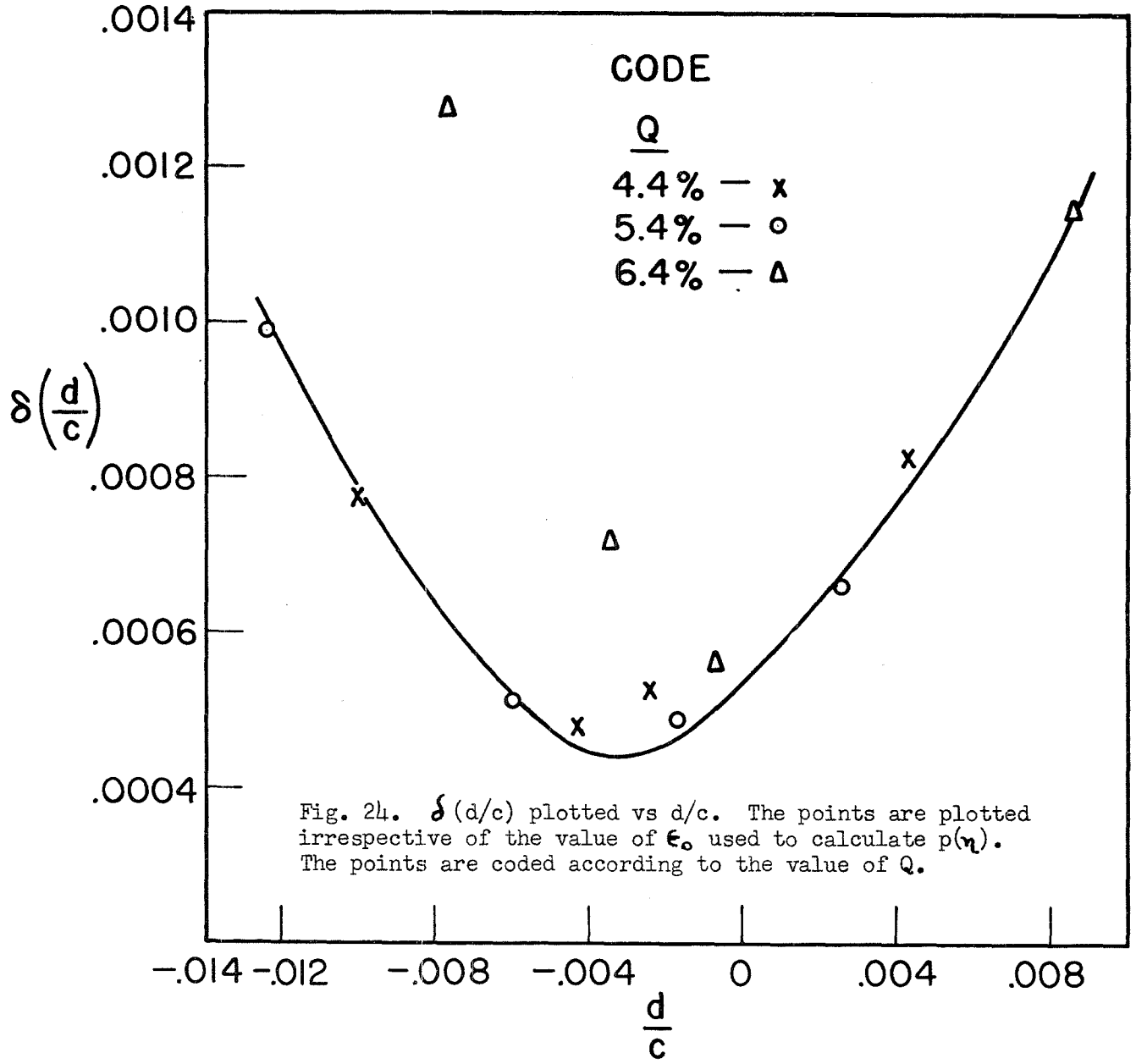

Fig. 24. δ (d/c) plotted vs d/c. The points are plotted irrespective of the value of ϵ_o used to calculate $p(\eta)$. The points are coded according to the value of Q.